INVESTIGATION OF THE SCHWANN CELL LINEAGE IN THE MOUSE SCIATIC NERVE:
AN ELECTROPHYSIOLOGICAL AND MORPHOLOGICAL STUDY

DISSERTATION

zur Erlangung des Grades eines
Doktors der Naturwissenschaften

Der Mathematischen-Naturwissenschaftlichen Fakultät
und
der Medizinischen Fakultät

vorgelegt

von

Nicole Fröhlich

aus Wurzen, Deutschland

Mai 2016

Tag der mündlichen Prüfung	08.09.2016
Dekan der Math.-Nat. Fakultät:	Prof. Dr. W. Rosenstiel
Dekan der Medizinischen Fakultät:	Prof. Dr. I. B. Autenrieth
1. Berichterstatter:	Dr. Maria Kukley
2. Berichterstatter:	Prof. Dr. Olga Garaschuk
Prüfungskommission:	Dr. Maria Kukley
	Prof. Dr. Olga Garaschuk
	Prof. Dr. Bernd Antkowiak
	Prof. Dr. Cornelius Schwarz

Erklärung / Declaration:

Ich erkläre, dass ich die zur Promotion eingereichte Arbeit mit dem Titel:

„**Investigation of the Schwann Cell Lineage in the mouse sciatic nerve:**

an electrophysiological and morphological study“

selbständig verfasst, nur die angegebenen Quellen und Hilfsmittel benutzt und wörtlich oder inhaltlich übernommene Stellen als solche gekennzeichnet habe. Ich versichere an Eides statt, dass diese Angaben wahr sind und dass ich nichts verschwiegen habe. Mir ist bekannt, dass die falsche Abgabe einer Versicherung an Eides statt mit Freiheitsstrafe bis zu drei Jahren oder mit Geldstrafe bestraft wird.

I hereby declare that I have produced the work entitled

*“***Investigation of the Schwann Cell Lineage in the mouse sciatic nerve:**

an electrophysiological and morphological study*”,*

submitted for the award of a doctorate, on my own (without external help), have used only the sources and aids indicated and have marked passages included from other works, whether verbatim or in content, as such. I swear upon oath that these statements are true and that I have not concealed anything. I am aware that making a false declaration under oath is punishable by a term of imprisonment of up to three years or by a fine.

Tübingen, den 04.05.2016 .....

Datum / Date Unterschrift /Signature

INDEX

ABBREVIATIONS

4-AP	4-Aminopyridine
ACh	Acetylcholine
AMPA	A-amino-3-hydroxy-5-methyl-4-isoxazolepropionic acid
ATP	Adenosine triphosphate
BSA	Aovine serum albumin
CAP	Compound action potential
CD68	Cluster of Differentiation 68
CGP	(3-Aminopropyl) ethylphosphinic acid hydrochloride
CNS	Central nervous system
CTZ	Cyclothiazide
DAPI	2-[4-(Aminoiminomethyl)phenyl]-1*H*-Indole-6-carboximidamide hydrochloride
DIC	Differential interference contrast
eGFP	Enhanced green fluorescent protein
FAK	Focal adhesion kinase
FCS	Fetal calf serum
GFAP	Glial fibrillary acidic protein
HMG	High mobility group domain
IBA1	Ionized calcium-binding adapter molecule 1
IR DIC	Infrared differential interference contrast
iSC	Immature Schwann cells
LJP	Liquid junction potential
LY341495	(2S)-2-Amino-2-[(1S,2S)-2-carboxycycloprop-1-yl]-3-(xanth-9-yl) propanoic acid
MBP	Myelin basic protein
Mec	Mecamylamine hydrochloride
MLA	Methyllycaconitine
NF-kB	Nuclear factor of k light polypeptide gene enhancer in B cells
NGF-R	Nerve growth factor
NMDA	N-methyl-D-aspartate
Oct6	Octamer-binding transcription factor-6
OEC	Olfactory ensheathing cells
OPC	Oligodendrocyte precursor cells
PBS	Phosphate buffered saline
PFA	Paraformaldehyde

PI	Propidium iodide
PNS	Peripheral nervous system
PPADS	Pyridoxalphosphate-6-azophenyl-2',4'-disulfonic acid tetrasodium salt
$R_{membran}$	Membrane resistance
R_{series}	Series resistance
SC	Schwann cell
SCE	Schwann cell enhancer
SCP	Schwann cell precursor cells
Sox10	SRY (sex determining region Y)-box 10
TBS	Tris-buffered saline
TEA	Tetraethylammonium
TM	Transmembrane domains
TTX	Tetrodotoxin
V_h	holding potential

LIST OF FIGURES

LIST OF TABLES

ABSTRACT

Two Schwann cell (SC) types are present in the peripheral nervous system: myelinating and non-myelinating SCs. Both types originate from the same progenitor, the immature SC, which develops from neuronal crest cells. The sequential expression of transcription factors and developmental markers characterize the distinct SC types in the lineage. The electrophysiological properties of these cells are only rarely studied in ex vivo slices so far. Furthermore, only a few studies investigated the different SC types in embryonic and early postnatal vertebrate. We want to determine and characterize SCs in ex vivo slices. We developed a new preparation of sciatic nerve slices of late embryonic (E16-18) and early postnatal mice (P0-P2). Using patch clamp recording and immunohistological analyses, we could (dependent on the age) characterize two (E16-E18) or four (P0-P2) electrophysiologically different SC types. These SC types differ in their expression of voltage-dependent Na^+ and K^+ channels. First analyses show that they express TEA and 4-AP sensitive delayed rectifing K^+ channels. During patch-clamp recordings we included a fluorescent dye into the pipette solution, so we could combine the electrophysiological properties of the different SC types with their morphological features. These analyses show that SCs before birth display higher number of processes and branches whereas SCs after birth have longer but a lower number of processes and less branches.

First hint that SCs could express neurotransmitter receptors for glutamate was shown in invertebrate. Furthermore, neurotransmitters, including glutamate, are able to induce changes of SC membrane potential in the giant squid axons (Villegas, Evans et al. 1987, Lieberman and Sanzenbacher 1992). Moreover, different studies done in cell culture (Liu and Bennett 2003) or with immunohistochemical methods (Dememes, Lleixa et al. 1995) show that SCs in vertebrates could express different types of glutamate receptors. Using the fast pressure-application system, we want to investigate whether SCs in acute slices express functional ionotropic glutamate receptors and whether SC types differ in their expression. Application of 1mM Glutamate induced an inward current in at least two SC types and in both developmental stages/age groups. The majority of the evoked current is sensitive to the AMPA/kainate blocker GYKI53655, indicating that functional glutamate receptors of the AMPA/kainate type are expressed.

1. INTRODUCTION

In the last decades glial cells became more and more important in the field of neuroscience. They start their history as 'nerve glue'. The name was given by Virchow in its book 'Cellularpathologie' in 1858. But first noted they have been even early, in 1824, by Rene Dutrochet. He just described them as 'globules' that glued between nerve fibers. Later, Otto Deiters classified glial cells as cells which are lacking an axon. His first drawings show most probably a white matter oligodendrocyte. In the next year's more and more details became emerge, Golgi showed that some glial cells are associated with blood vessels. His student Pio del Rio-Hortega, in 1920, classified glial cells in the four still existing groups: protoplasmic in gray matter, neuroglia in white matter, mesoblastic microglia, and interfascicular glia (today known as oligodendrocytes) (Fig. 1.1; (Somjen 1988, del Rio-Hortega 1993)).

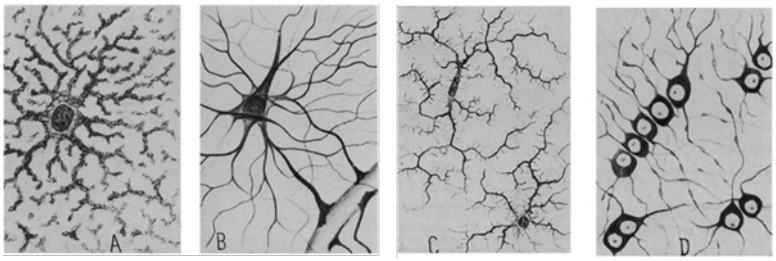

Fig. 1.1 Illustration of the four types of interstitial cells in the human nervous tissue
A. Protoplasmic neuroglia from the gray matter. B: Neuroglia of the fibrous type from white matter. C: Microglia. D: Interfascicular glia, or oligodendrocytes, from the white matter of the brain (Somjen 1988, Fig. 4).

Their function was long time and is even now very debated. The eponym described them as connective tissue, which fills the space in between neurons and hold them together. Golgi was given them already distinct functions; because of their close relation to blood vessels he speculated that they are maybe important for the support of neurons with nutrients. Nageotte discovered secretory vesicles in glial cells and reasoned therefore that they are able to release substances (Nageotte 1910). Santiago Ramon y Cajal supported the idea of his brother, Pedro Ramon y Cajal; he proposed that glial cell processes insulate nerve fibers. Furthermore already Virchow states the possibility that these cells play an important role during diseases and brain pathologies.

1.1. GLIAL CELLS IN THE CENTRAL NERVOUS SYSTEM

In these days glial cells in the vertebrate central nervous system are divided in three subgroups: Microglia, Astrocytes, Oligodendrocytes (Fig. 1.2).

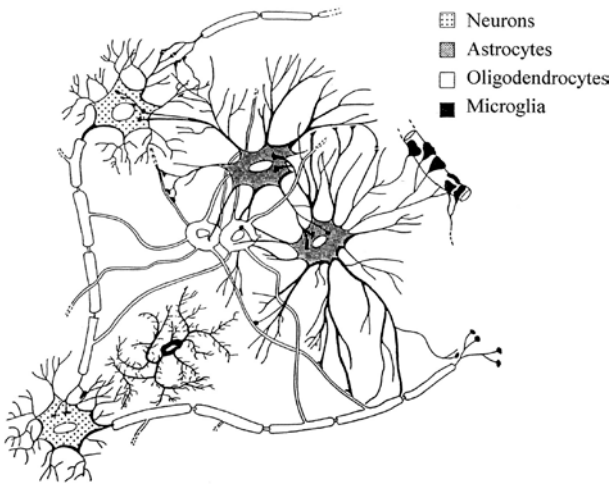

Fig. 1.2 Schematic drawing of the different glial cell types in the CNS.
The drawing shows their interaction with each other and neurons. Modified from (Baumann and Pham-Dinh 2001).

1.1.1. MICROGLIA

Microglia are the resident macrophages of the CNS (Fujita and Kitamura 1975). They originate from the haematopoetic stem cells and represent an important group of glial cells in the brain (Prinz and Priller 2014). They build the primary immune cells of the CNS and react to tissue damage, produced by injury, inflammation or in reactions of pathogen. This reaction leads to a change from the resting to the activated state. In this state not only the morphology changes, they also start to produce among other things pro-inflammatory cytokines, prostaglandin and NO (Saijo and Glass 2011). Furthermore recent studies show that microglia supply different factors (e.g. brain-derived neurotrophic factor) and mediators that influence synaptic plasticity (Parkhurst, Yang et al. 2013). In addition microglia seems to have as well an affected on synaptic pruning (Paolicelli, Bolasco et al. 2011).

To summarize, microglia cells are the major immune cells of the CNS and play an important role during non-healthy states of the brain. Yet newer studies show their impact in the healthy state as they also influence plasticity.

1.1.2. ASTROCYTES

The term ‘astrocyte’ is a description of the stellate (latin: astrum) appearance of this cell type. The cell is characterized by a lot of branched processes, which end at blood vessels and synapses. Already the morphology indicates the function of these cells. The historical role of astrocytes was the basic support of neurons (e.g. pH control, neurotransmitter uptake,

water transport, potassium conductance, regulation of the blood flow) in the CNS, supported as well by the close contact of these cells to the blood stream (Kimelberg 2007). More recent studies give astrocytes important new roles. They are able to regulate and influence synaptic formation, maturation, pruning and elimination (Clarke and Barres 2013). A special features of astrocytes is the connection between each other via gap junctions, which leads to the formation of a syncytium that transfer Ca^{2+} waves over longer distances and acts as a functional network (Nagy and Rash 2000). They became a global player in neuroscience, because of their various interactions with neurons, and more and more studies underline their importance in the healthy and diseased CNS.

1.1.3. OLIGODENDROCYTES

Oligodendrocytes are the myelinating cells of the CNS. One oligodendrocyte is able to myelinate up to 40 axons (Baumann and Pham-Dinh 2001). Myelin is important for increasing the conduction velocity of axons in the CNS, as the myelin sheaths build an insulating layer around the axons (Baumann and Pham-Dinh 2001, Miron, Kuhlmann et al. 2011). Remyelination has an important function in the CNS. This process is not performed by already existing mature oligodendrocytes, in fact oligodendrocyte precursor cells (OPC) are the source for new maturing and myelinating oligodendrocytes (Gensert and Goldman 1997, Carroll, Jennings et al. 1998, Levine and Reynolds 1999). These OPCs build a special group of glial cells in the CNS. This large pool of cells is able to proliferate and/or to differentiate even in adult hood (Alonso 2000, Dawson, Polito et al. 2003, Mori, Wakabayashi et al. 2009). OPC exhibit another very interesting feature. Different groups demonstrated that these cells do not only express receptors for different neurotransmitter, they are also able to contact axons via a synaptic-like structure (Bergles, Roberts et al. 2000, Kukley, Capetillo-Zarate et al. 2007, Ziskin, Nishiyama et al. 2007, Karadottir, Hamilton et al. 2008). The function of these connections is still under investigation.

The description of the three glial subtypes of the CNS clearly shows that glial cells are more than supporting cell that fill the gaps in between neurons. They more and more become an equivalent partner of their bigger brother the neuron.

1.2. GLIAL CELLS IN THE PERIPHERAL NERVOUS SYSTEM

Also in the peripheral nervous system distinct glia cells are discovered. They are often associated with a special part of the neuron or a neuronal subtype.

1.2.1. SATELLITE GLIA

The neuronal cell bodies of the parasympathetic and sympathetic, as well as the dorsal root ganglia are covered by a special glial subtype called satellite glia. Satellite glia cells are flattened cells that enwraps the somata of neurons (Huang, Gu et al. 2013). They share distinct characteristics with the brain astrocytes; like GFAP and gap junction expression. Like astrocytes they react to injury with the upregulation of GFAP, in addition also morphological changes, an increase in gap junction expression and the production of proinflammatory cytokines could by observed (Cherkas, Huang et al. 2004, Liu, Sun et al. 2012).

1.2.2. ENTERIC GLIA

Another unique glial type in the PNS is the enteric glia. It is located in the gastrointestinal tract. They are important for the homeostasis of the enteric neurons (Bush, Savidge et al. 1998). Recent studies show that enteric glia is involved in the majority of gut functions, like motility, mucosal secretion and host defence. Furthermore this glial type is reacting to different neurotransmitter, e.g. acetylcholine and ATP, with intracellular Ca^{2+} increase (Boesmans, Cirillo et al. 2013). Like astrocytes in the brain, enteric glia express gap junctions and building a syncytium that transfer Ca^{2+} waves over longer distances and acts as a functional network (Maudlej and Hanani 1992).

1.2.3. PERISYNAPTIC SCHWANN CELLS

Axon terminals at the neuromuscular junctions are covered with terminal glia (perisynaptic Schwann cells). Perisynaptic Schwann cells are closely opposed to the terminal and the release site; in addition the expression of different neurotransmitter receptors (e.g. acetylcholine, glutamate and ATP) could be demonstrated. This specific location and receptor expression enables the cells to detect and modulate synaptic transmission (Robitaille 1995, Rochon, Rousse et al. 2001). They play an important role in stabilizing nerve terminals and influence the re-growth of axons after denervation (Son, Trachtenberg et al. 1996).

1.2.4. OLFACTORY ENSHEATHING CELLS

Olfactory ensheathing cells (OEC) cover the CNS and PNS part of the primary non-myelinated olfactory axons. They surround several axons with their cytoplasm. They support and guide the axons during the lifelong continual regeneration or after damage back to the CNS (Boyd, Skihar et al. 2003, Higginson and Barnett 2011). Several studies show that the implantation of OECs in the spinal cord after injury promotes the axon regeneration and remyelination which leads to an increase in the functional recovery (Santos-Benito and Ramon-Cueto 2003).

1.2.5. SCHWANN CELLS

Schwann cells, as the myelinating glia of the peripheral nervous system were discovered by Theodor Schwann, a german biologist. In the middle 1800s during his time in the lab of Müller he identified sheaths of cells that surround peripheral nerve axons. In addition Remark described in his doctoral thesis from 1836 sheath (Schwann cells) that surround nerve fibers. Furthermore Remark distinguishes between myelinating and non-myelinating axons (Remak, 1836). In 1932 Nageotte summarizes the current state with the statement: 'It (the Schwann cell) maintains singularly close anatomical and physiological relations with the neurite but, in this synthesis, the two protoplasms always remain distinct (Causey and Hoffman 1956). Until the 1950 it was still unclear whether the Myelin itself is a part of the Schwann cell. Hess summarized in his publication from 1953 what is so fare known about the relationship between axons and Schwann cells. Schwann cells are described as ‘fine fenestrated veil extending over the intermodal segment, perhaps sending trabeculae into the myelin sheath.’ (Hess and Lansing 1953). He postulated in his publication based on electron microscopy investigations that the myelin is a part of the Schwann cell which is surrounding one single fiber, whereas several non-myelinating fibers get engulfed by the protoplasm of a single Schwann cell and its outer limiting membrane (Fig. 1.3 (Hess and Lansing 1953)).

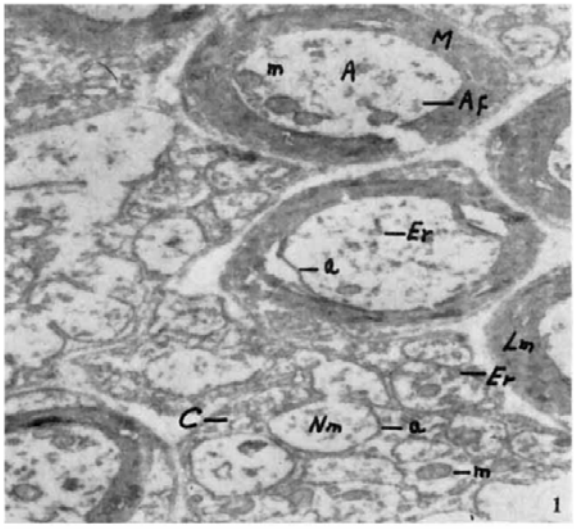

Fig. 1.3 One of the first electron microscopy pictures from the adult sciatic nerve of guinea pig.
The cross-section shows: A axon, C Schwann cell cytoplasm, M myelin, m mitochondria, Nm non-myelinated fibers. Modified from Hess and Lansing 1953.

The invention of electron microscopy introduced the possibility to describe cellular and subcellular structures. In the next years quite some publications investigated the morphological features of Schwann cells in longitudinal- and cross-sections of the adult peripheral nerves in different species (Hess and Lansing 1953, Geren and Schmitt 1954, Causey and Hoffman 1956). The nucleus of a myelinating Schwann cells in the adult peripheral nerves shows an exaggerate spindle shape (Hess and Lansing 1953) and the cell holds only a small amount of cytoplasm and is relatively thin (Geren and Schmitt 1954). The cytoplasm contains mitochondria and sparsely endoplasmic reticulum (Hess and Lansing 1953).

1.3. SCHWANN CELL DEVELOPMENT

1.3.1. SCHWANN CELL PRECURSOR CELLS

Schwann cells are the myelinating cells of the peripheral nervous system (PNS). They develop out of neuronal crest cells. One part of these neuronal crest cells migrates out of the trunk region of the neuronal tube in a ventral direction to develop into glia of the PNS (Jessen and Mirsky 2005). At around the embryonic day 12-13 (E12-13) in mice these cells develop to Schwann cell precursor cells (SCP) (Jessen, Brennan et al. 1994, Dong, Brennan et al. 1995). SCPs are characterized by a relatively small amount of cytoplasm and an irregular shaped nucleus. Thin sheets are extended from the soma and surround the axon bundles and spreading in between the axons (Jessen, Brennan et al. 1994). These are the first cells in the Schwann cell lineage that express the transcription factor SRY (sex determining region Y)-box 10 (Sox10). It is required for the survival and maintenance of the whole Schwann cell

lineage (Kuhlbrodt, Herbarth et al. 1998, Finzsch, Schreiner et al. 2010). Sox proteins express one special high mobility group domain (HMG), which enables them to bind to a sequence-specific DNA region (Wegner 1999). The special tertiary structure of the protein can during the binding process lead to architectural change of the DNA; in addition the binding to different promoter can affect the development of the transcription complex. Sox10 is especially important during the early Schwann cell development; nevertheless it is expressed and needed during the whole Schwann cell lineage (Britsch, Goerich et al. 2001). To discriminate SCP from other cells in the nerve tissue the low affinity nerve growth factor receptors (NGF-R) was as well used. Experiments with NGF-R+ cells show that these early SCPs failed to express S100 in a recognizable level (Jessen, Brennan et al. 1994). SCP cells are in close contact with axons, it is well established that they need each other for survival (Garratt, Britsch et al. 2000, Garratt, Voiculescu et al. 2000, Britsch, Goerich et al. 2001). The nerve contains axon bundles, existing of densely packed axons and SCPs. SCPs surround the axons bundle and also found in between the axons (Jessen, Brennan et al. 1994). They are highly proliferative and underwent rapid apoptosis if they lose the contact to axons (Jessen, Brennan et al. 1994, Dong, Brennan et al. 1995). At this stage of the development nerves have a compact structure with only a few vessels and connective tissue. SCP and axons are closely contiguous and both express N-cadherin. N-cadherin seems to play an important role during very early nerve and Schwann cell development. It seems to be essential for the formation of contacts between Schwann cells, which build the perfect base for the axon outgrowth (Wanner, Guerra et al. 2006). The next developmental stage, immature Schwann cells appear when the axons have reached their final destination and the first electrical activity appears (Ziskind-Conhaim 1988, Wanner, Guerra et al. 2006). During the phase of axon outgrowth and nerve formation only SCP are surrounding axons (Jessen, Brennan et al. 1994).

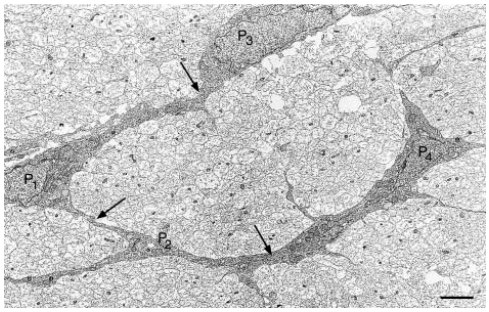

Fig. 1.4 Schwann Cell Precursors are in close contact the axons.
Electron microscopy picture from four SPC (P1-P4) in the rat hind-limb nerve cross section at E15. Nuclei of the cells are labeled with P1-P4. Scale bar: 0.7µm. Modified from (Jessen and Mirsky 1999).

1.3.2. IMMATURE SCHWANN CELLS

The transition between SCP and immature Schwann cells (iSC) happens around the embryonic day 16. It is characterized by the down regulation of N-cadherin and the up regulation of S100, GFAP and O4 (Mirsky, Dubois et al. 1990, Jessen, Brennan et al. 1994, Wanner, Guerra et al. 2006). The process of migration is completed and the iSCs are in close contact with a bundle of axons (Woodhoo and Sommer 2008). During this stage of development the proliferation reaches its peak (between E15-19) (Yu, Feltri et al. 2005). It has been shown that the proliferation is induced by axons (Komiyama and Suzuki 1992). Laminins, which are the major component of the Schwann cell surrounding basal lamina, also promotes the proliferation (Yu, Feltri et al. 2005). In addition Neuregulin-1, which is expressed by neurons, is an important survival factor for Schwann cells. (Li, Tennekoon et al. 2001). Survival and proliferation from iSC is promoted by several signals, which can originate from axons, autocrine signals or components from the basal lamina.

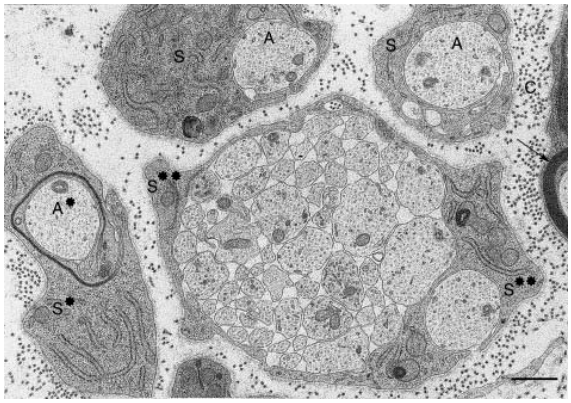

Fig. 1.5 Immature Schwann cells enclose a bundle of axons with different diameters. Electron microscopy picture from a newborn mouse sciatic nerve cross section. S** shows two iSC that enclose axons; S pro-myelinating Schwann cell which engulf a single axon; S* myelinating Schwann cell which starts to build the first layer of myelin. Scale bar: 0.6µm. Modified from (Jessen and Mirsky 1999).

The interaction between iSC and axons plays an important role during this phase of the development. Because in this period the processes called 'radial sorting' is taking place.

Radial sorting describes the process in which iSC separate the large diameter axons to build 1:1 relationship. During this process the iSC sends cytoplasmic processes into the group of axons and separate the large diameter axons (Woodhoo and Sommer 2008). Webster performed in 1973 an electron microscopy study in which he described the processes the first time: 'axons to be myelinated appeared to progress radially from a bundle to a 1:1 relationship with a Schwann cell at the sheath's outer margin' (Webster, Martin et al. 1973). Small diameter axons stay together in groups and get engulfed by a non-myelinating Schwann cell. The regulation of this process is still not very deeply reviewed. Studies show that the interaction between laminins expressed by the basal lamina and the receptors, β1-

integrins, expressed by Schwann cells is important (Feltri, Graus Porta et al. 2002). Also other genes that are closely related the laminin – β integrin interaction/basal lamina have an impact on radial sorting, e.g. members of the Rho GTPases (Benninger, Thurnherr et al. 2007, Nodari, Zambroni et al. 2007) or the focal adhesion kinase (FAK) (Grove, Komiyama et al. 2007). Dependent whether Schwann cells engulf several axons or myelinate one single axon they are divided in two groups; the non-myelinating and myelinating Schwann cells.

1.3.3. PRO-MYELINATING SCHWANN CELL

After the process of radial sorting one single iSC stays in contact with one axon. This interaction leads to the activation of a molecular program to build myelin. The process is under strict transcriptional control. Fig. 1.5 shows the appearance of a pro-myelinating Schwann cell in a newborn mouse sciatic nerve section (the cell is labeled with S). In the first step Oct6 is activated. Oct6 (octamer-binding transcription factor-6) belongs to the group of POU domain transcription factors and initiates the transition from pro-myelinating Schwann cell to myelinating Schwann cells. The expression of Oct6 is induced in iSC and peaks in the stage of pro-myelinating and early myelinating Schwann cells (Scherer, Wang et al. 1994, Arroyo, Bermingham et al. 1998). Oct6 is regulated by axonal or extracellular signals that interact via the Oct6 Schwann cell enhancer (SCE). To achieve the full enhancer activity a dimeric Sox10 binding to the SCE is needed (Finzsch, Schreiner et al. 2010, Jagalur, Ghazvini et al. 2011). A tight interaction between Sox10 and Oct6 is therefore needed to induce the activation and expression of Krox20. Mice lacking Oct6 show a transient arrest in the pro-myelinating status and a delay in the onset of myelination (Jaegle, Mandemakers et al. 1996). The activation of Krox20 by Oct6 and Sox10 elevate the pro-myelinating Schwann cell in the stage of a myelinating Schwann cell (Zorick, Syroid et al. 1999). The number of pro-myelinating Schwann cells is at the day of birth the highest and decline with their maturation to myelinating Schwann cells in the rat nerve (Friede and Samorajski 1968).

1.3.4. MYELINATING SCHWANN CELL

In the pro-myelinating phase the myelinating is induced by the strong interaction between Sox10 and Oct6, which leads to the activation of Krox20. The major transcription factor controlling different genes important for myelination is Krox20 (Topilko, Schneider-Maunoury et al. 1994). In mice lacking Krox20 the Schwann cells remain in the phase of pro-myelinating Schwann cells and failed to develop further. In addition Krox20 is also needed

for the maintenance of the myelination (Zorick, Syroid et al. 1999, Decker, Desmarquet-Trin-Dinh et al. 2006). As the inducible depletion of Sox10 in the adult nerve shows, it is also important for the maintenance of the myelin (Bremer, Frob et al. 2011). But also the axon plays an important role in the activation of the myelination. Neuregulin 1, expressed by axons, interacts with the Erb2/3 receptor at Schwann cells and acts via the activation of the transcriptions factor NF-kB (nuclear factor of k light polypeptide gene enhancer in B cells) (Garratt, Britsch et al. 2000). This special interaction is as well important for the thickness of the myelin sheath that is made (Michailov, Sereda et al. 2004). In addition the level of NRG1 Type III expressed by axons determines whether the axon gets ensheathed or myelinated. Large diameter axons express a high level of NRG1, which leads to the formation of myelin sheaths; whereas small diameter axons with a low level of NRG1 get only ensheathed (Taveggia, Zanazzi et al. 2005, Brinkmann, Agarwal et al. 2008). The interaction between axons and Schwann cell, as well as the intrinsic transcription factor activation of Schwann cells play major roles in the processes of myelination. Myelinating Schwann cells are characterized by the expression of the transcription factor Krox20 and Sox10; the proteins for myelination like P0 and MPB are also specific for this cell type in the peripheral nervous system.

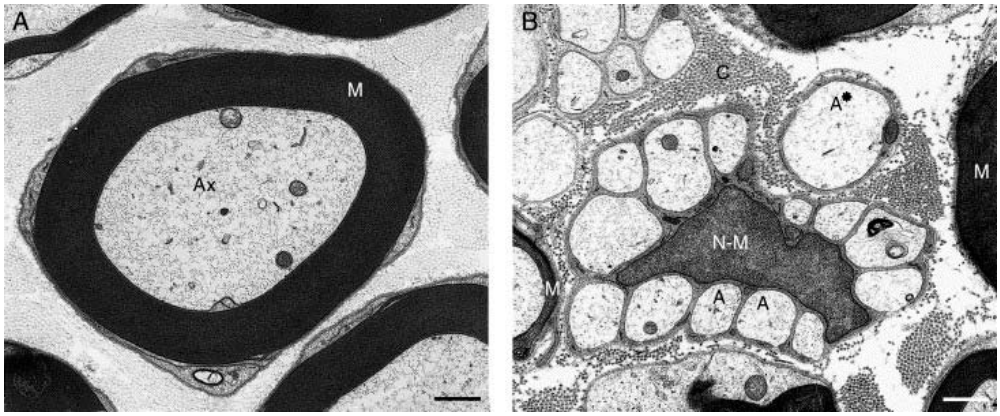

Fig. 1.6 Myelinating and non-myelinating Schwann cells in the adult sciatic nerve.
Cross section of the adult sciatic nerve of a rat shows in A a myelinating Schwann cell which forms several layer of compact myelin (M) around the axon (ax). Scale bar: 0.5µm. B Non-myelinating Schwann cell (N-M) which engulfs 13 small diameter axons (A). A* presents a non-myelinating Schwann cell which covers only one single axon. Scale bar:0.5µm. Modified from (Jessen and Mirsky 1999)

1.3.5. NON-MYELINATING SCHWANN CELL

During the process of radial sorting large diameter axons get separated by the processes of iSC. These iSC in contact with one large axon start the differentiation into myelinating Schwann cells. The remaining small diameter axons are clustered by non-myelinating Schwann cells, the Remak bundle (Webster, Martin et al. 1973). The axons within one remark bundle are separated from each other by processes of the non-myelinating Schwann cell (Aguayo, Bray et al. 1976). The marker profile of non-myelinating Schwann cells is quite close to that of iSCs; as both are positive for Sox10, GFAP and O4. In contrast, as the cells are lacking Krox20, P0 and MBP discrimination from myelinating Schwann cells is possible.

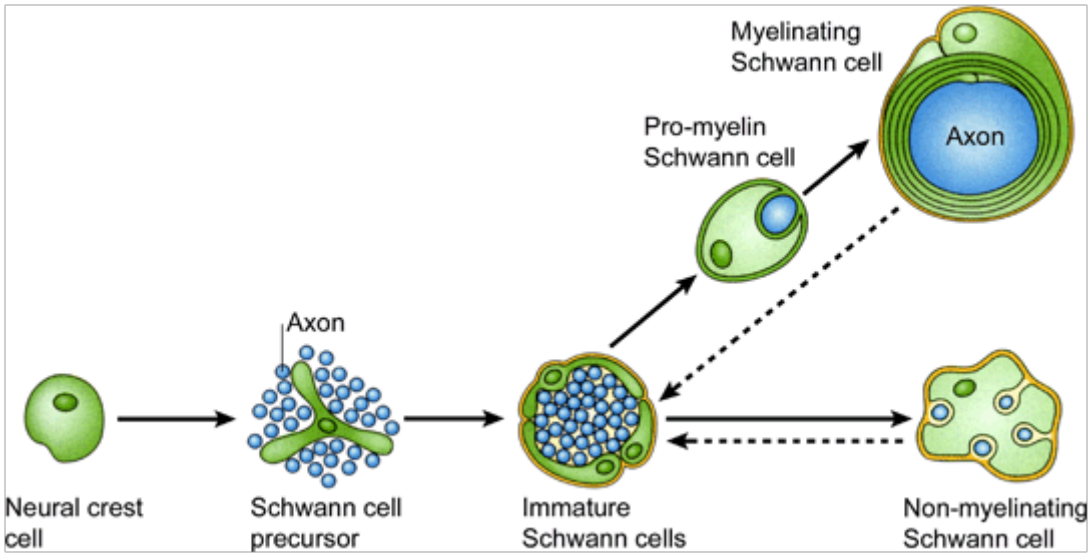

Fig. 1.7 Schematic drawing of the major steps in the Schwann cell development.
The origin of all Schwann cells is the neuronal crest cell. At the age of E12-13 the first transition take place into Schwann cell precursor. The second common developmental step is the passage to Immature Schwann cells, which takes place around E16 in mice. Until this step the development of non-myelinating and myelinating Schwann cells is the same. At the birth of the animals immature Schwann cells develop further into myelinating and non-myelinating Schwann cells (Jessen and Mirsky 2005).

As immature Schwann cells start to differentiate into myelinating and non-myelinating Schwann cells they leave the cell cycle. In contrast to the majority of neurons and glial cells Schwann cells are able to de-differentiate and re-enter the cell cycle in response to injury. This process is accompanied by axonal degeneration and myelin breakdown. The described phenotype of Schwann cells in the injured nerve is comparable with iSC (Jessen and Mirsky 2005). The de-differentiated Schwann cells build the surrounding for the re-growing axons and proceed with the re-myelination of these axons (Bosse 2012). NRG1 seems to play as well an important role during this process (Fricker, Lago et al. 2011, Stassart, Fledrich et al.

2013). Nevertheless the process of axonal regeneration and remyelination is a well-organized task and details are still under investigation.

1.4. ELECTROPHYSIOLOGICAL PROPERTIES OF SCHWANN CELLS

With the development of the patch-clamp technique it has been demonstrated that the presence of voltage-gated channels is not restricted to excitable cells. Early studies show the presence of voltage-gated channels at glial cells (Bevan, Chiu et al. 1985), T lymphocytes (Cahalan, Chandy et al. 1985) and also Schwann cells. Studies performed in rabbit neonatal and adult cultured Schwann cells indicate the expression of voltage-gated sodium channels in at least a subset of Schwann cells (Chiu, Schrager et al. 1984, Shrager, Chiu et al. 1985, Howe and Ritchie 1990). The kinetic properties of these voltage-gated sodium channels are comparable with that in neurons (Chiu, Schrager et al. 1984). Additional evidence for the expression of several voltage-gated sodium channel subtypes could be found in Schwann cells using in situ hybridization and RT-PCR (Oh, Black et al. 1994).

The presence of voltage-gated potassium channels was investigated by different groups. They show the presence of fast activating and inactivating (I_A) channels, fast activating and slow inactivating (I_D) channels and slow activating and inactivating (I_K) channels (Konishi 1989, Wilson and Chiu 1990, Baker, Howe et al. 1993, Baker and Ritchie 1996, Sobko, Peretz et al. 1998) (Tab. 1). All studies were performed in cultured or freshly dissected Schwann cells.

Tab. 1 Overview of the three reviewed voltage-gated potassium channel classes.

	I_A	I_D	I_K
Kinetics	fast & transient	fast & sustained	slow & sustained
$Tau_{activation}$	~ 1ms	<10ms	>10ms
Pharmacology	sensitive to high 4-AP (5mM)	sensitive to low 4-AP (50µM)	sensitive to TEA
Electrophys. separation	prepulse protocol to (-110mV) – (-40mV)	prepulse protocol to -40mV	prepulse protocol to -40mV
	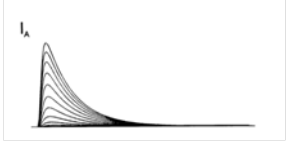		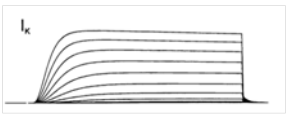

The traces are reproduced from (Locke and Nerbonne 1997).

Chiu and colleagues discovered in 1984 4-Aminopyridine (4-AP) sensitive voltage-gated potassium channels in Schwann cells cultured for eight days from newborn rat sciatic nerve (Chiu, Schrager et al. 1984). Also cultured rabbit neonatal Schwann cells show the presence of at least two different 4-AP and Tetraethylammonium (TEA) sensitive channels (Howe and Ritchie 1988). Furthermore enzymatically dissociated newborn Schwann cells of the mouse sciatic nerve express voltage-gated potassium channels that are sensitive to the potassium channel blocker TEA, Quinine and 4-AP (Konishi 1989). Baker and colleagues investigated especially the delayed-rectifying potassium channels in cultured Schwann cells from newborn rabbits. They used the sensitivity of the channels to 4-AP and their kinetics to divide them into two groups. The majority of Schwann cells express both of the two different types of 4-AP sensitive channels, whereas a minority is only expressing a single type. Giving the first indication that Schwann cells differ in their expression of voltage-gated channels (Baker, Howe et al. 1993, Baker and Ritchie 1996). Whole cell patch-clamp recordings performed in freshly isolated rat sciatic nerve Schwann cells from different age groups revealed the reduction of somatic voltage-gated potassium channels with increasing age and myelination (Wilson and Chiu 1990). In addition recordings performed at the paranodal region of adult Schwann cells show the presence of voltage-gated potassium channels at the paranodal region of myelinating Schwann cells (Wilson and Chiu 1990). Immunohistochemical investigations of voltage-gated potassium channels in the sciatic nerve of young rats discovered a subtype dependent distribution of the channels. Dependent from the subtype they can be specifically expressed at the juxtaparanodal region or perinuclear, intracellular compartments (Mi, Deerinck et al. 1995). This supports the idea that voltage-gated channels are clustered at special region and are not equally distributed across the Schwann cell surface, as it is reported for many other cell types. This spatial clustering of voltage-gated channel may indicate the functional role. As they are positioned close to the voltage-gated channels expressed by axons in the nodal region they may play a role in potassium regulation at this specific part of the axon especially during axonal activity. Furthermore, cultured neonatal Schwann cells decrease proliferation when voltage-gated potassium channels are blocked (Konishi 1989, Sobko, Peretz et al. 1998). Also semiquantitative RT-PCR shows the down-regulation of voltage-gated potassium channels in the mouse sciatic nerve from P1 to P40 (Sobko, Peretz et al. 1998).

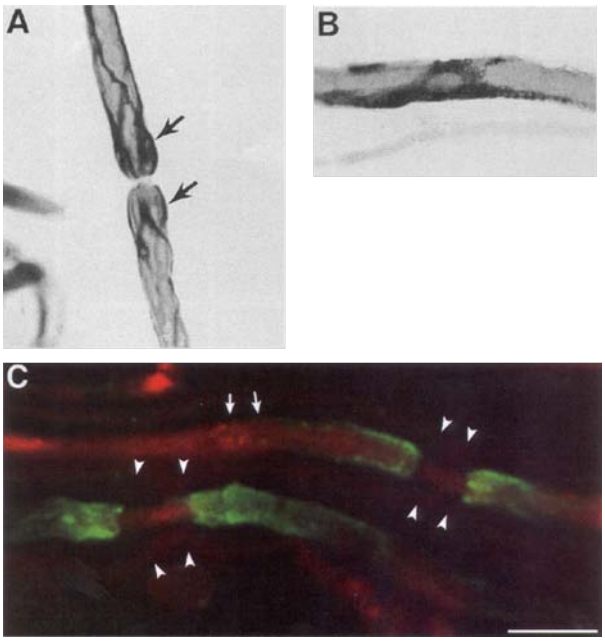

Fig. 1.8 Localization of voltage-gated potassium channels in rat sciatic nerve Schwann cells.
A-B: Immunoreactivity against the voltage-gated potassium channel (Kv1.5) in a teased nerve preparation. Labeling was present in the nodal (A) and in the perinuclear (B) region.
C: Immunohistochemical staining against Kv1.1 channels (green) and neurofilament (red) in cryosectioned nerve slices. Scale bar: 10µm. Modified from (Mi, Deerinck et al. 1995)

Schwann cells in the sciatic nerve are at least in culture able to express different voltage-gated channels. The studies also show that Schwann cells differ in their expression of channel and may change the channel expression during development. The channels seem to be clustered specially at the paranodal region of the myelinating Schwann cell. The functional role of these channels is still not clear. However, some experiments performed in cultured Schwann cells show their impact on potassium buffering at the nodal region and proliferation of Schwann cells.

1.5. NEUROTRANSMITTER RECEPTOR EXPRESSION IN SCHWANN CELLS

1.5.1. NEUROTRANSMITTER

One possibility to transfer information from one cell to the other in the nervous system is the interaction via neurotransmitter. In neurons the action potential propagates along the axon and leads to a Ca^{2+}-dependent release of neurotransmitter from vesicles at the presynaptic site of the synapse. The synapse is a very specific structure of the neuron that passes a signal from one neuron to the other via a small gap, called synaptic cleft. The pre-synaptic cell is releasing endogenous chemicals into the synaptic cleft, which travel through the cleft and bind at a specific receptor expressed by the postsynaptic cell. This important interaction was discovered and started to be investigated in the 1950 (Fatt and Katz 1950, Fatt and Katz 1952, Katz 1971, Katz 2003). More than 100 various neurotransmitters exist in

the nervous system; but the major excitatory neurotransmitters are glutamate, acetylcholine (ACh) and purinergic signals, whereas GABA and glycine are the major inhibitory neurotransmitter. The neurotransmitter binding receptors at the postsynaptic site can be divided into two large groups: (1) ligand-gated ion channel receptors (ionotropic receptors) that result in a fast neurotransmission and (2) receptors coupled to second messenger system (metabotropic receptor) that leads to a slower and more prolonged response. (1) Ligand-gated ion channel receptors get activated by the binding of the neurotransmitter, which leads to the opening of the channel pore. Dependent from the neurotransmitter positively or negatively charged ions enter the cell and lead to a change of the membrane potential. The postsynaptic cell gets de- or hyperpolarized. (2) The neurotransmitter binding to the metabotropic receptor initiate a complex signaling cascade from the cell surface to the cell interior. The activation leads to the segregation of G-proteins, which interact directly with other ion channels or other proteins (e.g. enzymes) that produce intracellular second messenger. They lead to a variety of physiological responses by regulating ion channels, enzyme activity and many other processes. Furthermore, the signal can transfer to the nucleus and may lead to long lasting gene expression changes. The majority of ionotropic glutamate receptors are located at the region facing directly the presynaptic release site, which is called the postsynaptic density, where as the second class of neurotransmitter receptors, the metabotropic receptors, are most of the time positioned around the postsynaptic density.

Glutamate plays an important role in the neurotransmission of the peripheral nervous system. It is one of the major excitatory neurotransmitter of the ascending sensory neurons from the periphery to the central part of the nervous system. There are three families of ionotropic glutamate receptors: N-methyl-D-aspartate (NMDA), a-amino-3-hydroxy-5-methyl-4-isoxazolepropionic acid (AMPA) and kainate receptors. They are named after their preferred agonist. Ionotropic glutamate receptors are composed of four large subunits that form the central ion pore that is permeable for cations. All subunits share some common features. They consist of three hydrophobic transmembrane domains (TM1, 3, 4) and one cytoplasm-facing re-entrant membrane loop (TM2). The n-terminus is located at the extracellular space and comprises one of the two ligand binding domains. The second ligand binding domain resides in the long extracellular loop between TM3 and 4. The c-terminus is intracellular located and important for trafficking and anchoring (Dingledine, Borges et al.

1999, Traynelis, Wollmuth et al. 2010). Two molecules of glutamate or other agonist bind at the specific ligand binding sites of AMPA and Kainate receptors and lead via a fast conformational change to the rapid opening of the ion channel pore. The permeability for the different cations varies depended from the subunit composition. The four different AMPA subunits (GluA1-4) are very well characterized. Whereas the subunits GluA1, GluA3 and GluA4 are permeable for sodium, potassium and calcium; the GluA2-subunit is impermeable for calcium. But not only the cation permeability is dependent from the subunit composition, also the receptor trafficking and assembly are strongly influenced (Isaac, Ashby et al. 2007). Another important property of the AMPA receptors is the fast desensitization of the receptor, which is mediated by a conformational change in the subunits. One of the most potent allosteric modulator of desensitization is cyclothiazide (CTZ) which is operating by stabilizing the formation of the dimer and thereby leaving the channel opened (Mayer and Armstrong 2004).

The first evidence that Schwann cells express neurotransmitter receptors was determined in the invertebrate nervous system. Different electrophysiological experiments performed in squid generated the idea of the neurotransmitter receptor expression in Schwann cells. Villegas published in 1972 his first paper about Schwann cell axon interaction in squid. They monitored with sharp electrode recordings the membrane potential of Schwann cells in the squid. A long lasting hyperpolarization of the Schwann cell membrane potential after a prolonged stimulation of the axons was described. They were not able to reproduce this hyperpolarization by a single stimulation pulse (Villegas 1972). In the next years he studied intensively the discovered connection. He could demonstrate that the hyperpolarizing response could by mimicked by the application of nicotine, whereas muscarine has no effect at the Schwann cell membrane potential (Villegas 1975). The hyperpolarization could be blocked with D-tubocurarine and is therefore mainly mediated by ACh receptors located at the cell surfaces facing the neighboring axons and the adjacent Schwann cells (Villegas 1975, Rawlins and Villegas 1978). Liebermann and colleagues as well performed stimulation experiments on squid giant axons. They also showed membrane potential changes in Schwann cells measured with sharp electrode after electrical stimulation of the squid giant axon (Lieberman, Abbott et al. 1989, Lieberman and Sanzenbacher 1992). Schwann cells show a short depolarization that was followed by a long hyperpolarization of the membrane potential in response to electrical stimulation. Further investigations showed that both

components are dependent from the activation of glutamate receptors and that the hyperpolarization is in addition dependent from ACh receptors (Evans, Reale et al. 1991, Evans, Reale et al. 1991). A clear link between these two actions could be not drawn with the experiments performed at this time and is still unclear. Both groups demonstrate the presence of neurotransmitter receptors in squid Schwann cells.

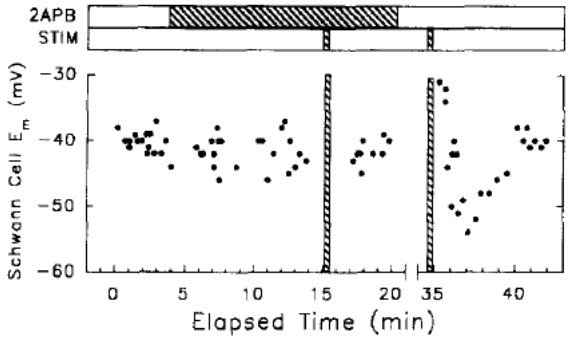

Fig. 1.9 Stimulation of the squid giant axon. The stimulation leads to a short depolarization followed by a hyperpolarization in the Schwann cell membrane potential. 2-APB (2-amino-4-phosphonobutyrate) is blocking both components of the membrane change. From (Lieberman and Sanzenbacher 1992)

Further studies performed in vertebrates explore the expression of different neurotransmitter receptors in Schwann cells. Immunohistochemical stainings for different glutamate receptors in the human skin accidentally discovered the expression of glutamate receptors in a Schwann cell processes (Kinkelin, Brocker et al. 2000). In addition light and electron microscopic immunohistochemical studies in the peripheral vestibular system of rats and guinea pigs exhibit the presence of AMPA receptors in Schwann cells (Dememes, Lleixa et al. 1995). Early postnatal cultured Schwann cells from the rat sciatic nerve demonstrate the release of ATP after glutamate application, which indicated the presence of glutamate receptors at the cultured Schwann cell surface (Liu and Bennett 2003).

The electrophysiological studies performed in invertebrates indicate the presence of neurotransmitter receptors for ACh and glutamate at the surface of Schwann cells. As well immunohistochemical studies performed in different animal models underline the presence of neurotransmitter receptors at Schwann cell.

1.6. THE SCIATIC NERVE AS A MODEL SYSTEM

The sciatic nerve is the major hind mixed nerve in the peripheral nervous system. It originates from the spinal segments L4-L6. It starts unifascicular and splits distally in two and even more peripheral in four fascicles (Schmalbruch 1986, Prodanov and Feirabend 2007). The middle part of the rat sciatic nerve consists out of myelinated motor axons (6%), myelinated (23%) and non-myelinated (48%) sensory axons and non-myelinated (23%) sympathetic axons (Schmalbruch 1986).

The structure of the rat newborn sciatic nerve is very well described. The nerve consists of axon bundles (containing up to 15 axons) that are surrounded by Schwann cells. Large diameter axons in bundles where not normally distributed, they are more often located peripheral more close to the Schwann cell surface. They are already in the processes of been separated from the bundle. Single axons engulfed by a single Schwann cell are as well present. Only a few axons located in the newborn nerve show an enlargement that was classified as a growth cone (Webster, Martin et al. 1973). At the day of birth almost no myelin was observed (Webster 1971, Webster, Martin et al. 1973, Jenq, Chung et al. 1986). At the third day of life the structure of the nerve already changed. The number of axons per bundle became smaller and the number of single Schwann cell axon interaction becomes larger. In addition now many of them contain one to three layers of myelin (Webster, Martin et al. 1973). The number of axons and Schwann cells increased from birth to day three (Webster, Martin et al. 1973). At day 7 after birth a large increase in the number of isolated and myelinated Schwann cells was seen. They were arranged in small families. Furthermore the myelin thickness and the axon diameter correspond closely. The number of Schwann cells increased again during this time, while the number of axons stayed the same (Webster, Martin et al. 1973). Especially the number of myelinating Schwann cells increased by five-fold and provides half of the total Schwann cell population in the nerve at this age. Also the number of axon bundles engulfed by Schwann cells increased, but the number of axons in the bundle decreased (Webster, Martin et al. 1973). In animals older than P5 a reduction in the total number of axon could by observed. The myelination peaks in the first two weeks of live and stays stable until adulthood (Jenq, Chung et al. 1986). The only change that occurs is that in average the axon diameter gets smaller and the myelin sheaths thinner (Jenq, Chung et al. 1986). In the adult sciatic nerve 1/3 of axons are myelinated whereas 2/3 of axons are

only engulfed by non-myelinating Schwann cells (Jenq, Chung et al. 1986, Schmalbruch 1986).

The sciatic nerve of the mouse represents the perfect model system for our study. As the major peripheral nerve it enables us to investigate the Schwann cell lineage already during the very early steps of the development. In addition as a mixed nerve, containing myelinating and non-myelinating Schwann cells, it provides the possibility to study all Schwann cell types and their progenitors in one preparation.

RESEARCH GOAL

Schwann cells are one of the peripheral glial cell types. Their major important role is the myelination or engulfment of axons. Quite some research has been performed to investigate the marker expression of the different Schwann cell types during the Schwann cell development. The already performed research in the field of electrophysiology shows that Schwann cells are able to express voltage-gated sodium and potassium channels, but the majority of studies was performed in cultures or teased Schwann cells. It is known that Schwann cells, as well as other cell types change their expression pattern of different channels when they are in culture. In addition the majority of electrophysiological studies have been performed in animals after birth or even adult animals. The development of Schwann cells is at these age groups already in its last steps, an investigation of the early developmental stages in the Schwann cell lineage is not possible. The electrophysiological properties of Schwann cells in their natural surrounding are relatively unexplored.

The main goal of this study was the electrophysiological and morphological investigation of Schwann cells in a more natural environment. We established a new preparation to investigate Schwann cells in situ. The sciatic nerve as the major mixed nerve was used as a model system. As one of the biggest nerves in the mouse a preparation in early developmental stages was possible. This fact enables us to investigate also the early stages of the Schwann cell lineage development. In addition the presence of myelinated and non-myelinated axons provides the possibility to analyze the whole Schwann cell lineage. The first time a study that combines a detailed electrophysiological and morphological characterization of Schwann cells in the sciatic nerve slices was performed.

The sciatic nerve preparation provides in addition the option to investigate the interaction between Schwann cells and axons in situ. Former studies showed that the neurotransmitter release is not restricted to the synaptic region; it also takes place along the axons. To our knowledge that is the first time that a preparation in mammals was performed in which the contact between the axons and the Schwann cells stays intact. We started to investigate the possible connection vie neurotransmitter release and receptor expression between the axons of the sciatic nerve and the different Schwann cell types with the help of electrical stimulation.

2. MATERIAL AND METHODS

All experiments for this study were carried out in C57BL/6N (Charles River strain code 027) and TgN(GFAP-EGFP)GFEC-FKi mice (gift from Prof. Frank Kirchhoff, University of Saarland, Institute for Physiology). In TgN(GFAP-EGFP)GFEC-FKi mice the enhanced green fluorescent protein (eGFP) is expressed under the promoter of the human glial fibrillary acidic protein (GFAP). GFAP is a marker for a certain sub-type of Schwann cell (details about GFAP are discussed further in the results part related to immunohistochemistry). Unfortunately the eGFP signal was too weak to use it for our patch-clamp experiments. Nevertheless the mice were used for morphological analyses independent from the GFAP signal. Animals were housed at room temperature (24-26°C) in a 12h light/dark cycle room and given ad libitum access to water and food. All procedures were performed in accordance with the guidelines of the Regierungspräsidium Tübingen.

2.1. PREPARATION

2.1.1. NERVE PREPARATION FROM E16-18 ANIMALS

Pregnant mice were anaesthetized by inhaling 5% isofluoran-oxygen mixture in an anaesthetic apparatus for small animals with evaporator (IsoFlo, Eickemeyer). After the induction of a deep anaesthesia the isofluoran concentration was reduced to 1.5–2.5%. The depth of anaesthesia was proved by the toe pinch. The body temperature was kept at 36°C with the heating pad (Happy Hamster, 8 Watts, Fenix) and was controlled with the help of a rectal thermometer. The eyes were covered with eye ointment (Bepanthen Augen- und Nasensalbe) to protect them from dehydration.

In deep anaesthesia the extremities of the mouse were fixed. The surgery area was disinfected and covered with Gaze (Gazin©, Mullkompresse, Luhmann & Rauscher). The abdomen was opened (circa 3cm) with the help of a small scissor. The uterus with fetuses was moved out from the abdomen with the help of a little pressure at the abdomen sides. After this the fetuses were removed out of the uterus one by one. For this the uterus was opened with a small cut, followed by a ligature of the supporting uterine artery and vein. Directly after the removal of the fetus from the uterus, it was decapitated. The fetus was fixed with a back facing upwards in a dish filled with sylgard silicone (WPI Inc.). The upper

part of the back leg was opened by two cuts made with a scalpel. The muscle tissue above the nerve was carefully removed to expose the sciatic nerve. The nerve was dissected and removed from the animal with fine forceps. After the removal of all fetuses the anaesthetized mother mouse was sacrificed by decapitation.

2.1.2. *Nerve preparation from P0-2 animals*

The early postnatal animal was rapid killed by decapitation and fixed at a dish filled with sylgard silicone with the back facing upwards. The upper part of the back leg was opened with two cuts made with a scalpel. The muscle tissue above the nerve was carefully removed to expose the sciatic nerve. The nerve was dissected and carefully removed with fine forceps.

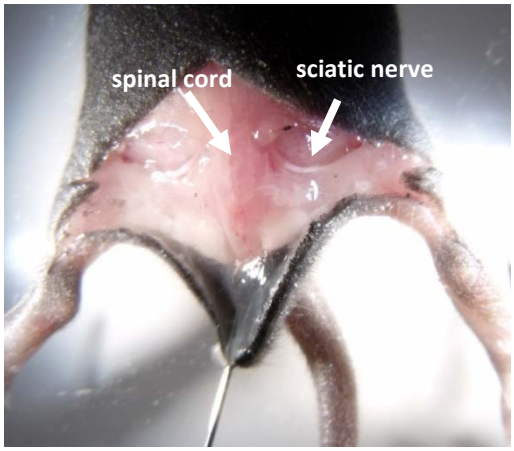

Fig. 2.1 Sciatic nerve preparation.
Opened back side of a C57BL/6N mouse during the preparation of the sciatic nerve. The sciatic nerve is clearly visible after the gentle removal of the overlaying muscle tissue.

2.1.3. *Slice preparation*

After removal of the sciatic nerve from a fetus or a neonatal mouse, the nerve was stored shortly (five to ten minutes) in an ice-cold high Mg^{2+} artificial cerebrospinal fluid (Prep-ACSF) containing the following (in mM): 124 NaCl, 1.25 NaH_2PO_4, 10 $MgSO_4$, 2.7 KCl, 26 $NaHCO_3$, 2 $CaCl_2$. Several nerves were collected and embedded in 36°C warm 2.5% low melting agarose (Plaque Agarose, Biozym) dissolved in ACSF. Subsequently the agarose with the nerves was cooled down for 3min on ice. During this time the agarose gets solid. Thereafter the agarose block was cut with the help of a razor blade into several small rectangles. Each rectangle contained a single nerve. Up to seven rectangles were glued to the specimen holder and fixed in the cutting chamber of the vibratome (VT1200S, Leica Biosystems). The chamber was then filled with ACSF containing the following (in mM): 124 NaCl, 1.25 NaH_2PO_4, 1.3 $MgSO_4$, 2.7 KCl, 26 $NaHCO_3$, 2 $CaCl_2$; pH 7.4, osmolality 300-310 mOsm/kg; gassed with a 95% O_2 and 5% CO_2 mixture. Afterwards 100µm thick longitudinal slices from the sciatic nerve

were produced. The slices were stored for 30min in a heated interface chamber (34°C) and constantly perfused with ACSF. Afterwards the slices were cooled down to room temperature and the experiments were started. The slices could be stored alive over several hours in the interface chamber at room temperature.

2.2. VOLTAGE-CLAMP RECORDING

Individual nerve slices were transferred to the recording chamber and mounted on a glass slide coated with Poly-L-Lysine (0.05%, Sigma). A small platinum grid was put above the slice in order to hold it at the position and prevent the movements of the slice during recording. Each slice fixed like this was incubated for 5min at 35°C with collagenase (0.1%, sigma) dissolved in ACSF. The collagenase pre-treatment was needed to facilitate access of the patch pipette to the membrane of Schwann cells. Afterwards the recording chamber with the slice was positioned on the stage of the upright microscope (Nikon Eclipse FN), equipped with differential interference contrast (DIC) optics and the filter set for Lucifer Yellow and Alexa568. During the whole experimental procedure the slice was continuously rinsed with oxygenated ACSF. The microscope was also equipped with a charge-coupled camera (COHU CCD camera), to observe the field of view via the monitor. Initially the Nikon Plan 4x/0.10 objective was used to position the sciatic nerve slice in the field of view. Subsequently, identification and selection of cells for patch clamp experiments and almost all electrophysiological recordings were performed with the Nikon NIR Apo 60x/1.0 water immersion objective. All patch-clamp experiments were performed at room temperature using ACSF as extracellular solution. The intracellular solution was K^+-gluconate based and contained the following (in mM): 125 K^+gluconate, 2 $MgCl_2$, 0.5 EGTA, 10 HEPES, 20 KCl, 3 NaCl; pH7.3, osmolality 280-290 mOsm/kg. For post-hoc morphological and immunohistochemical analyses Lucifer Yellow (0.1% final concentration, Sigma) or Alexa568 (0.02% final concentration, Invitrogen) was added to the intracellular solution.

Cells for patch clamp recordings were identified using the infrared differential interference contrast (IR DIC) microscopy. Patch clamp pipettes (Borosilicate glass, GB150F-8P, 0.86x1.50x80mm with filament, SCIENCE PRODUCTS GmbH) were pulled with a vertical puller (Narishige Model PC-10). The pipette resistance was between 5-7MΩ when filled with K^+-gluconate solution. The cells were hold at a holding potential (V_h) of -80mV using the amplifier EPC8 (Heka Intruments, Lambrecht/Pfalz, Germany). The holding potential was

corrected for the liquid junction potential (LJP) by offsetting the amplifier to -13mV before forming a gigaseal. The LJP was calculated with the help of the Liquid Junction Potential Calculator (JPCalcW, Peter H Barry, Dept of Physiology, School of Medical Sciences, University of New South Wales, Sydney, Australia & Axon Instruments, Inc. California, USA). Data were collected using the acquisition software 'Recording Artist' from Richard C. Gerkin (School of Life Sciences, Arizona State University, USA) for Igor Pro (WaveMetrics Inc., Lake Oswego, USA). Recorded cells were accepted for analyses and included into the dataset if the series resistance (R_{series}) was below 40 MΩ, the change of R_{series} during the experiment was smaller than 30%, and the offset change was not higher than ±5mV.

2.2.1. Electrophysiological identification of the different Schwann cell types

For these experiments K^+-gluconate based intracellular solution was used. A holding potential (V_h) of -80mV was used as starting point to apply different voltage step protocols. The first classification of Schwann cells was based on the properties of the total outward current and the voltage-independent leak current. To acquire these parameters 10 depolarizing steps from -80mV to 20mV with 10mV increment and with duration of 400ms were applied and analyzed.

Voltage-gated sodium channel

The expression of voltage-gated sodium channels was investigated with the help of TTX, a voltage-gated sodium channel blocker. Ten depolarizing steps from -80 to 20mV were applied with 10mV increment. The protocol after the bath application of 1µM TTX was subtracted from the protocol before the application. The remaining inward current represents the TTX-sensitive voltage-gated sodium current.

$Tau_{activation}$ was determined from the remaining inward current by fitting an exponential curve to the rising phase of the current evoked by the voltage-step to 10mV. The peak of the current was measured at 10mV.

Voltage-gated potassium channels

All experiments for detailed analyses of potassium channels were recorded in the presence of 1µM TTX and 100µM $CdCl_2$, to block voltage-gated sodium channels and calcium currents. Two different approaches were used to investigate the different channel expression: (1)

different pre-pulse protocols and (2) pharmacology. (1) Voltage-gated outward potassium channels were activated with two different pre-pulse protocols: (a) Pre-pulse to -110mV for 500ms followed by depolarizing steps from -80mV to 20mV with 10mV increment to activate all potassium currents; (b) Pre-pulse to -40mV for 500ms followed by depolarizing steps from -80mV to 20mV with 10mV increment to activate only the delayed rectifying potassium channels. (2) Two different potassium channels blockers, 4-Aminopyridine (4-AP, Sigma) and Tetraethylammonium chloride (TEA, Sigma), were applied to investigate voltage-gated potassium channels. 4-AP (5mM) was dissolved in the bath solution shortly before the experiment and TEA (25mM) was substituted for NaCl in the bath solution on an equimolar basis. The drugs were applied via the bath. Depolarizing steps from -80 to 20mV were applied before and after the drug application

To distinguish the presence of I_A type current the protocol with the pre-pulse to -40mV was subtracted from the protocol with the pre-pulse to -110mV. The remaining outward current represents the I_A-like current. The application of 4-AP was used as a second approach to distinguish the I_A-like current from the other voltage-gated potassium channels. The I_K- and I_D-like currents were investigated by the different pre-pulse protocols; in addition the application of 4-AP and TEA was used for separation.

Signals were low-pass filtered at 10kHz (7-pole Bessel -3dB) before digitization and sampled with a sampling rate of 20kHz (ITC-18, HEKA Instruments). Data were analyzed using a custom written macros for IGOR Pro. Series resistance (R_{series}) was evaluated from the transient current in response to a 10mV depolarizing step. The calculated R_{series} was between 15 and 40MΩ.

$$R_{series} = \frac{V}{I_{peak}}$$

Membrane resistance ($R_{membran}$) was computed as the difference between the total resistance, measured at the steady state current (350ms after the onset of the voltage-steps) in response to a 10mV depolarizing step, and the R_{series}.

$$R_{total} = \frac{V}{I_{steady\ state}} \qquad R_{membrane} = R_{total} - R_{series}$$

The leak current was estimated at the first 10mV step from the holding potential, assuming that no voltage-gated channels open at that potential. It was measured 350ms after the

onset of the voltage step. All depolarizing steps were offline leak subtracted. Therefore a template of the first depolarizing step to -70mV was produced with the help of an exponential fit. This template was later on used to subtract the leak current from the following depolarizing steps. Therefore the template was multiplied with a factor that corresponds to the applied voltage steps. From the leak subtracted traces the peak und steady state current for the voltage-gated sodium and potassium currents were evaluated. The peak current was defined as the maximum value reached during the first 20ms of the applied voltage step to 10mV. Furthermore the steady state or plateau current was determined as the current remaining after 350ms of the onset of the voltage step to 10mV. Mono-exponential or double-exponential fits to the rising phase of the curve were used to determine the activation time constants ($Tau_{activation}$) of the different sodium and potassium channels present in Schwann cells. Rise time was calculated as the time it takes for the current to rise from 20% to 80% of the maximum current.

2.2.2. PRESSURE APPLICATION

The fast pressure application was used to investigate the expression of functional neurotransmitter receptors at the different Schwann cell types. The neurotransmitter (1mM glutamate) was focally delivered to the cell through a glass pipette (opening: 3-4.5µm) with the help of the fast pressure-application system (PDES-01 AM, NPI Electronic Instruments). The pressure pipette was positioned 18–23µm away from the patched cell. The neurotransmitter was applied for 30ms with a pressure of 5psi. The interpulse interval between the different trials was 40s. All glutamate pressure-application experiments were performed in ACSF containing voltage-gated sodium channel antagonist (TTX, 1µM, Alomone labs), NMDA receptor antagonist (CPP, 10µM, Tocris), metabotropic receptor antagonist (LY341495, 50µM, Tocris), $GABA_A$ receptor antagonist (Picrotoxin, 100µM, Sigma), $GABA_B$ receptor antagonist (CGP55845, 5µM, Tocris), P2 purinergic receptor antagonist (PPADS, 30µM, Ascent Scientific), nicotinic ACh receptor antagonist (Mecamylamine, 50µM, Sigma), α7-containing nicotinic ACh receptor antagonist (MLA, 200nM, Sigma), metabotropic ACh receptor antagonist (Atropine, 10µM, Sigma), and the allosteric modulator of AMPA receptors (CTZ, 50µM, Ascent Scientific); otherwise it is stated in the text. To examine the presence of AMPA/kainate receptor GYKI53655 (30µM, Abcam) was applied via the bath. Philanthotoxin (10µM, Sigma) was used to investigate the presence of GluA2-receptors at the different Schwann cell types. The responses were low pass filter at 3kHz and recorded

with a sampling frequency of 20kHz (ITC-18, HEKA Instruments). Data recording and analyses were done with IGOR Pro and the acquisition software 'Recording Artist' from Richard C. Gerkin.

2.2.3. STIMULATION

Electrical stimulation was used to investigate the interaction between Schwann cells and axons in the peripheral nerve. Experiments for electrical stimulation were performed with K^+gluconate-based intracellular solution and in ACSF with or without increased calcium concentration to 2.5mM, as extracellular solution. The isolated pulse stimulator (A-M Systems, SCIENCE PRODUCTS GmbH, Hofheim, Germany) was used to evoke action potentials in the axons of the sciatic nerve slice. Different stimulation electrodes were used: bipolar stimulation electrodes (SCIENCE PRODUCTS GmbH) or monopolar glass stimulation electrodes (Borosilicate glass, SCIENCE PRODUCTS GmbH). Single or paired (with 40-100ms interpulse interval) rectangle pulses with different duration were applied every 15-45sec. Stimulus trains were applied each 1min (10 or 100 at 100Hz). The responses were low-pass filtered at 1kHz and digitized with 10 or 20Hz sampling frequency (ITC-18). Data recording and analyses were done with IGOR Pro and the acquisition software 'Recording Artist' from Richard C. Gerkin. All stimulation experiments were performed with NMDA receptor antagonist (CPP, 1µM) and the allosteric modulator (CTZ, 50mM) in the bath, otherwise it's stated in the text.

Extracellular stimulation

To evaluate the healthiness of the axons in the slice, the action potential propagation was investigated with the help of extracellular stimulation. A large axon bundle was electrical stimulated with the isolated pulse stimulator with the help of bipolar stimulation electrode on one side of the nerve. The compound action potential (CAP) was recorded with an extracellular electrode that was placed at the sciatic nerve ending of the opposing side.

2.3. MORPHOLOGY AND IMMUNOHISTOCHEMISTRY

During the electrophysiological recording the cells were filled with a fluorescent dye (Lucifer Yellow or Alexa568). Directly after the removal of the patch-pipette the slice with the filled cell was transferred in a Petri dish and fixed overnight at 4°C with 4% Paraformaldehyde (PFA, Roth) dissolved in phosphate buffered saline (PBS) containing the following (in mM): 267 NaCl, 4.3 Na_2HPO_4, 1.6 NaH_2PO_4; pH 7.4. Afterwards the slice was washed with PBS six times for 10min each at room temperature. In some cases additional staining for different cellular markers was performed, see section antibody staining. After the performed staining the slices were transferred to coated object slides (SuperFrost© Plus Objektträger, Langenbrinck) and dried for at least two hours (2h) before the slices were mounted with VECTASHIELD (VECTASHIELD Mounting medium, Linaris) and framed with clear nail polish.

2.3.1. ANTIBODY STAINING

Immunohistochemical stainings have been performed under two different conditions: (1) free-floating slices or (2) cryosections. (1) The 100µm free-floating slices were shortly before the start of the staining transferred in 24-well plates. All steps during the staining procedure were performed under permanent shaking. (2) A re-sectioning at the cryostat in thinner slices (20µm) was needed, to obtain a satisfactory staining result for some antibodies. In order to prevent slices obtained for cryosectioning from damages occurring during the freezing process they were incubated in 30% sucrose in PBS overnight at 4°C. Afterwards the slices were embedded in Tissue-Tek (Tissue-Tek® O.C.T.™ compound, Sakura) and immediately frozen at -150°C for at least 1h. Re-sectioning to 20µm slices was done at the cryostat (Leica, CM3050S) at around -20°C. Slices were dried for 2h and stored at -20°C. Shortly before the start of the staining, the object slides with the slices were defrosted. In order to reduce the amount of reagent needed, the slices were surrounded with pap pen (Invitrogen).

The following protocol was used for the cryosectioned and free-floating slices. At the beginning of the staining the slices were washed 4 times with PBS at room temperature for 10min. To reduce the background signal because of unspecific antibody binding and to increase the penetration potential of the antibody the slices were incubated in blocking solution for 2h at room temperature. The blocking solution contained: 10% fetal calf serum (FCS), 1% bovine serum albumin (BSA) and 0.3% Triton-X100 in PBS. Afterwards the primary

antibody was applied overnight at 4°C in blocking solution. At the next day the slices were washed with PBS 6 times for 10min each at room temperature. The secondary antibody was added in blocking solution at room temperature for 3h. The following washing step, 3 times for 10min in Tris-Buffered Saline (TBS) was performed at room temperature. TBS was containing the following (mM): 770 NaCl, 500 Sigma 7-9; pH 7.6. Nuclei were visualized with DAPI, which was applied for 5min diluted in TBS at room temperature. Subsequently the slices were washed with TBS 3 times each for 10min. In the last step of the staining protocol aqua bidest was shortly applied (1min) to reduce the formation of salt crystals during the drying process.

During all stainings a negative control was processed, the slices incubated only with the secondary antibody alone did not result in any staining. For double labeling experiments antibodies were applied sequentially, first the 1th primary antibody followed by the 1th secondary antibody; afterwards the 2th primary antibody and the 2th secondary antibody. Antibody details are summarized in table 2 and 3. The free-floating slices were transferred to coated object slides in aqua bidest and dried for at least 2h. The slices stained directly at the object slides were also dried for at least 2h. Afterwards the slices were mounted with VECTASHIELD and framed with clear nail polish.

Tab. 2 Primary antibodies

antigen	slice preparation	host Species	dilution	specificity of the marker	company
Sox10	cryosections	polyclonal rabbit	1:50	all Schwann cells	DCS Diagnostics
MBP	floating slices	monoclonal rat	1:250	myelinating Schwann cells	Abcam
GFAP	cryosections/ floating slices	polyclonal rabbit	1:250	Immature Schwann cells, non-myelinating Schwann	DAKO
IBA1	floating slices	polyclonal rabbit	1:500	activated and non-activated microglia/macrophages	Wako
CD68	floating slices	monoclonal rat	1:100	activated microglia/macrophages	Serotec
Neurofilament 200kDa	cryosections/ floating slices	polyclonal chicken	1:1000	axonal marker	Abcam
DAPI	cryosections/ floating slices	-	1:5000	nuclear counterstaining	Sigma

Tab. 3 Secondary antibodies

antibody	species	dilution	company
Alexa488	goat anti-rabbit	1:500	Invitrogen
Alexa488	anti-rat	1:500	Invitrogen
FITC	donkey anti-chicken	1:500	Dianova
Cy5	donkey anti-chicken	1:500	Dianova
Cy5	goat anti-rabbit	1:200	Biomol/Rockland
Biotin-SP-conjugated	goat anti-rat	1:200	Dianova
Streptavidin-Cy5		1:200	Biomol/Rockland

2.4. IMAGE ACQUISITION AND ANALYSES

All fluorescent images were acquired with the confocal laser scanning microscope (LSM710, Carl Zeiss Microscopy GmbH) and the acquisition software ZEN 2009 (Carl Zeiss Microscopy GmbH) using the Plan-Apochromat40x/1.3 oil immersion objective (Carl Zeiss Microscopy GmbH) and the EC Plan-Neofluor 10x/0.30 (Carl Zeiss Microscopy GmbH). The following parameters were used to image the different fluorochromes: (a) DAPI: excitation 405 (Diode 405-30) and emission bandpass 410-460nm; (b) Alexa488: excitation 488 (Argon), Multi-band pass filter (MBS) 488/561/633, emission bandpass 505-559nm; (c) Alexa568: excitation 561 (DPSS 561-10), MBS 488/561/633 and emission bandpass 585–632; (d) Alexa633: excitation: 633nm (HeNe633), MBP 488/561/633 and emission bandpass 664-688. The pinhole for multi-channel scans was adjusted to one airy unit of the longest wavelength. The optical section was determined by the pinhole size and was usually around 1µm. To evaluate colocalization between Schwann cell marker and filled cells, as well as for morphological analyses z-stack images were taken in half optical section intervals. The whole cell was imaged in a z-stack. The laser power was adjusted in the way that the brightest part of the cell (in most of the cases the soma) was not overexposed. To ensure that all small processes are scanned in some cases a second image was acquired where the intensity was increased. Negative controls were imaged with exactly the same parameters like the corresponding staining.

For morphological and co-localization analyses pictures were transferred to ImageJ and the BioVoxxel Toolbox. For morphological analyses the z-stack images were processed to a maximum projection. The total length of the cell, thickness of the processes, number of primary processes and number of branches were estimated. The total length of the cell was estimated as the distance between the endings of the two longest processes. The thickness of the processes was measured at a defined distance from the cell soma (20µm) (Fig. 2.2). All processes that originate directly from the soma were named and counted as primary processes. Dependent on the number of branches, the cell was classified in the following groups: (a) no branches, (b) up to 3 branches, (c) between 3-7 branches, (d) more than 7 branches (Fig. 2.2). Cells that are located on top of the slice or exhibit bubbles as a patch clamp or preparation artefact were excluded from the dataset. Data analysis and statistics were done with IBM SPSS Statistics (IBM, Armonk, New York). The normal distributions of the data were tested with the Shapiro-Wilk's test. Afterwards a parametric or non-parametric Levene's test was used to assess the equality of variances for a variable in the different groups. Dependent on the results of the pre-test we used analysis of variance (ANOVA; post-hoc test: tukey) or the Mann-Whitney U test to state the statistical significance. Data are shown in mean±SEM and the p values are presented in the text, figures or tables.

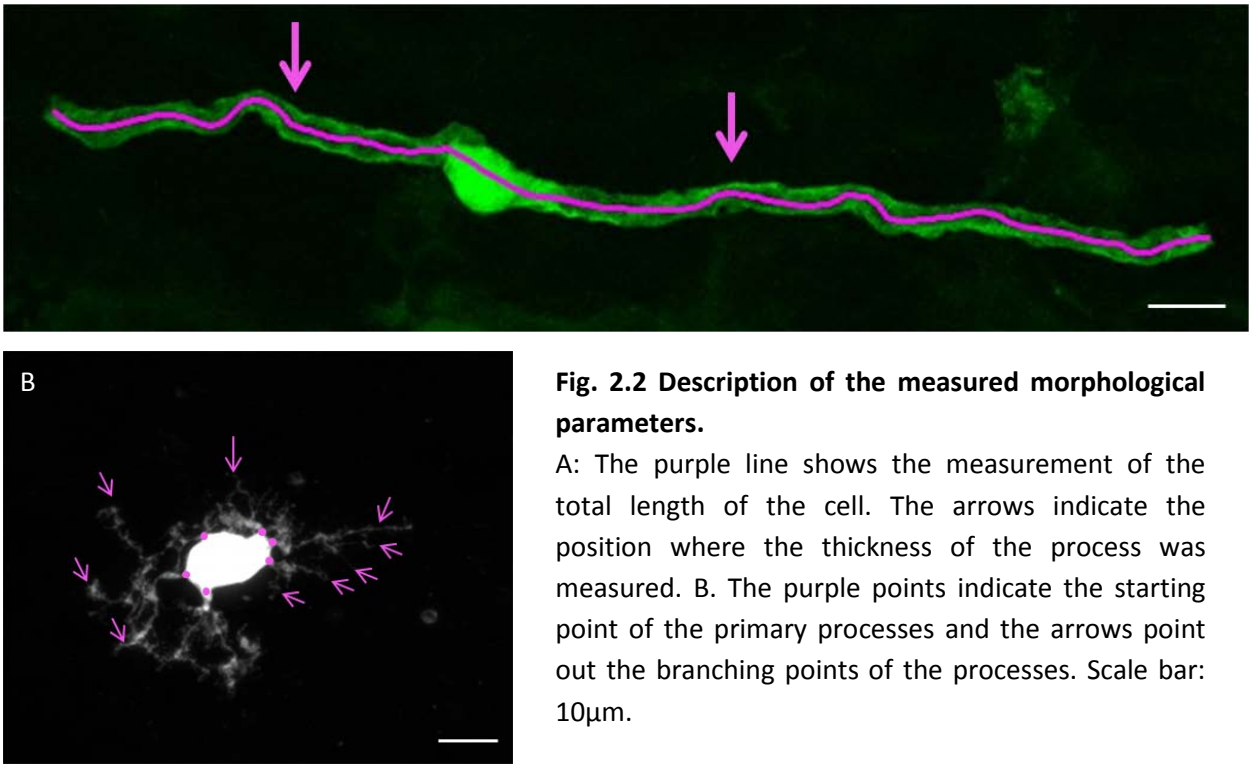

Fig. 2.2 Description of the measured morphological parameters.
A: The purple line shows the measurement of the total length of the cell. The arrows indicate the position where the thickness of the process was measured. B. The purple points indicate the starting point of the primary processes and the arrows point out the branching points of the processes. Scale bar: 10µm.

2.5. CELL COUNTING

The number of Sox10 and IBA1 positive cells was counted in slices in the different age groups. For this a 50x100µm counting window was included into a z-stack image in ImageJ (Fig. 2.3). To avoid a biased setting, the window was included before the channel of interest was switch on. At first all DAPI positive cells were counted in the window, cells that were touching the two boarders indicated in magenta were counted, cells that are in direct contact with the white boarders were excluded from counting (Fig. 2.3). In a second step the numbers of Sox10 or IBA1 positive cells were counted with the same procedure.

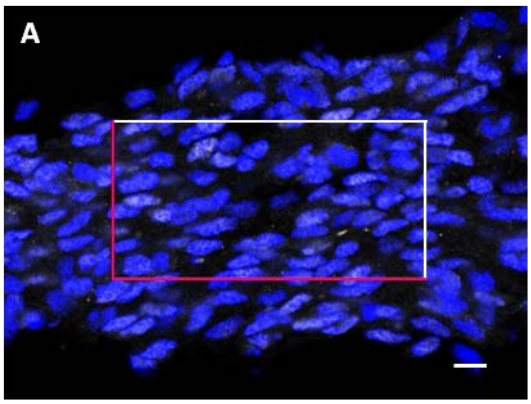

Fig. 2.3 Counting procedure in the sciatic nerve slice.
A: Image of a sciatic nerve slice with an included counting window (50x100µm). The different colored sides of the rectangle indicate the counted (magenta) and not counted (white) boarders of the counting window. Scale bar: 10µm.

3. RESULTS

3.1. PREPARATION

Most of the experiments in the Schwann cell research field are performed in more or less artificial systems, as already discussed in the introduction. Our aim was to investigate Schwann cell in a more natural surrounding therefore we developed a new preparation to produce slices from the sciatic nerve of a mouse for electrophysiological investigation and morphological characterization. The new preparation of these slices is in detail described in the methods part. In brief, sciatic nerve slices were freshly collected from embryonic and early postnatal animals and shortly after that embedded in low melting agarose. The embedding is needed to produce a cutting block for the vibratome and to allow the cutting of longitudinal slices from the nerve. The produced 100µm longitudinal slices of the sciatic nerve from embryonic and early postnatal animals, enables us to investigate the different properties of the Schwann cells in situ. Fig. 3.1 shows the typical appearance of the slices under the patch-clamp microscope with DIC optics. Under these conditions somata (Fig. 3.1 arrows) of Schwann cells and axons (Fig. 3.1 arrowhead) are without a doubt specifiable, therefore electrophysiological patch-clamp recordings from Schwann cells are feasible in this preparation.

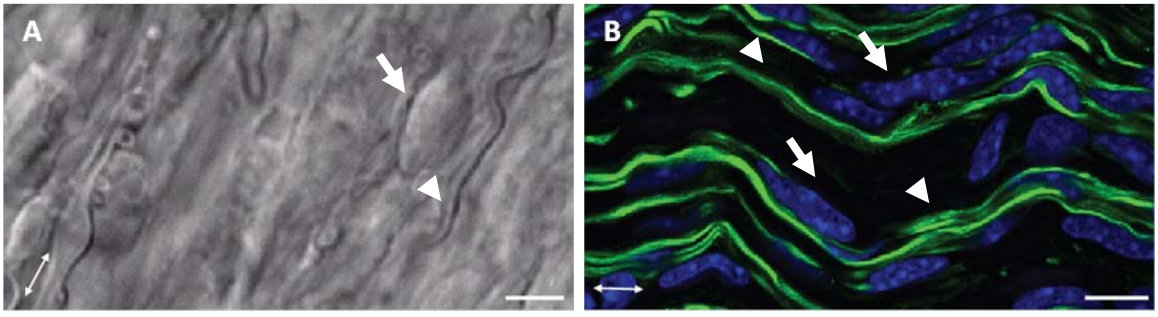

Fig. 3.1 Preparation of sciatic nerve slice from the mouse.
A: DIC picture of the 100µm slice from the sciatic nerve. B: Post-hoc immunohistochemical staining of a different slice with antibodies directed against Neurofilament 200kD (green) and Hoechst (blue). Arrows point towards somata and arrowheads point toward axons. Arrow with two arrowheads indicates the running direction of the axons. Scale bar: 10µm

We concentrated on two different age groups: embryonic day 16-18 (E16-18) and postnatal day 0–2 (P0-2). We considered these two age groups because of different reasons. The first and most important reason was that the development of the Schwann cell lineage starts

very early. As we were interested in all different types and developmental stages of the Schwann cell lineage, a preparation during the embryogenesis was necessary. Sciatic nerve preparation before E16 appeared to be difficult: the nerve was visible but its consistence was so fragile, that removal of the nerve was not possible without destructing the tissue structure. We were concerned that this destruction can affect the results of our electrophysiological and morphological characterization. For that reasons the first age group was determined to E16-18. In the age of E16 the sciatic nerve contains a mixture of Schwann cell precursors and their followers the immature Schwann cells. As the mature Schwann cells appear in the sciatic nerve around birth, the second investigated age group was defined between P0-2. The two age groups allow us to explore a wide range of different developmental stages in the Schwann cell lineage from early progenitors to the mature Schwann cell.

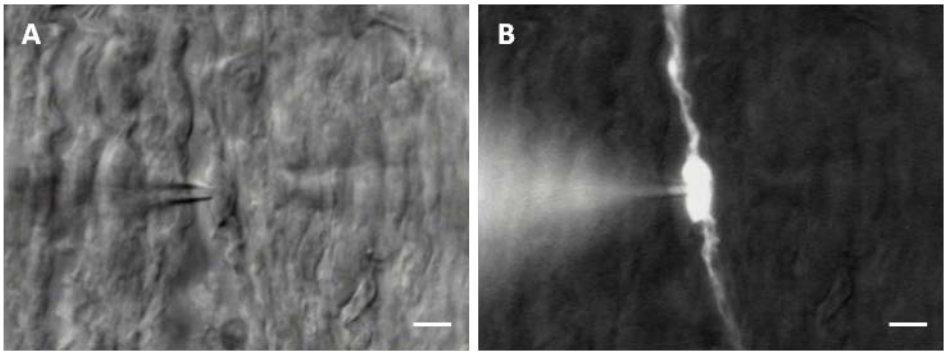

Fig. 3.2 Patch clamp recording of a Schwann cell in sciatic nerve slice.
A: Representative picture during a Schwann cell patch clamp recording under DIC optics. The patch pipette and the patched soma are clearly visible. B: The patched cell was during their recording filled with a fluorescent dye (in this case Alexa568). The picture was made shortly before the removal of the pipette. The filled soma of the patched cell with two filled processes is clearly visible. Scale bar: 10µm.

We used the propidium iodide (PI) staining in slices of the nerve to evaluate the proportion of dead cells. PI is membrane impermeant and excluded from healthy cells. It can only enter the nucleus and interact with the DNA by intercalating between the bases if the membrane is already perforated. We observed only a small number of PI positive cells in our nerve slices. Therefore we can conclude that the process of the sciatic nerve slice preparation, as well as the maintenance of the slices didn't destroy or induce death in large number of cells. The maintenance of the nerve morphology after the cutting procedure was proofed with the post-hoc staining of all nuclei with DAPI and for axons with Neurofilament NF-220. These staining demonstrated that the nerve was densely packed with nuclei and that the axons run

in parallel to each other through the nerve (Fig. 3.1). An immoderate destruction of the nerve tissue through the preparation could be ruled out.

In addition compound action potential (CAP) recordings were performed in different age groups to demonstrate the healthiness of the axons after the cutting process. The CAP is the summation of all individual evoked action potentials of the different axons in the nerve (Buchanan, Harper et al. 1996). The recorded CAP in the nerve preparation from E16-18 (n=2, Fig. 3.3) and adult (n=2, Fig. 3.3) mice illustrated the existence of intact axons in the 100µm slice of the sciatic nerve of the mouse. To confirm the dependence of the recorded CAP from voltage-gated sodium channels 1µM TTX was applied. The application completely abolished the CAP recorded in embryonic and adult sciatic nerve slices (Fig. 3.3, magenta traces). The CAP recordings illustrated the presence of axons that are able to propagate action potential over a long distance in the sciatic nerve slice and show thereby the healthiness of the axons after the cutting process.

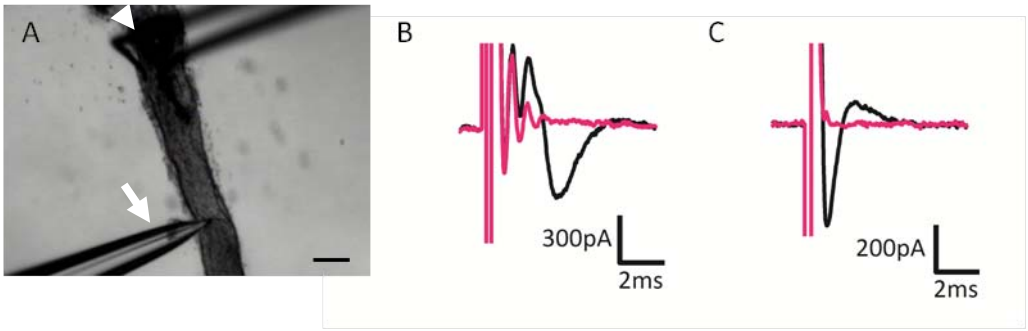

Fig. 3.3 Compound action potential recordings in the sciatic nerve slice.
A: DIC picture during the CAP recording. The recording pipette (arrow) and the bipolar stimulation electrode (arrowhead) are positioned at the opposing sides in the sciatic nerve slice. Scale bar 60µm. B-C: Averaged traces of the CAP before (black) and after TTX (magenta) application in sciatic nerve slices from E16-18 (B) and adult (C) animals.

We established a new preparation of sciatic nerve slices that enables us to investigate the electrophysiological and morphological properties of Schwann cells in their natural environment. Immunohistochemical stainings as well as compound action potential recordings demonstrate the feasibility of our preparation and the quality of our slices.

3.2. ELECTROPHYSIOLOGICAL CHARACTERIZATION OF SCHWANN CELLS IN THE MOUSE SCIATIC NERVE

The new established slice preparation of the mouse sciatic nerve allows us to perform whole-cell patch clamp recordings of Schwann cells in their intact surrounding. In the first step of our investigation we used a basic depolarizing voltage step protocol to characterize Schwann cells by the presence of voltage independent and voltage dependent channels.

Ten depolarizing voltage steps were applied from the holding potential (V_h) of -80mV to 20mV with 10mV increments. Using this protocol we could dependent from the age group distinguish up to four different cell types. We called these cells: Type 1, Type 2, Type 3 and Type 4 cells. Figure 3.4 shows the response of the different Schwann cell types to the depolarizing voltage steps.

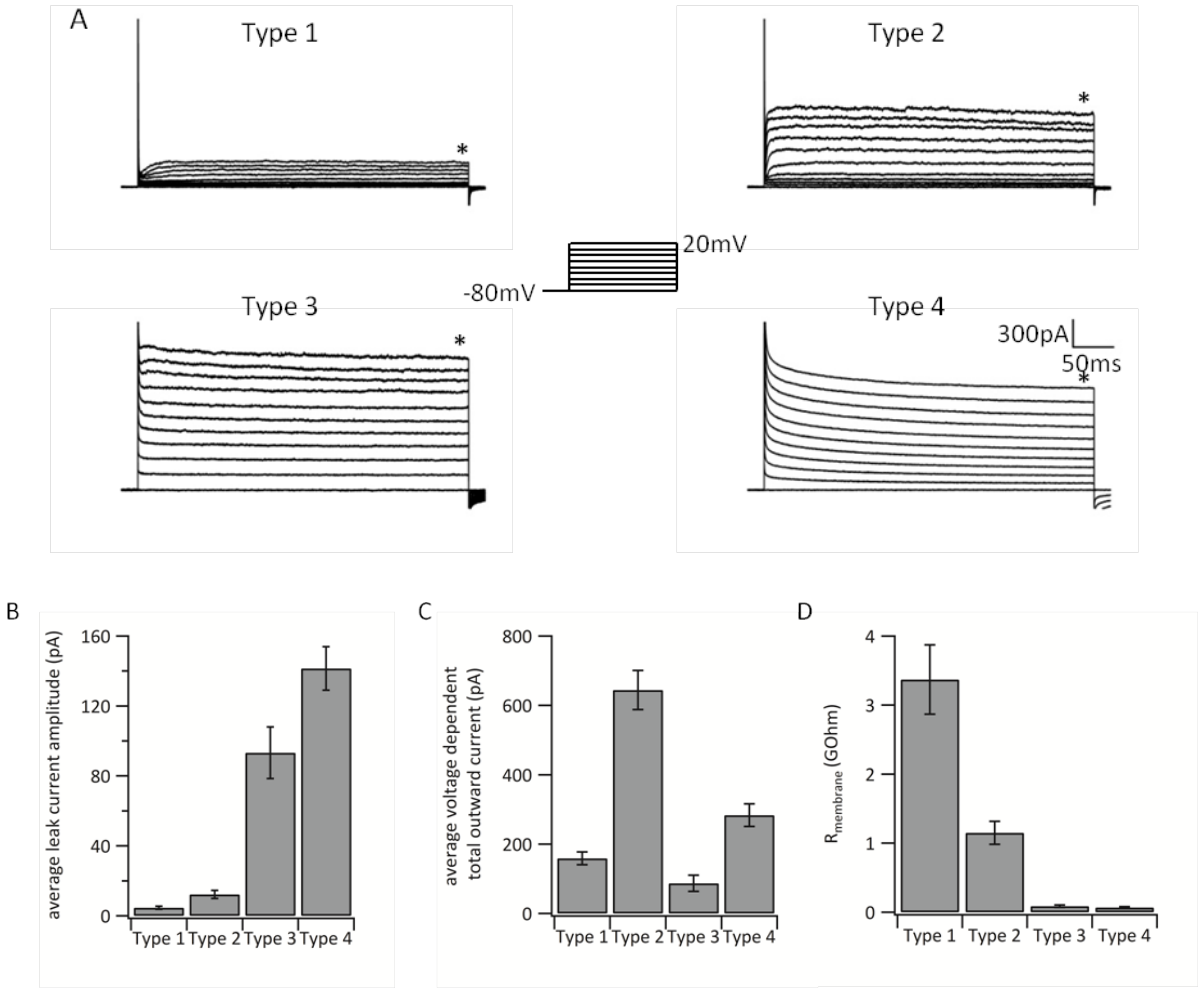

Fig. 3.4 Four electrophysiological different Schwann cells types.
Whole-cell voltage clamp recordings of responses to depolarizing voltage steps from -80mV to 20mV with 10 mV increment. Recordings were performed directly after the breaking into the cell. A: The raw traces showing current responses of Schwann cell of Type 1 to 4 to a series of depolarizing

voltage steps. The insert shows the applied voltage clamp protocol. B-D: Summary bar-graphs of the average amplitudes of the leak current (B), total voltage dependent outward current (C) and membrane resistance (D) of four different Schwann cell types studied. To estimate the leak current amplitude we used voltage step from -80mV (holding potential) to -70mV. The amplitude was measured at the time-point indicated by the star in part A. The total voltage dependent outward current amplitude was measured from the leak-subtracted voltage step from -80mV (holding potential) to +10mV. The amplitude was measured at the time-point indicated by the star in part A. Membrane resistance was calculated at -70mV. Data present in mean+/-SEM.

The applied depolarizing voltage step protocol from the holding potential of -80mV to 20mV with 10mV increments enables us to investigate the presence of the voltage independent leak current, voltage dependent outward current and the membrane resistance. To estimate the leak current amplitude we used the voltage step from the holding potential (-80mV) to -70mV. The amplitude was measured at the time-point indicated by a star in part A of Fig. 3.4. The voltage-dependent outward current was estimated from the leak subtracted voltage step from -80mV (holding potential) to +10mV. The amplitude was measured at the time-point indicated by a star in part A of Fig. 3.4. The procedure of the leak current subtraction and calculation of the leak current and voltage-dependent total outward current is in detail described in the methods part. To calculate the membrane resistance we used the voltage step from -80mV (holding potential) to -70mV. The detailed calculation for the membrane resistance is described in the methods part.

We assume that the majority of the voltage-dependent outward current is mediated by voltage-gated potassium channels. Nevertheless as we didn't used an antagonist for voltage-gated calcium and sodium channels in the bath, we cannot completely exclude that a proportion of the measured outward current is promoted by calcium and/or sodium channels. Voltage-gated sodium channels that opened during the depolarizing voltage steps show a fast rise and decay kinetic in neurons (Catterall 2000), oligodendrocyte precursor cells (Berger, Schnitzer et al. 1992, Steinhauser, Kressin et al. 1994) and Schwann cells (Shrager, Chiu et al. 1985). Also voltage-gated calcium currents recorded in cultured Schwann cells exhibit in the majority of cases a transient appearance (Amedee, Ellie et al. 1991). As we measure the total steady state voltage-dependent outward current 350ms after the onset of the voltage step a participation of fast inactivating sodium and calcium channels at the measured current could be almost completely ruled out.

We found that Schwann cells of Type 1 possess the smallest amplitude of voltage-independent leak current with 4.6±0.8pA (n=19) from all investigated Schwann cell types. Also Schwann cells of Type 2 revealed a small leak current amplitude with 12.2±2pA (n=16). In contrast to the previous types, Schwann cells of Type 3 display a much higher leak current amplitude with 93.3±15pA (n=6). The highest amplitude of the voltage-independent leak current could be observed in Schwann cells of Type 4 with an average leak current amplitude of 141.5±12pA (n=15).

The average voltage-dependent outward current amplitude that we detected for Type 1 Schwann cells in our study was 158.8±19pA (n=19). Schwann cells of Type 2 display the highest voltage-dependent outward current amplitude of all cells with 644.14±56pA (n=16), whereas Schwann cells of Type 3 and 4 show a much smaller amplitude. The smallest amplitude of the voltage-dependent outward current was exhibited by Schwann cells of Type 3 with 86.95±23pA (n=5). Compared to high leak current of Type 4 cell, the average amplitude of the total voltage-dependent outward current was with 283.73±32pA (n=12) relatively small.

The last parameter that we want to discuss in the first part of the electrophysiological investigation was the membrane resistance. We showed that Schwann cells of Type 1 exhibit by far the highest membrane resistance with 3.37±0.5GΩ (n=20) of all investigated Schwann cell types. The membrane resistance of Type 2 Schwann cells was with 1.15±0.2GΩ (n=20) approximately three times smaller than that of Type 1 cells. Schwann cells of Type 3 and Type 4 show both a small membrane resistance with 89.1±16MΩ (n=7) and 69±12MΩ (n=19) respectively.

The table 4 summarizes the values of the averaged voltage-independent leak current, the average total voltage-dependent outward current and the membrane resistance, in addition the statistical parameters are included.

Tab. 4 Summary table of the four electrophysiological different Schwann cell types.

	n	leak current (pA)	n	total voltage dependent outward current (pA)	n	$R_{membrane}$ (GΩ)
Schwann cell type						
Type 1	19	4.62±0.9pA	19	158.82±19	20	3.37±0,5
Type 2	16	12.26±2.3	16	664.14±56	20	1.15±0,2
Type 3	6	93.3±15	5	86.9±23	7	0.08±0,01
Type 4	15	141.5±12	12	283.7±32	19	0.06±0,01
Statistical analyses						
Type 1 versus 2		p<0.001		p<0.001		NS
Type 1 versus 3		p<0.001		NS		p<0.001
Type 1 versus 4		p<0.001		p<0.001		p<0.001
Type 2 versus 3		p<0.001		p<0.001		p<0.001
Type 2 versus 4		p<0.001		p<0.001		p<0.001
Type 3 versus 4		NS		p<0.001		NS

NS: not significant

In summary Schwann cells of Type 1 displayed the lowest amplitude of the voltage-independent leak current, whereas Type 2 cells possess the highest amplitude of the voltage-dependent total outward current of all Schwann cell types. Both cell types possess a relative high membrane resistance with >1GΩ in comparison to the two remaining types. Type 3 and Type 4 cells exhibit high amplitude of the voltage-independent leak current. The lowest average amplitude of the voltage-dependent steady-state outward current was measured in Type 3 cells. The first electrophysiological analyses of Schwann cell in the mouse sciatic nerve show, that we can clearly distinguish four electrophysiological different Schwann cell types. A more detailed analysis of the expressed voltage-dependent potassium and sodium channels follows in a next chapter.

Tab. 5 Distribution of the four Schwann cell types in the two age groups

	Type 1	Type 2	Type 3	Type 4
E16 – 18	**+**	**+**	**-**	**-**
P0 – 2	**+**	**+**	**+**	**+**

Distribution of the electrophysiological different Schwann cell types in the two investigated age groups. '+' means that the cell type was present and '–' means that the cell type was not present in this age group.

We studied the distribution of the different Schwann cell types in the two investigated age groups of mice: E16-18 and P0-2. Schwann cell of Type 1 and 2 could be found in both age groups, whereas Schwann cells of Type 3 and 4 could be only found in the older, more

developed age group of P0-2 mice (Tab. 5). We therefore think that Schwann cell of Type 3 and 4 seem to be more developed cell types in the Schwann cell lineage.

Schwann cells of Type 3 are only very rarely investigated during this study. The probability to patch this type was during the whole study relatively low. There could be different reasons for this problem. One reason could be that this cell type was particularly sensitive to the destruction during the preparation process. We can almost completely rule out this possibility because of the low number of cells positive for the PI staining. Another possible explanation is that only a few cells of this specific type are present in the age groups that were investigated in our study. Some developmental stages of the Schwann cell lineage appear in the sciatic nerve after birth (e.g. myelinating and non-myelinating Schwann cells). Therefore the described type might be only rarely present in the investigated age group. For the explained reasons it was not always possible to patch enough cells for a statistical analyses, nevertheless I will present the data of these Schwann cell type.

In summary, the first patch clamp experiments performed in sciatic nerve slices exhibit the presence of four electrophysiological different Schwann cell types. We could show that the four types can be distinguished by the voltage-independent leak current, the voltage-dependent total outward and the membrane resistance. The investigation of the distribution of the cell types in the two age groups shows that Schwann cell of Type 1 and 2 are present in both age groups whereas Schwann cell Type 3 and 4 are only present in the older age group.

3.3. Investigation of voltage-gated channels in the different Schwann cell types.

In the previous part the total voltage-dependent outward current and the leak current were reviewed. In the following section we want to take a closer look at the voltage-gated sodium and potassium channels that are present in the different Schwann cell types. Voltage-gated sodium and calcium channels are an important pathway for sodium and calcium ions entry, which are known to mediate several cellular functions (e.g. neurotransmitter release, hormone secretion, gene expression).

3.3.1. *VOLTAGE-GATED SODIUM CHANNELS*

Upon visual inspection of the depolarizing voltage steps a small inward current was only visible in Type 2 Schwann cells. To further investigate the presence of voltage-gated sodium channels in Schwann cells of Type 2 we applied 1µM TTX, to specifically inhibit voltage-dependent sodium channels. Depolarizing voltage steps from -80mV to 20mV with 10mV increment before and after the drug application were applied. To identify the currents blocked by the antagonist, the traces under the different conditions were subtracted from each other.

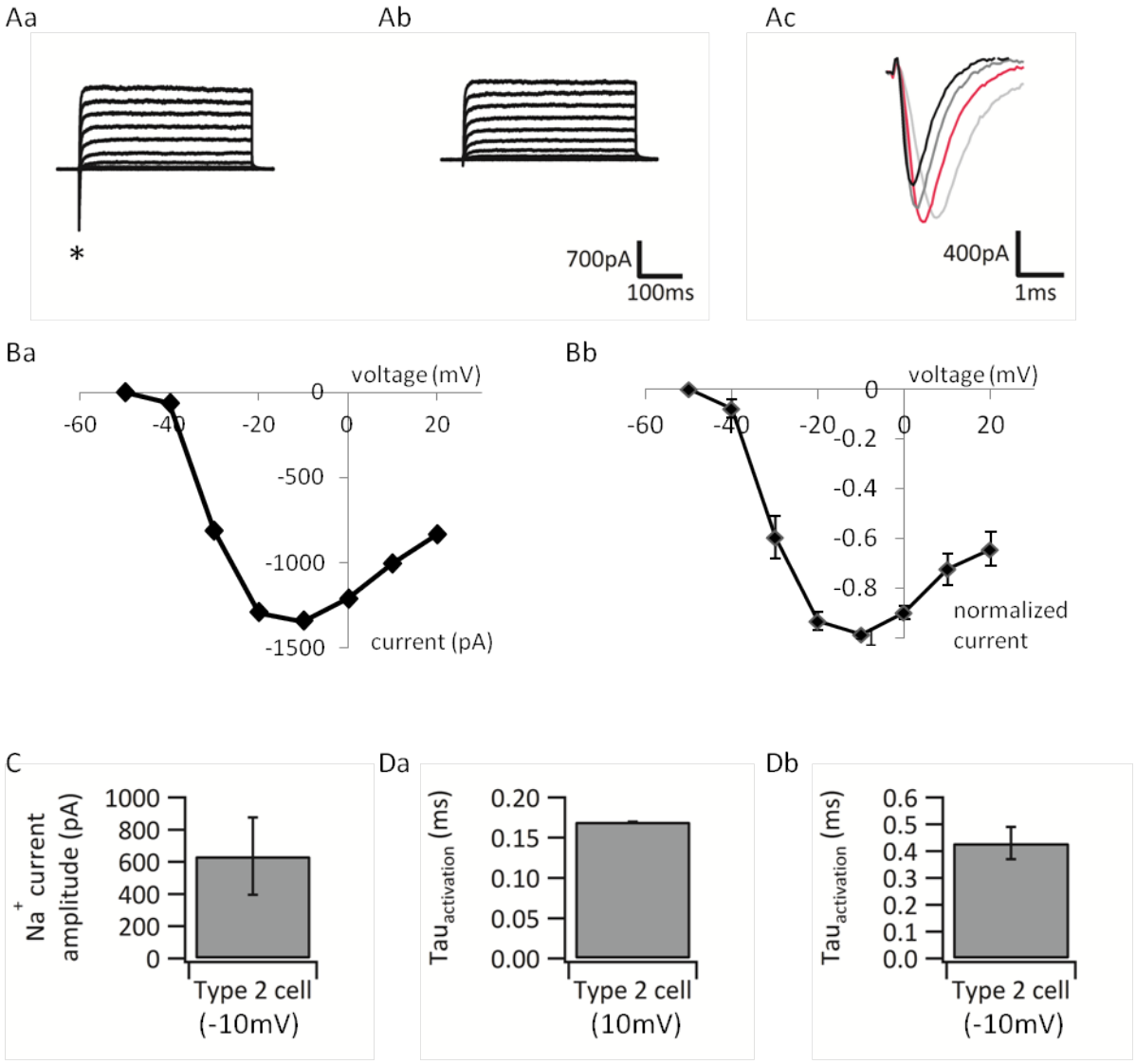

Fig. 3.5 Schwann Cells of Type 2 express voltage-gated sodium channels.
A: Leak subtracted example traces showing currents recorded in Type 2 Schwann cells before (Aa) and after (Ab) the application of TTX (1µM) upon a series of depolarizing voltage steps. The star indicates the inward sodium current. Ac: Leak subtracted example traces at +10 (black), 0 (dark grey), -10mV (magenta) and -20mV (light grey) indicate TTX-sensitive fast inward current. Ba: I-V

relationship of the voltage-gated sodium current showed in A. Bb: Normalized I-V relationship of the voltage-gated sodium current that represents five different experiments. C: Bar graph of the average TTX-sensitive current amplitude activated upon a depolarizing voltage step to -10mV (n=5). D: Bar graph of the averaged rise time of the fast inward current in Type 2 cells activated upon a depolarizing voltage step to +10mV (n=5, Da) and -10mV (n=5, Db). Data presented in mean±SEM.

These experiments demonstrate that under these conditions 5 out of 7 Schwann cells of Type 2 (71%) express a voltage-dependent inward current. Fig. 3.5 shows the typical fast transient inward current triggered by depolarizing the membrane potential. During the series of depolarizing voltage steps the current was detectable at a voltage step to the membrane potential of approximately -40mV and peaked at a membrane potential of -10/-20mV. The sodium current amplitude varied between cells and was between 133 and 1341pA; the average peak current amplitude upon a depolarizing voltage step to -10mV was 635.5±240pA. The time constant characterizing the activation kinetics of sodium channels was derived from fitting a single exponential to the rise of the sodium current. With increasing depolarization the activation time of the sodium current becomes faster. The evoked fast inward sodium current had an averaged activation time constant ($Tau_{activation}$) of 430±60µs (n=5) upon a depolarizing voltage step to -10mV and 170±10µs (n=5) upon a depolarizing voltage step to +10mV (Fig. 3.5). Thus the recorded fast transient current, shows the typical properties of voltage-gated transient sodium currents recorded in neurons (Patlak 1991). Electrophysiological recordings in neurons showed dependent from the species an activation time constant in the range of 100-200µs at a depolarizing voltage step to +10mV (Gilly, Gillette et al. 1997). Comparisons with older experiments performed in cultured rabbit Schwann cells reported with approximately 800µs time-to-peak (Howe and Ritchie 1990) a slower rise time. One possible reason for this discrepancy could be the described changes of kinetic properties under cultural conditions. Further details will be discussed in the discussion part.

In a second step we exposed Schwann cell of Type 2 to 1µM TTX, a specific voltage-gated sodium channels antagonist, and to 100µM $CdCl_2$, an antagonist of voltage-gated calcium channels. We applied depolarizing voltage steps from -80mV to 20mV with 10mV increment before and after the drug application. To identify the currents blocked by these two antagonists, the traces under the different conditions were subtracted from each other. We compared the activation time ($Tau_{activation}$) and the peak current amplitude of the two

different conditions (only 1µM TTX or 1µM TTX and 100µM $CdCl_2$) in Type 2 Schwann cells (Fig. 3.6).

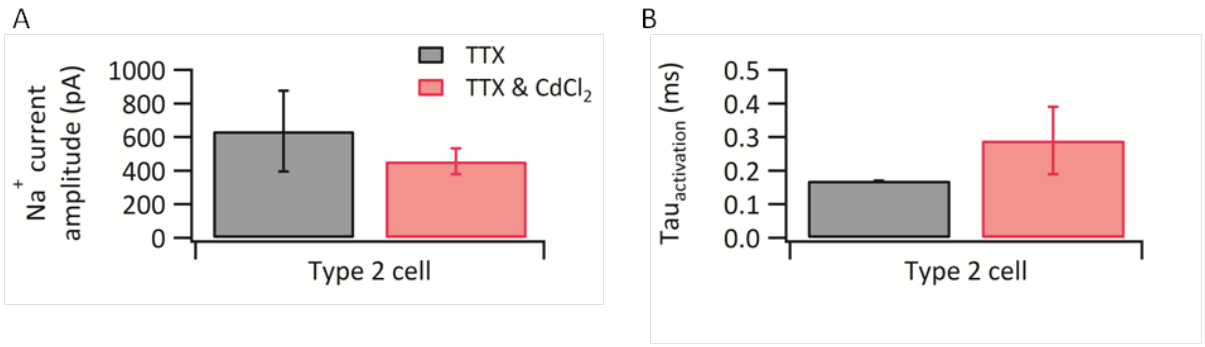

Fig. 3.6 Comparison of the current amplitude and activation time under two different conditions of Type 2 Schwann cells. A: Comparison of the peak current amplitude after the application of TTX (n=5; grey) or TTX and $CaCl_2$ (n=7; magenta) in Type 2 Schwann cells. B: Comparison of the activation time of the fast transient inward current after the application of TTX (n=5, grey) or TTX and $CdCl_2$ (n=6, magenta). Data present as mean±SEM.

The comparison of the peak current amplitude blocked by TTX alone or by TTX and $CdCl_2$ from Type 2 Schwann cells showed no significant difference (t-test: $p>0.05$), which indicated that there are no additional channels expressed, which are blocked solely by $CdCl_2$. The activation time ($Tau_{activation}$) is under the TTX and $CdCl_2$ conditions slower, but the difference is as well not statistical significant (t-test; $p>0.05$). Nevertheless, the slower activation time of the channels blocked by TTX and $CdCl_2$ might indicate an expression of small proportion of calcium channels blocked by $CdCl_2$ which is not sufficient to induce a significant difference. Further experiments could be performed with elevated extracellular barium substituted for calcium, which may amplify the calcium mediated current (Sontheimer 1994).

Experiments with TTX and $CdCl_2$ in the bath were performed and analyses as describe above in Type 1 (n=9), Type 3 (n=2) and Type 4 (n=3) Schwann cells. The three different Schwann cells types exhibit no fast transient inward current that was blocked by TTX or $CdCl_2$. We therefore conclude that Type 1, 3 and 4 express no voltage-gated sodium and calcium channels. In contrast 7 out of 11 Type 2 Schwann cells (64%) revealed an inward current that was blocked by our two drugs.

In conclusion, Schwann cells of Type 2 posses TTX-sensitive voltage-dependent sodium channels. First investigations show comparable kinetics with sodium channels in the CNS and

in Schwann cells. In contrast Type 1, 3 and 4 Schwann cells do not exhibit voltage-gated sodium and calcium channels.

3.3.2. Ca^2-INDEPENDENT VOLTAGE-GATED POTASSIUM CHANNELS

The first investigation of the different Schwann cells types was done without any inhibitor in the bath solution. As voltage-gated potassium channels seems to play an important role not only for the action potential propagation in neurons but also for the regulation of different physiological processes (e.g. proliferation in glial cells) (Konishi 1989), we wanted to investigate the presence of these channels in the different Schwann cells types in the sciatic nerve slice. To isolate the proportion of the voltage-gated potassium current from the total voltage-gated outward current, we used TTX and $CdCl_2$ to block the participation of voltage-gated sodium and calcium channels.

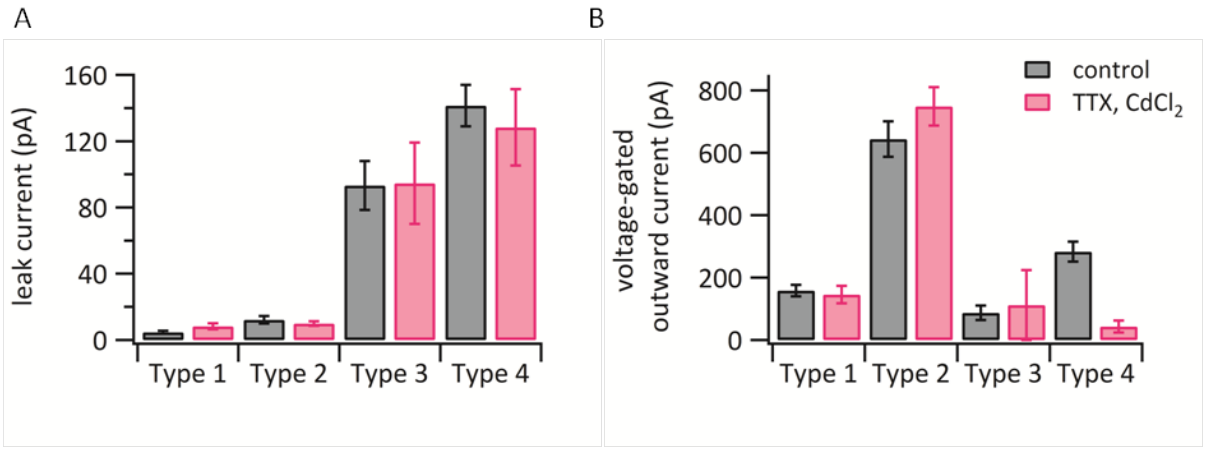

Fig. 3.7 Comparison of the leak current and the voltage-gated outward current after the application of TTX and $CdCl_2$.

A: Comparison of the leak current estimated as described before with (magenta) and without (black) 1µM TTX and 100µM $CdCl_2$ in the bath. B: Summary bar graph of the total voltage-gated outward current (black) and the Ca^{2+}-independent voltage-gated outward potassium current (magenta) in the different Schwann cell types. The majority of the voltage-gated outward current is mediated by Ca^{2+}-independent voltage-gated potassium channels. Data present as mean±SEM.

We first wanted to estimate the difference between the total voltage-dependent outward steady state current, obtained without TTX and $CdCl_2$ in the bath, and the outward voltage-gated potassium current, acquired with both drugs in the bath. We applied depolarizing voltage steps from the holding potential of -80mV to 20mV with 10mV increment and subtracted the condition with the two drugs in the bath from the control condition. The steady state current was evaluated approximately 350ms after the start of the voltage step from the holding potential to +10mV from the subtracted traces. The steady state current

amplitude was selected as the parameter to compare, because under control conditions the possible presence of fast transient voltage-gated sodium channels would interfere with the peak current amplitude and influence the measurements. The comparison shows that there is no difference between the two steady state voltage-dependent currents in Type 1 (n=11), Type 2 (n=22) and Type 3 (n=2) cells (Fig. 3.7). The majority of the steady state voltage-dependent current that is activated by depolarizing voltage steps are originating from Ca^{2+}-independent voltage-gated potassium channels. Type 2 cells clearly exhibit the highest voltage-gated steady state potassium current of all four subtypes with an average steady state current amplitude of 749.38±62pA (n=22). A much smaller steady state current amplitude was evaluated in Type 1 Schwann cells with an average voltage-dependent steady state current amplitude of 145.82±28pA (n=11) and in Type 3 Schwann cells with 112.13±112pA (n=2). Schwann cells of Type 4 seem to be an exception; they display a distinct difference between the average voltage-dependent total outward current and the voltage-gated outward potassium current. Under control condition (without TTX and $CdCl_2$ in the bath) the total voltage-dependent steady state outward current was in average 283.73±32pA (n=12), whereas with the two blocker in the bath the isolated average voltage-dependent steady state potassium current was only 57.55±18pA (n=3). One possible explanation for this effect might be the relatively small n number for the average voltage-dependent outward potassium current. The n number of the experiments performed without TTX and $CdCl_2$ is much higher with 12 experiments. In addition the variation within the group of Type 4 Schwann cells under the conditions with TTX and $CdCl_2$ in the bath was high. The steady state amplitude of the voltage-gated potassium current varied between 0 and 91pA. The low n number in combination with the high variety in the estimated values may cause the difference between the total steady state voltage-dependent outward current and the steady state voltage-dependent potassium current. Nevertheless it might be possible that the majority of the steady state voltage-dependent outward current is mediated by channels which are sensitive to TTX and $CdCl_2$.

In summary, we showed that the majority of the voltage-gated steady state outward currents are mediated by the isolated voltage-dependent steady state potassium currents in Schwann cells of Type 1, Type 2 and Type 3. Only Schwann cells of Type 4 exhibit a high total voltage-gated outward current and a smaller voltage-dependent potassium current isolated in the presence of blockers for voltage-gated sodium (TTX) and calcium channels ($CdCl_2$).

Upon visual inspection we recognized, that dependent from the Schwann cell types, the voltage-gated outward potassium currents seem to differ in their kinetics and as well in their peak and steady state current amplitudes. We therefore decided to investigate the voltage-gated potassium currents more in detail. We hypothesized that the different Schwann cells types vary in their expression of I_A, I_D and I_K currents. To investigate the differences we used two different approaches: (1) electrophysiological and (2) pharmacological approach.

3.3.2.1. Fast and transient voltage-gated Ca^{2+}-independent potassium currents

Electrophysiological approach

We first used the electrophysiological approach to test whether the different Schwann cell types express A-type potassium channels. To isolate this current, we applied two different voltage steps paradigms. During the first paradigm a pre-pulse to -110mV for 500ms was directly before the depolarizing voltages steps with a length of 400ms applied. Directly after the applied pre-pulse, the depolarizing voltage steps start from -80mV to 20mV with 10mV increment. This protocol leads to an activation of all voltage-gated potassium channels expressed by the investigated cell. The second voltage steps paradigm was applied with a pre-pulse to -40mV for 500ms directly before the depolarizing voltage steps with a length of 400ms. Directly after the applied pre-pulse, the depolarizing voltage steps start from -80mV to 20mV with 10mV increment. The second paradigm selectively inactivates the channels mediating the I_A potassium current. The subtraction of the second paradigm with a pre-pulse to -40mV from the first paradigm with a pre-pulse to -110mV, at the corresponding voltages, exposes the hidden I_A current.

We applied the two pre-pulse voltage steps paradigms to Type 1 and Type 2 cells to uncover the existence of I_A currents in this cell types. We decided to investigate only these two Schwann cells types because of the lower total steady state voltage-dependent outward current expressed by Type 3 and 4 Schwann cells. The majority of channels expressed by Type 3 and Type 4 Schwann cells are voltage-independent leak channels.

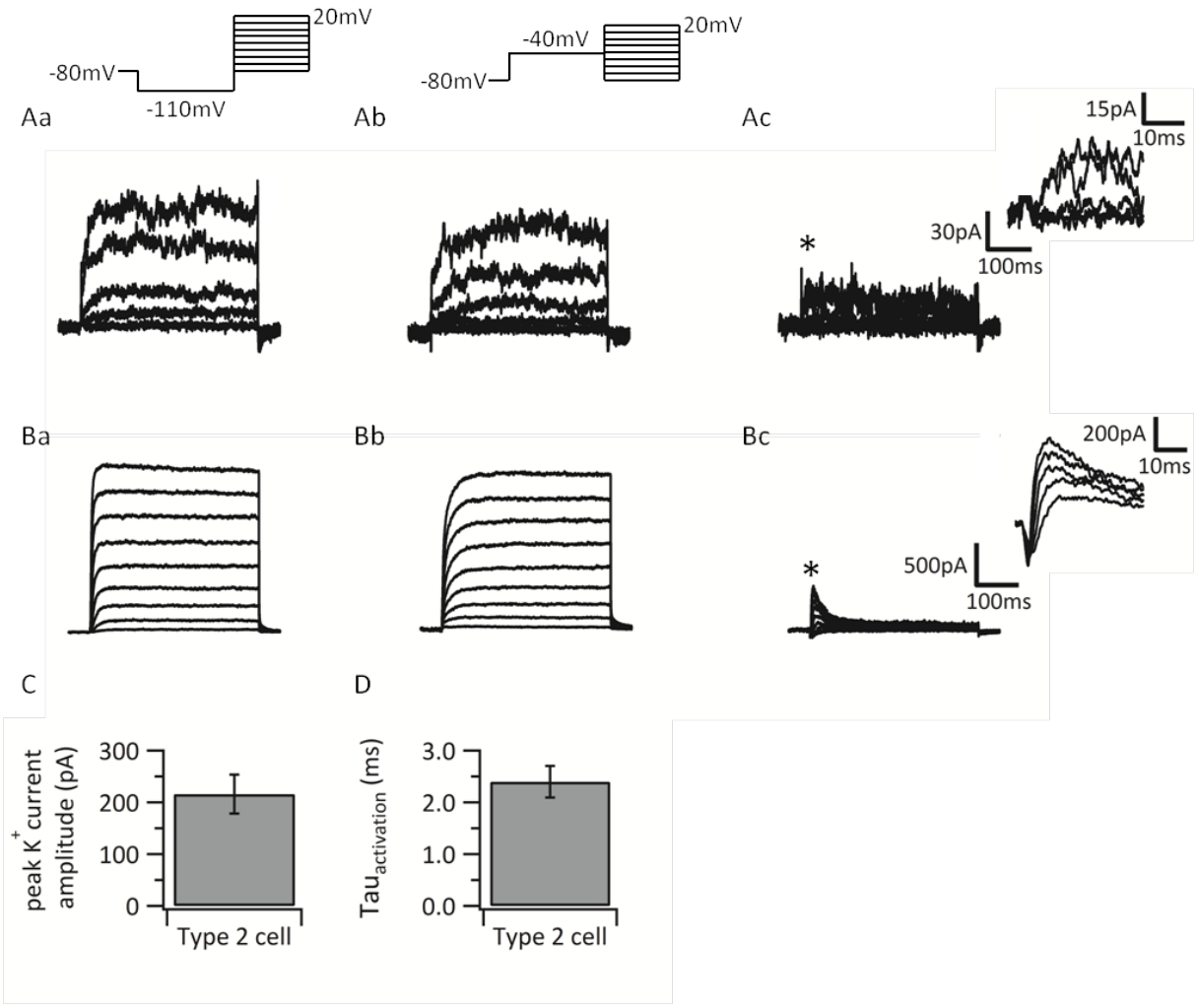

Fig. 3.8 Schwann cells differ in the kinetic and amplitude of the fast and transient potassium currents uncovered by the application of different pre-pulse protocols.

A-B: Leak subtracted example traces showing outward currents recorded in Type 1 (A) and Type 2 (B) Schwann cells upon a series of depolarizing steps preceded by a pre-pulse to -110mV (Aa, Ba) and to -40mV for 500ms (Ab,Bb). For clarity reasons only each second voltage step (the voltage steps from the holding potential of -80mV to -60, -40, -20, 0 and 20) in Type 1 cells is presented. Ac-Bc: Currents obtained after the subtraction shown in Ab from those in Aa, and traces shown in Bb from those in Ba. The insert shows the expanded traces at the position indicated with the star in the original trace. C: Summary bar graph showing the average peak current amplitude from Type 2 Schwann cells at the voltage steps to +10mV. D: Summary bar graph showing the $Tau_{activation}$ from the fast potassium current in Type 2 Schwann cells obtained from an exponential fit to the rising phase of the current at the voltage step to +10mV.

The voltage step paradigms performed in Type 1 cells (n=4) showed that these cells do not express voltage-gated potassium channels with a fast and transient kinetic. In contrast 12 out of 15 Type 2 cells (80%) showed an I_A-like current. The average peak current amplitude measured at +10mV was 216±37pA (n=12). The mean time constant of activation

($Tau_{activation}$) of I_A–like current at a voltage step to +10mV in Type 2 cells was 2.4±0.3ms (n=11).

Schwann cells diver not only in the expression of voltage-gated sodium channels, they also seem to differ in the expression of the fast and transient voltage-dependent potassium channels. Our experiments show that Type 2 cells express fast and transient potassium channels, with kinetic properties comparable with other studies performed in Schwann cells, glial cells or neurons. Furthermore Schwann cells of Type 1 seem to express no fast and transient potassium currents.

Pharmacological approach

Another option to investigate the presence of I_A-like voltage-gated potassium channels in the different Schwann cell types is the specific blockage of the channel by an inhibitor. A potent blocker described in the literature is 4-Aminopyridine (4-AP). It is established that it is blocking dependent from the concentration I_A-like potassium currents (high concentration of 4-AP, 5mM) and in addition also I_D-like currents (low concentration, 50µm) (Storm 1990, Beck, Ficker et al. 1992, Albert and Nerbonne 1995, Locke and Nerbonne 1997). Our recordings clearly show that the large I_D-like voltage-gated potassium current expressed by Schwann cells of Type 2 superpose the fast and transient voltage-dependent I_A-like current (Fig. 3.8) in the subtracted traces. The same effect is affecting the results of Type 1 Schwann cells. Therefore analyses of the kinetic and the amplitude of the I_A-like voltage-gated potassium current are not possible, because of the large I_D-like voltage-gated potassium current blocked as well by 4-AP. Nevertheless our recordings show the blockage of the I_A-like potassium current in Type 2 Schwann cells by 4-AP.

3.3.2.2. Sustained Ca^{2+}-independent voltage-gated potassium channels

After the investigation of the fast and transient voltage-dependent potassium current in the previous chapter, we next wanted to analyze the presence of sustained Ca^{2+}-independent voltage-gated potassium channels. This group can be divided into two sub-groups: the fast (I_D) and the slow (I_K) activating outward sustained potassium currents (Storm 1990, Albert and Nerbonne 1995, Locke and Nerbonne 1997). We used two approaches to investigate these currents: (1) electrophysiological and (2) pharmacological.

Electrophysiological approach

First we applied a series of depolarizing voltage steps; starting from the holding potential of -80mV to +20mV with an increment of 10mV in Type 1 and Type 2 Schwann cells. The investigation of voltage-dependent sustained potassium currents was only performed in Type 1 and Type 2 Schwann cells, as the other two types, Schwann cells of Type 3 and 4, express only a small amount of voltage-gated potassium channels. In the case of Type 1 cells we used the depolarizing voltage step protocol without any pre-pulse paradigm to activate the sustained voltage-gated outward potassium currents and calculate the kinetics of the activated currents. As shown in the previous part, this cell type doesn't express I_A currents that would affect the kinetics of the sustained currents. As we used the rising phase of the current to measure the mean activation time ($Tau_{activation}$) of the sustained currents, an additional activation of the fast and transient voltage-gated I_A-like current would overlay with the rising phase of the sustained currents and modify the activation time. Therefore we used the depolarizing voltage step protocol with a pre-pulse paradigm in Type 2 Schwann cells. A pre-pulse to - 40mV for 500 ms was applied directly before the depolarizing voltage steps. The pre-pulse applied during that paradigm is selectively inactivating the I_A-like voltage-gated potassium current. Thereby an influence of the fast and transient I_A-like current at the activation kinetic of the sustained voltage-gated outward currents can be excluded.

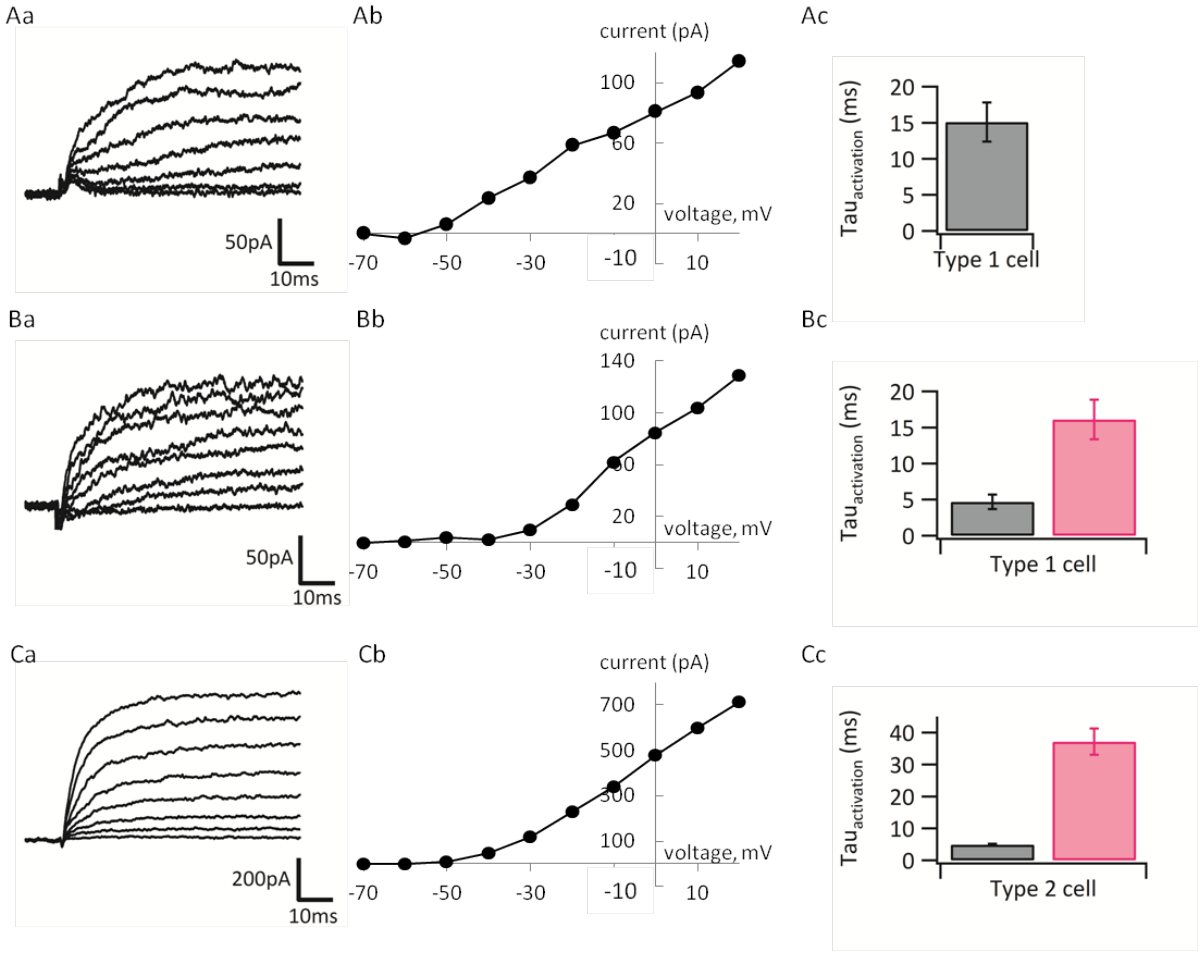

Fig. 3.9 Schwann cells in the sciatic nerve slices express potassium channels mediating sustained voltage-gated potassium currents.
Aa, Ba: Leak subtracted example traces showing sustained currents in two different subgroups of Type 1 Schwann cells (Aa, Ba) upon a series of depolarizing voltage steps starting from the holding potential of -80mV to 20mV with 10mV increment. Ca: Leak subtracted example traces from the depolarizing voltage step protocol with a pre-pulse paradigm to -40mV for 500ms from a representative Type 2 cell. Ab, Bb, Cb: Steady state amplitude of the voltage-dependent potassium current at the different applied potentials shown in part Aa, Ba and Ca of the figure. Ca-Cc: Summary bar graph of the activation time constants determined by mono (Ac) or double exponential (Bc, Cc) fit from the rising phase upon a depolarizing voltage step from -80mV to +10mV. Data present in mean±SEM.

For each cell we performed leak subtraction as described in Material and Methods. We then studied the activation kinetic of the sustained outward potassium currents, as well as their amplitude.

In Type 1 Schwann cells measurable steady state outward potassium current was detected during the depolarizing voltage steps to potentials more positive than -40mV (n=11). Fitting an exponential function to the rising phase of the current showed that in approximately half of the Type 1 cells (5 out of 11) the current was well fitted with a single exponential (Fig.

3.9). The time constant of activation ($Tau_{activation}$) at the voltage step to +10mV was 15.1±3ms. In the remaining cells (6 out of 11) the activation phase of the current could by well fitted with a double exponential fit. The $Tau_{activation}$ measured at depolarizing voltage steps to +10mV were: 4.7±1ms and 16.1±3ms (Fig. 3.9). As the slow time constant in these six cells was not statistically different from the activation time constant of the other five cells, we pooled the data. We conclude that Schwann cells of Type 1 express potassium channels mediating an sustained outward current with an average time constant of activation of 15.6±2ms (n=11). A subpopulation of these cells expresses in addition an outward current with approximately 3 times faster kinetic ($Tau_{activation}$ was 4.7±1ms). The measured activation time constants of the sustained outward potassium currents in Type 1 Schwann cells are comparable to those of the delayed rectifier current I_K ($Tau_{activation}$ = approx. 14ms) and I_D ($Tau_{activation}$ = approx. 4ms) measured in cultured Schwann cells (Baker, Howe et al. 1993) and in neurons (Storm 1990, Albert and Nerbonne 1995, Locke and Nerbonne 1997). The details of this comparison are given in the discussion part of the thesis.
Next we examined the amplitude of the described potassium currents in Type 1 Schwann cells. The total steady state potassium current was measured approximately 350ms after the onset of the voltage step. The first subgroup of Type 1 cells, in which the rising phase of the current was fitted with a single exponential fit, showed an average steady state potassium current of 106.85±19pA. The second subgroup of Type 1 cells, where the rising phase of the current was best characterized by a double exponential fit, displayed total average steady state amplitude of 184.97±44pA. We found that approximately half (47.8±4%) of the sustained steady state current in these Type 1 subgroup is related to the fast sustained current with an activation time constant of 4.7±1ms. The other half (52.2±4%) of the sustained steady state current was mediated by the slower sustained outward current with an activation time constant of 16.1±3ms (Fig.3.9).

In Type 2 Schwann cells the measurable voltage-dependent steady state potassium current was detected during the depolarizing voltage steps to potentials more positive then -50mV (n=20). The activation phase of the sustained potassium current could be well fitted with an double exponential fit. The $Tau_{activation}$ measured at depolarizing voltage step to +10mV were: 4.9±0.2ms and 37.2±4ms (n=20). We conclude that all Schwann cells of Type 2 express a fast sustained potassium current, which is comparable with the fast delayed rectifier current I_D ($Tau_{activation}$ = approx. 4ms) in Type 1 Schwann cells, as well as in cultured Schwann

cells (Baker, Howe et al. 1993) and in neurons (Storm 1990, Albert and Nerbonne 1995, Locke and Nerbonne 1997). The second $Tau_{activation}$ was with 37.2±4ms approximately 10 times slower than the faster sustained component. The measured slow activation time constant in Schwann cells of Type 2 Schwann cells is in the rage of the delayed rectifier current I_K measured in different neurons in the CNS (Storm 1990). We conclude that all Schwann cells of Type 2 express delayed rectifier potassium currents of the faster I_D und the slower I_K type.

In addition we examined the amplitude of the voltage-dependent steady state outward current measured approximately 350ms after the onset of the depolarizing voltage steps to +10mV. The total average voltage-dependent outward current was 712.9±59pA. We found that approximately 2/3 (67.5±3%) of the total sustained voltage-dependent potassium is related to the fast current with an activation time constant of 4.7±0.2ms, whereas only 1/3 (32.3±3%) where mediated by the slower sustained voltage-dependent potassium current with an activation time constant of 37.4±4ms.

We conclude that Schwann cells of Type 1 and Type 2 express sustained voltage-dependent potassium currents. All Type 1 Schwann cells express the delayed rectifier current I_K, in addition half of the Type 1 cells express the faster delayed rectifier current of the I_D type. Type 2 Schwann cells which build a homogeneous group that posse delayed rectifier current of I_K and I_D type. Furthermore, the types differ in the subtypes of I_K channels that they express. Further details are given in the discussion part.

Pharmacological approach

As a second approach to study voltage-gated outward potassium currents in Schwann cells we used pharmacology. As our findings based on the electrophysiological approach suggested that Schwann cells of Type 1 and Type 2 possess channels mediating I_A, I_D, and I_K potassium currents we sought to separate these current using 4-Aminopyridine (4-AP) and Tetraethylamonium chloride (TEA). They are used in different studies to separate I_A and I_D, which are blocked by 4-AP, and I_K, which is blocked by TEA (Storm 1990, Beck, Ficker et al. 1992, Albert and Nerbonne 1995, Locke and Nerbonne 1997). 4-AP is dependent from the concentration blocking different voltage-dependent potassium currents. A low concentration (50µm) is blocking mainly the delayed rectifier potassium currents of the I_D type, whereas a high concentration (5mM) is blocking as well the fast and transient voltage-

dependent potassium current of the I_A type (Locke and Nerbonne 1997). The high concentration of 4-AP was used to block potassium currents of the I_A und I_D type in our study.

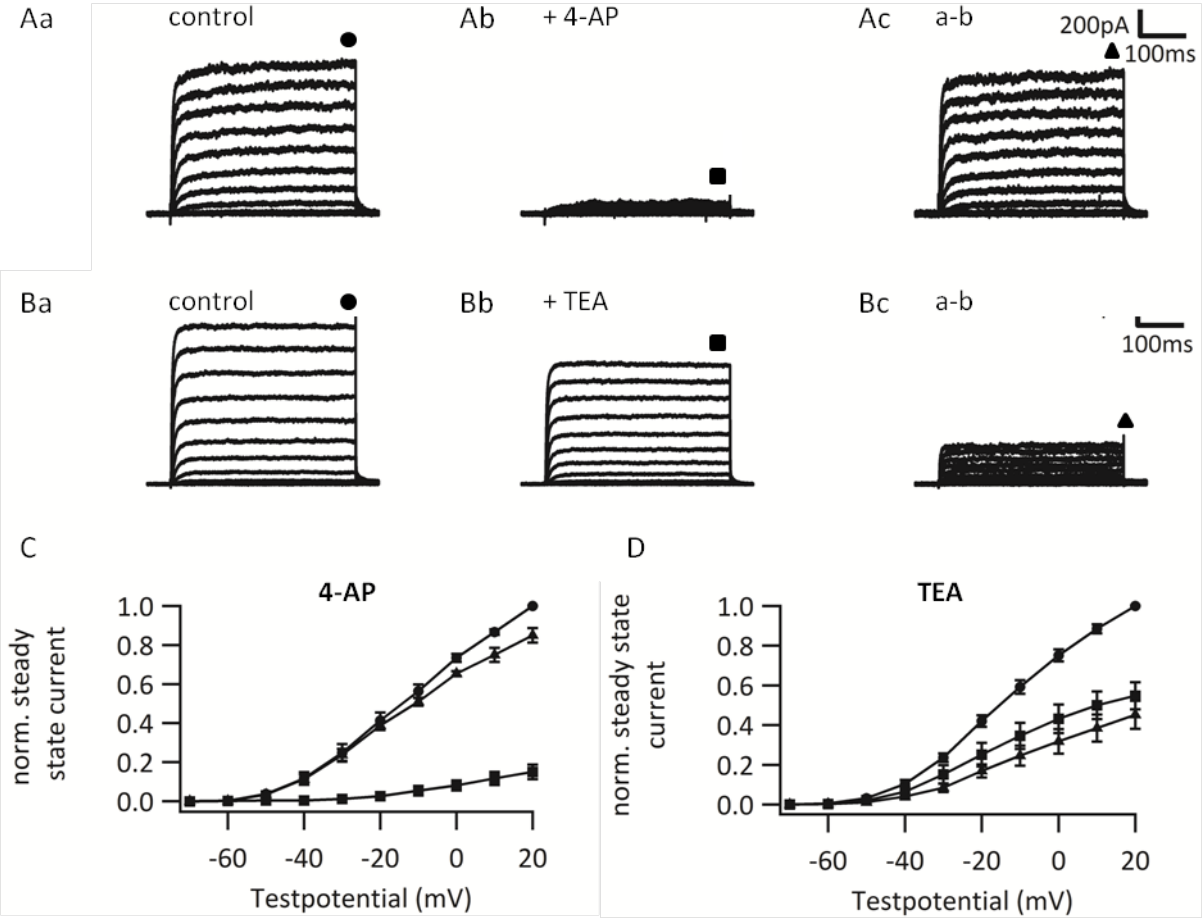

Fig. 3.10 Voltage-gated potassium channels expressed in Type 2 cells are inhibited by 4-Aminopyridine (4-AP) and Tetraethylamonium chlorid (TEA).

A-B: Leak subtracted outward currents recorded in Schwann cells of Type 2 during depolarizing voltage steps from -80mV to 20mV with 10mV increment under three different conditions: control (Aa, Ba), with 5mM 4-AP (Ab), with 25mM TEA (Bb). 1µM TTX and 100µM CdCl2 are present in the bath throughout the whole experiment. Ac, Bc: Currents obtained after the subtraction of the conditions with 4-AP (Ab) or TEA (Bb) from the control conditions (Aa, Ba). C, D: Comparison of the normalized total current amplitudes (●), the antagonist sensitive current (▲) and antagonist insensitive current (■) resulting from the traces in A and B plotted against the voltage. The data present mean+/-SEM.

We also recorded voltage-gated outwards potassium channels in Type 2 cell and applied 5mM 4-AP via the bath. Upon drug application the transient outward potassium current in Type 2 cells was completely blocked (n= 5). 4-AP in the concentration of 5 mM is expected to block I_A and I_D potassium currents (Locke and Nerbonne 1997). Therefore our data indicate that (a) Type 2 cells possess channels mediating I_A current, and (b) large proportion (87%) of

the sustained outward current in Type 2 cells is carried by channels mediating I_D current. These findings correspond more or less to the results which we obtained using the electrophysiological approach for separating different potassium currents: as described above, with that approach we found that approx. 2/3 of the sustained voltage-gated outward current in Type 2 cells is related to I_D current (with $Tau_{activation}$ = approximately 4ms).

Next we recorded voltage-gated outwards potassium currents in Type 2 cell and applied 25mM TEA via the bath. TEA is a blocker of I_K currents (Locke and Nerbonne 1997) and our findings so far indicate that ~13-30% of the sustained outward potassium current in Type 2 Schwann cells is mediated by I_K. Hence we expected that TEA will inhibit the sustained current by ~13-30%. However, we found that bath application of TEA blocked 44% of the total steady state voltage-gated outward current in Type 2 at +10mV (n=5). There could be different possible reasons for this discrepancy, one might be that a proportion of the voltage-gated potassium channels subtypes is sensitive to TEA and to 4-AP (Coetzee, Amarillo et al. 1999). It is known that 4-AP is not very selectively blocking I_A and I_D, former experiments revealed that as well some I_K subclasses are blocked by 4-AP (Storm 1990). It might be that Schwann cells of Type 2 express a subclass of I_K channels that is sensitive to 4-AP and to TEA.

Thus, we conclude that Schwann cells of Type 2 express both 4-AP-sensitive and TEA-sensitive outward potassium channels. Furthermore, our findings point to the fact that these channels mediate I_A, I_D, and I_K potassium currents. Yet more detailed experiments, e.g. using more specific blockers of different sub-types of potassium channels, are required in order to find out the quantitative contribution of each potassium current to the total voltage-gated outward current.

Schwann cells of the different types differ in their expression of voltage-dependent channels. Whereas Schwann cells of Type 1 and 2 show a low amplitude of the voltage-independent leak current and in relation a high amplitude of voltage-dependent currents, Schwann cells of Type 3 and 4 showed a high amplitude of voltage-independent leak current and in relation a small amplitude of voltage-dependent current. A detailed electrophysiological investigation of Type 1 Schwann cells revealed that they express sustained voltage-dependent potassium channels of the I_K and I_D type. Schwann cells of Type 2 express as the only Schwann cell type the fast and transient I_A-like current. In addition electrophysiological

and pharmacological investigations indicate that this type expresses a high proportion of sustained voltage-gated currents of the I_D and I_K type.

3.4. MORPHOLOGICAL ANALYSES OF THE ELECTROPHYSIOLOGICALLY IDENTIFIED SCHWANN CELL TYPES IN THE DEVELOPING MOUSE SCIATIC NERVE.

The morphological description of complete and intact Schwann cells was done so far only in cultured Schwann cells (Weiner, Fukushima et al. 2001) or in cross sections of the sciatic nerve (Webster, Martin et al. 1973). Our preparation gives us the possibility to investigate the morphology of the complete Schwann cell in the sciatic nerve, without minimal destruction of the surrounding tissue. To investigate the morphology of the different Schwann cell types in the mouse sciatic nerve we used two different fluorescent dyes: Lucifer Yellow and Alexa568. During the patch clamp recordings one of the dyes was included into the pipette solution. As a result the cytoplasm of the patched cell was replaced by the fluorescent internal solution. Directly after the recording the sciatic nerve slice containing the filled cell was fixed over night. To prevent confusions, only one cell per slice was filled. Lucifer yellow, a small fluorescent dye (molecular weight: 521.57g/mol, 457Da) was used in the beginning of our study to investigate the morphology of the Schwann cells. As Lucifer yellow is a small dye, fast filling of the soma and the processes could be observed. To be sure that the majority of small processes are filled with Lucifer yellow we compared the results with a second small fluorescent dye, Alexe568 (molecular weight: 730.74g/mol, ~600Da). We saw no differences between the filling of the Schwann cells and their morphology among the two different dyes, with exception of the brighter appearance of Alexa568-filled Schwann cells after the fixation process. We therefore decided to perform the following experiments with the brighter fluorescent dye Alexa568. Hence using this procedure a detailed analysis of the Schwann cell morphology in the mouse sciatic nerve in situ was possible.

Various morphological parameters were analyzed during our study. In particular, the total length of the cell, the number of primary processes, the thickness of the primary processes and the branching of the primary processes were investigated. The details about the measurements are described in the methods part. Statements about the size and

morphology of the cell soma were not made in our study, because we were concerned that these parameters could be affected by the removal of the patch clamp pipette.

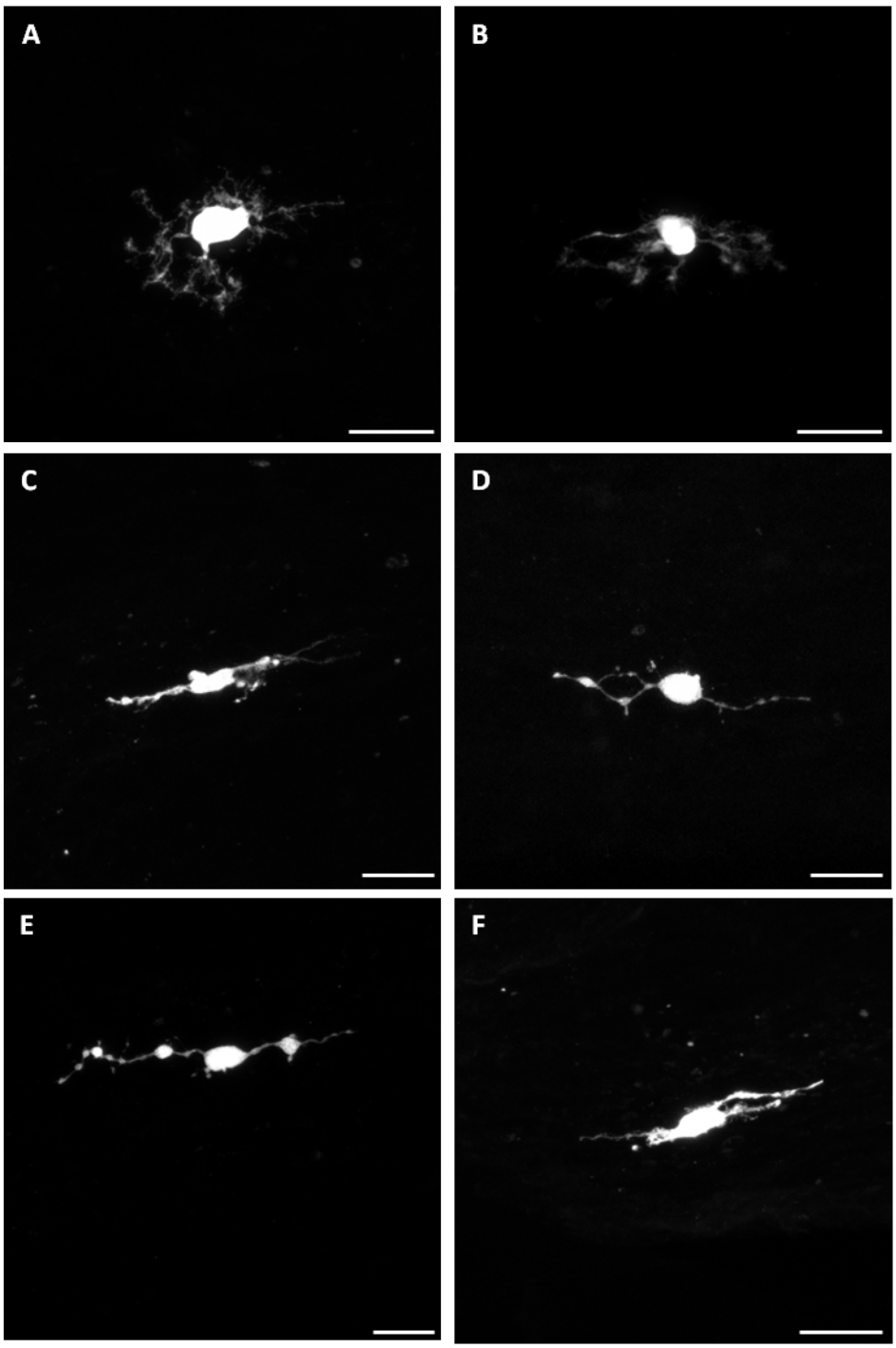

Fig. 3.11 Morphological appearance of Type 1 Schwann cells in the sciatic nerve slice.
A-F: Representative pictures of Type 1 Schwann cells filled with fluorescent dye during the patch-clamp recordings. Type 1 cells show stellate (A, B) or bipolar (C - F) morphology and in the majority of cases possess more than 2 primary processes that originate from the soma of the cell. This Schwann cell type exhibit the shortest total cell length of all Schwann cell types investigated in this study. Scale bar: 20µm.

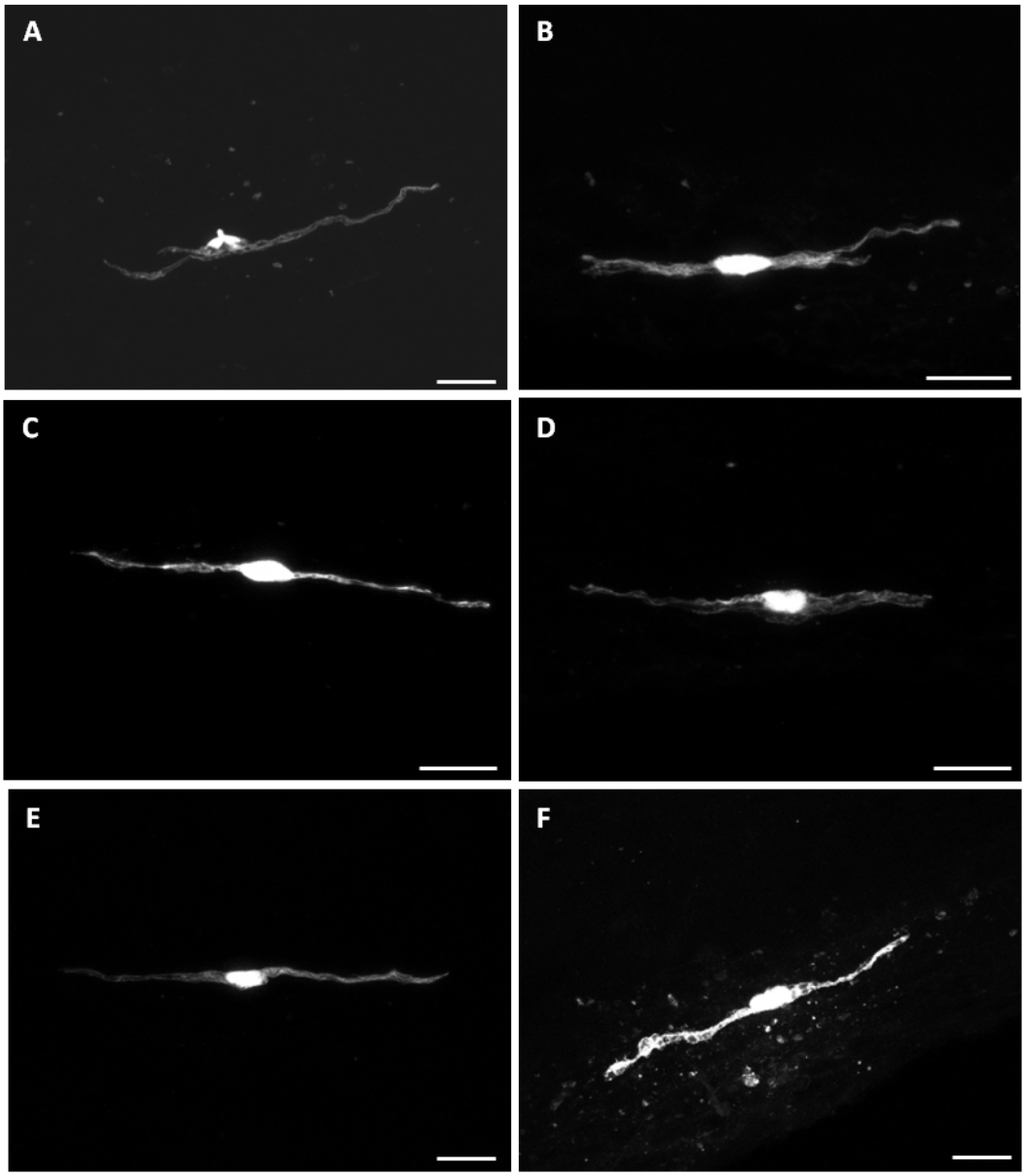

Fig. 3.12 Morphological appearance of Type 2 Schwann cells in the sciatic nerve slice.
A-F: Representative pictures of Type 2 Schwann cells filled with fluorescent dye during the patch-clamp recordings. All Type 2 Schwann cells show two primary processes that originate from the soma. Only a minority of Type 2 cells show branching (A,B). Scale bar: 20µm.

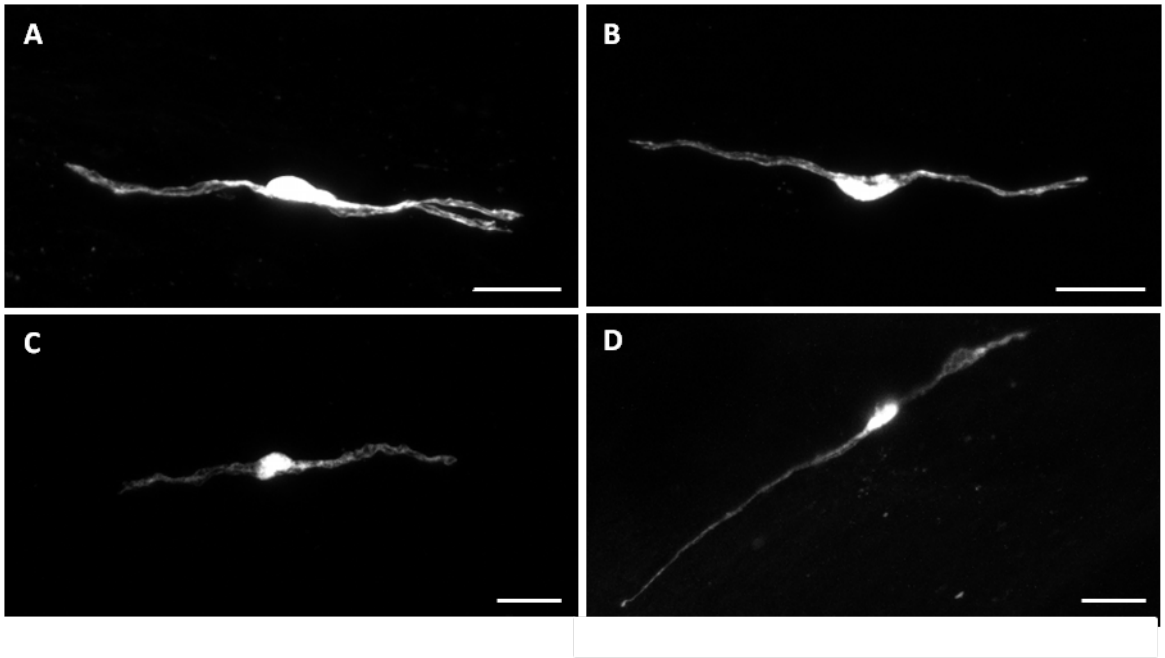

Fig. 3.13 Morphological appearance of Type 3 Schwann cells in the sciatic nerve slice.
A-D: Representative pictures of Type 3 Schwann cells filled with fluorescent dye during the patch-clamp recordings. All Type 3 Schwann cells show two primary processes that originate from the somata. One Type 3 Schwann cell shows a branching of the primary processes (A). Schwann cells of Type 3 are the longest of all investigated Schwann cell types. Scale bar: 20µm.

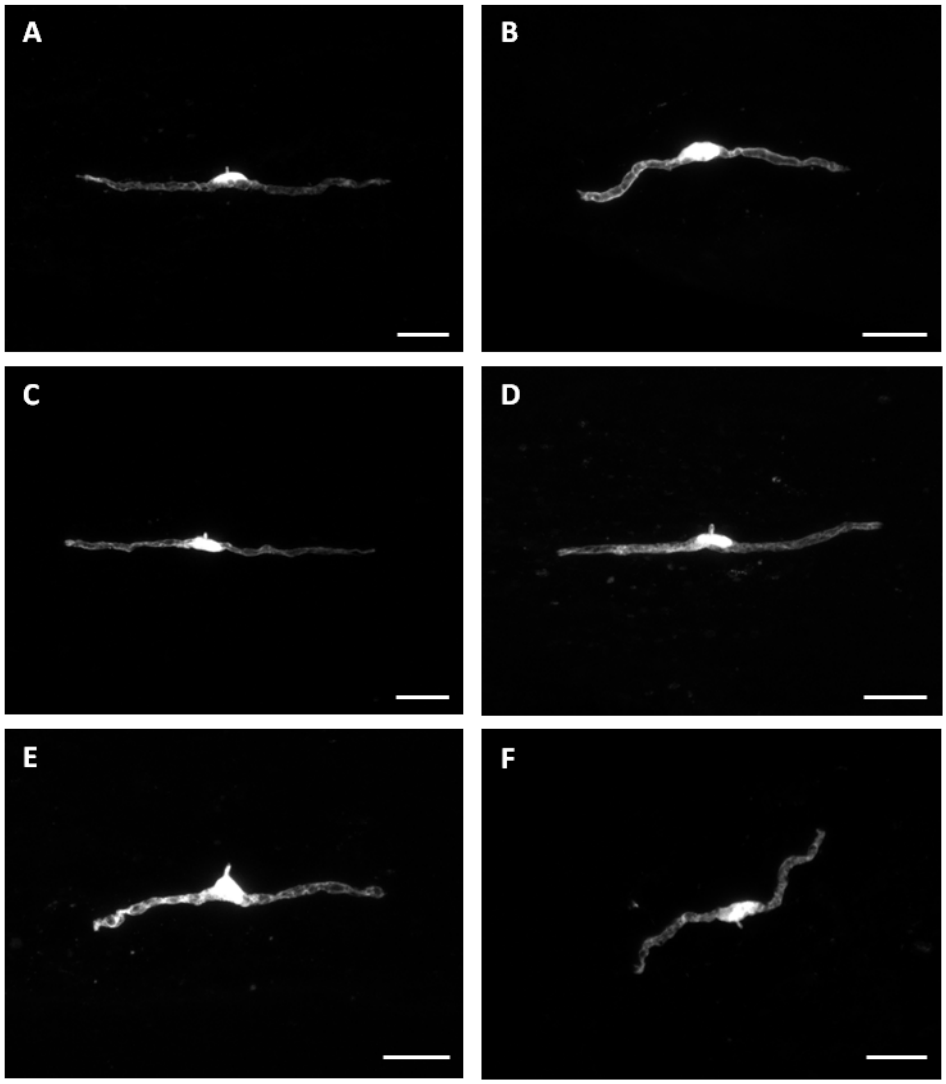

Fig. 3.14 Morphological appearance of Type 4 Schwann cells in sciatic nerve slices.
A-D: Representative pictures of Type 4 Schwann cells filled with fluorescent dye during the patch-clamp recordings. All Type 4 Schwann cells show two primary processes that originate from the somata. The processes are thick and never branched. Scale bar: 20µm.

Schwann cells of Type 1 show a stellate (Fig. 3.11 A&B) or elongated (Fig. 3.11 C-F) morphology. This cell type exhibited the highest number of primary processes from all investigated Schwann cell types, which originate from the centrally located somata. While all other Schwann cell types express in large part only two primary processes. In cells with a stellate appearance not all processes run in parallel with the axons (Fig. 3.11), whereas in cells with an elongated morphology the processes run in parallel to the axons (Fig. 3.11). In addition this cell type has the most branched and fine processes among all cell types investigated in this study: the average thickness measured at 20µm from the mid-point of the cell soma was 0.93±0.15µm (n=5). The total length of this cell type, estimated as the

distance between the end point of the two longest processes, equaled 66.89±6.53µm (n=8) and was the shortest among the studied cell types.

Schwann cells of Type 2 are characterized by a bipolar shape. The majority (seven out of eight cells) of Type 2 cells possessed two primary processes originating from the elongated soma. The processes run in parallel with the axons of the nerve. They are only in seldom cases branched and with an average thickness of 2.08±0.24µm (n=8) thicker than the processes of Type 1 Schwann cells. In addition the total length of the Type 2 Schwann cells is with 102.76±8.61µm (n=8) longer than the length of Type 1 Schwann cells.

Schwann cells of Type 3 exhibit a bipolar appearance, similar to Type 2 cells. The soma is elongated and gives rise to two primary processes. The total length of Type 3 cells is with 117.89±11.93µm (n=4) the longest of all cells studied. The thickness of the processes is 2.13±0.19µm (n=4) and is comparable to the thickness of the processes of Type 2 Schwann cells. Three out of four cells of Type 3 cells exhibited processes which were not branched while one cell showed one branching point in one of the two processes.

Schwann cells of Type 4 have a polarized appearance with two long primary processes. The nucleus is centrally located on top of the myelin sheath. The total length of Type 4 cells was with 101.09±5.57µm (n=10) one of the longest. The two primary processes originate from the centrally located elongated soma and extend along the axonal axis. The thickness of the processes was with 2.92±0.25µm (n=10) the largest of all other Schwann cell types investigated in this study. The processes of Type 4 Schwann cells are never branched. In addition the filling of the processes is not equally distributed along the processes. A brighter structure is running in spirals along the processes. This phenomena might result from the dye filling of the Schmidt-Lanterman incisures, a local stack of non-compacted myelin that spiral around the axon, and not of the compact myelin (Nave 2010).

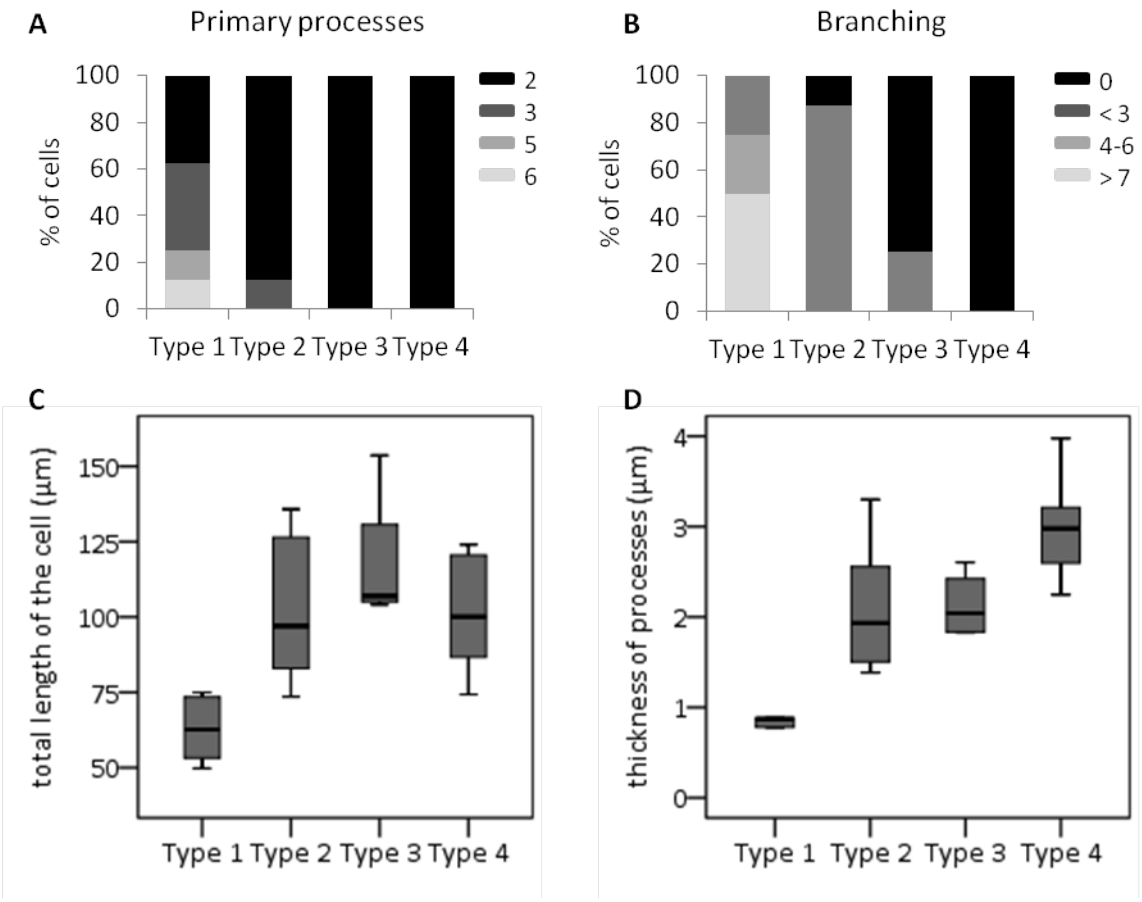

Fig. 3.15 Schwann cells of the distinct electrophysiological Types differ in their morphology.
A: Bar graph showing the distribution of the number of primary processes in the different Schwann cell types. The group of Type 1 cells has the highest proportion of cells with more than 2 primary processes. B: Bar graph showing the proportion of cells with branching processes. The largest number of branching is detected in the processes of Type 1 cells. C: The Box plot indicates the total length of the cell in µm. Type 1 is shorter than all other Schwann cell types. D: Box plot represents the thickness of the primary processes measured at the distance of 20µm distance from the middle of the soma. Type 1 shows the lowest variability, whereas the median thickness of the processes increases from Type 1 to Type 4 cells. Color-coding in (A) and (B) corresponds to the number of primary processes (A) or number of branches in the processes (B). Data in (C) and (D) presented as box plot represents the median together with the upper and lower quartiles as well as the minimum and maximum range values.

Tab. 6 Summary of the morphological parameters of the electrophysiologically different Schwann cell types in the mouse sciatic nerve.

	n	total length (µm)	n	thickness of the processes (µm)
Schwann cell type				
Type 1	8	66.88±6.5	5	0.92±0.2
Type 2	8	102.77±8.6	8	2.08±0.2
Type 3	4	117.89±11.9	4	2.13±0.2
Type 4	10	101.09±5.7	10	2.92±0.2
Statistical analyses				
Type 1 versus 2		p<0.05		p<0.05
Type 1 versus 3		p<0.05		p<0.05
Type 1 versus 4		p<0.05		p<0.001
Type 2 versus 3		NS		NS
Type 2 versus 4		NS		p<0.05
Type 3 versus 4		NS		NS

NS: not significant

The table represents the statistical analyses of two morphological parameters in the electrophysiological different Schwann cell types. The statistical significance was determined using One-Way ANOVA with post-hoc tukey HSD test.

Taking all the morphological data into account it becomes clear, that Schwann cells differ in their morphological appearance. While cells of all four types show a bipolar morphology, the group of Type 1 cells includes in addition cells with stellate morphology (Fig. 3.11). Type 1 Schwann cells represent the only cell type with more than two primary processes, and they are the only cell type whose processes show branching. The thickness of the processes is the smallest in Type 1 cells, and the largest in Type 4 cells, with Type 2 and Type 3 cells showing intermediate values for this parameter: Type 1 < Type 2 < Type 3 < Type 4 (Fig. 3.15, Table 6). The values of the total cell lengths are distributed slightly different between the Schwann cell types: Type 1 < Type 4 = Type 2 < Type 3 (Fig. 3.15, Table 6).

Studies in cultured Schwann cells and in teased nerve fibers show the presence of gap junctions in Schwann cells (Konishi 1990, Chanson, Chandross et al. 1993, Balice-Gordon, Bone et al. 1998, Meier, Dermietzel et al. 2004). We wanted to investigate the presence of gap junction in situ in our sciatic nerve slice preparation. During the experiments with two relatively small fluorescent dyes, Lucifer Yellow (molecular weight: 521.57g/mol, 457Da) and Alexa568 (molecular weight: 730.74g/mol, ~600Da) only the recorded cell was filled with a dye in all cases. We never observed labeling of neighboring cells in the sciatic nerve slices. These findings suggest that Schwann cells in the developing mouse sciatic nerve are not

coupled via gap junctions. An alternative explanation is, that the dyes used in our study are too big for the gap junctions in Schwann cells, as the earlier studies were performed with a smaller dye (376Da) (Balice-Gordon, Bone et al. 1998). In addition the charge of the dye may also play a role for the permeability of the gap junctions (Cao, Eckert et al. 1998). Further details will be presented in the discussion part.

Taken together, our analysis demonstrated that electrophysiologically distinct Schwann cell types in the developing mouse sciatic nerve also differ in their morphological appearance. Type 1 cells are the shortest cells among the four investigated cell types, and contain the largest number of primary processes. Type 3 cells are the longest cells, while Type 4 cells possess the thickest processes. The processes of Type 2, Type 3 and Type 4 cells (nearly) never show branching. With our approach we could not detect gap junctional coupling between Schwann cell in the mouse sciatic nerve slice.

3.5. EXPRESSION OF DIFFERENT SCHWANN CELL LINEAGE MARKERS IN THE ELECTROPHYSIOLOGICAL DIFFERENT SCHWANN CELL TYPES

So far we could demonstrate that, dependent from the age, up to four electrophysiological different Schwann cell types exist in the sciatic nerve in situ. In addition the conducted morphological analyses show that these types differ as well in their morphological appearance. To integrate our investigated Schwann cell types in the existing Schwann cell lineage we studied the expression of different Schwann cell lineage marker in the four Schwann cell types.

3.5.1. SRY-RELATED HMG-BOX 10 (SOX10)

As indicted in the introduction, Sox10 is expressed throughout the whole Schwann cell lineage and is one of the specific markers for this lineage (Kuhlbrodt, Herbarth et al. 1998, Britsch, Goerich et al. 2001, Finzsch, Schreiner et al. 2010). Hence it was used in this study to test whether the four electrophysiological different cell types belong to the Schwann cell lineage.

In the first step of the investigation we aimed to identify the proportion of Schwann cells in the sciatic nerve slices in situ. As Schwann cells build the majority of cells in the nerve at this age, we expect a high number of Sox10 positive cells in both investigated age groups (Finzsch, Schreiner et al. 2010). Therefore, we identified the percentage of Sox10 positive cells in our slice preparation in the two different age groups. Remarkably, the expression level of Sox10 can vary slightly during the development as well in the different cells of the Schwann cells lineage and therefore the brightness level of the staining maybe different from cell to cell. In coherence with its function as transcription factor, the two nuclear localization signals enables Sox10 to enter the nucleus and is most frequently detected in the nucleus (Rehberg, Lischka et al. 2002). In addition Sox10 is an active nucleocytoplasmic shuttle protein which means the protein is also able to leave and reenter the nucleus (Rehberg, Lischka et al. 2002). Therefore, a detection of Sox10 in the nucleus and in the cytoplasm is possible.

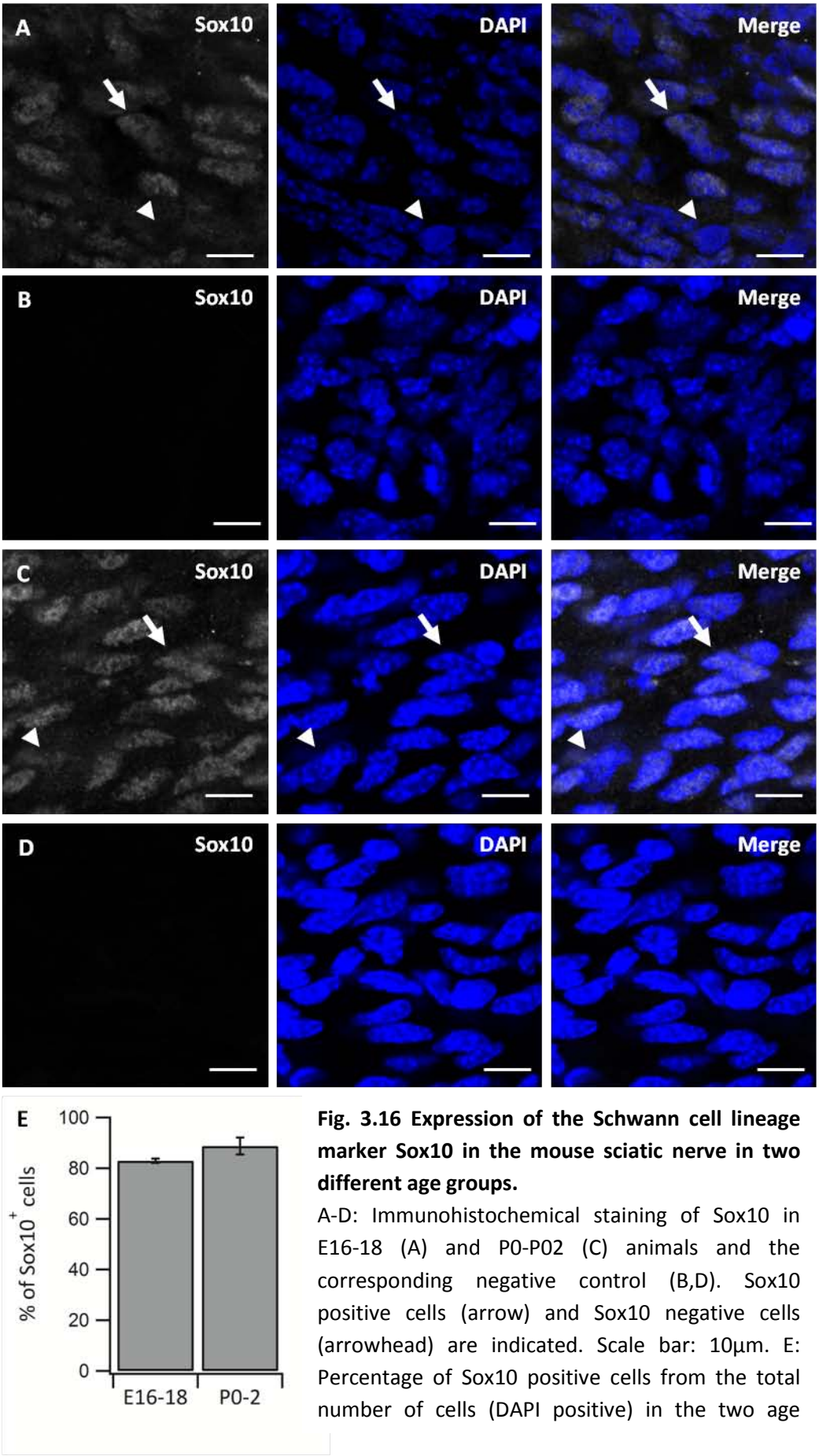

Fig. 3.16 Expression of the Schwann cell lineage marker Sox10 in the mouse sciatic nerve in two different age groups.

A-D: Immunohistochemical staining of Sox10 in E16-18 (A) and P0-P02 (C) animals and the corresponding negative control (B,D). Sox10 positive cells (arrow) and Sox10 negative cells (arrowhead) are indicated. Scale bar: 10µm. E: Percentage of Sox10 positive cells from the total number of cells (DAPI positive) in the two age

The staining of the sciatic nerve slices shows variability in the signal brightness between cells. In addition, we are able to see Sox10 staining equally distributed between nucleus and cytoplasm or exclusively in the cytoplasm. But in the majority of cases the staining is located in the nucleus of the cell (Fig. 3.16). We counted all cells that show a positive labeling for Sox10 independent from the brightness level and the staining pattern.

The quantification of our immunohistochemical Sox10 staining in the sciatic nerve slice shows, that in both age groups the majority of cells are positive for Sox10 (Fig. 3.16). The percentage of Sox10 positive cells was in P0-P02 animals with 88.7% (n=3 slices from three different animals) of the total cell number (DAPI positive cells) slightly higher but not significant different (t-test: $p>0.05$) than in the younger age group with 82.9% (n=3 slices from three different animals, Fig. 3.16).

Thus, our findings suggest that the majority of cells in the two investigated age groups are positive for Sox10 and therefore belong to the Schwann cell lineage.

Next, we used the established staining for Sox10 to test whether our four electrophysiological different cell types belong to the Schwann cell lineage. Therefore we performed the Sox10 staining on nerve slices containing Schwann cells filled with a fluorescent dye during patch-clamp recordings. The staining shows that six out of seven Type 1 cells tested are positive for Sox10. We tested Type 1 cells from both age groups (E16-18: n= 5; P0-2: n=2) and the result demonstrates that independent from the age of the animal Type 1 cells are positive for Sox10. Six out of seven Type 2 cells express the transcription factor Sox10. The staining was as well performed in both age groups, and demonstrated that the cells labeled positively for Sox10 both in late embryonic (n=4) and early postnatal animals (n=3) (Fig. 3.17). As Type 3 cell occur only rarely, during this work we could fill with a fluorescent dye only one cell of this type. Sox 10 staining demonstrated that this cell was positive for Sox10 (Fig. 3.17).

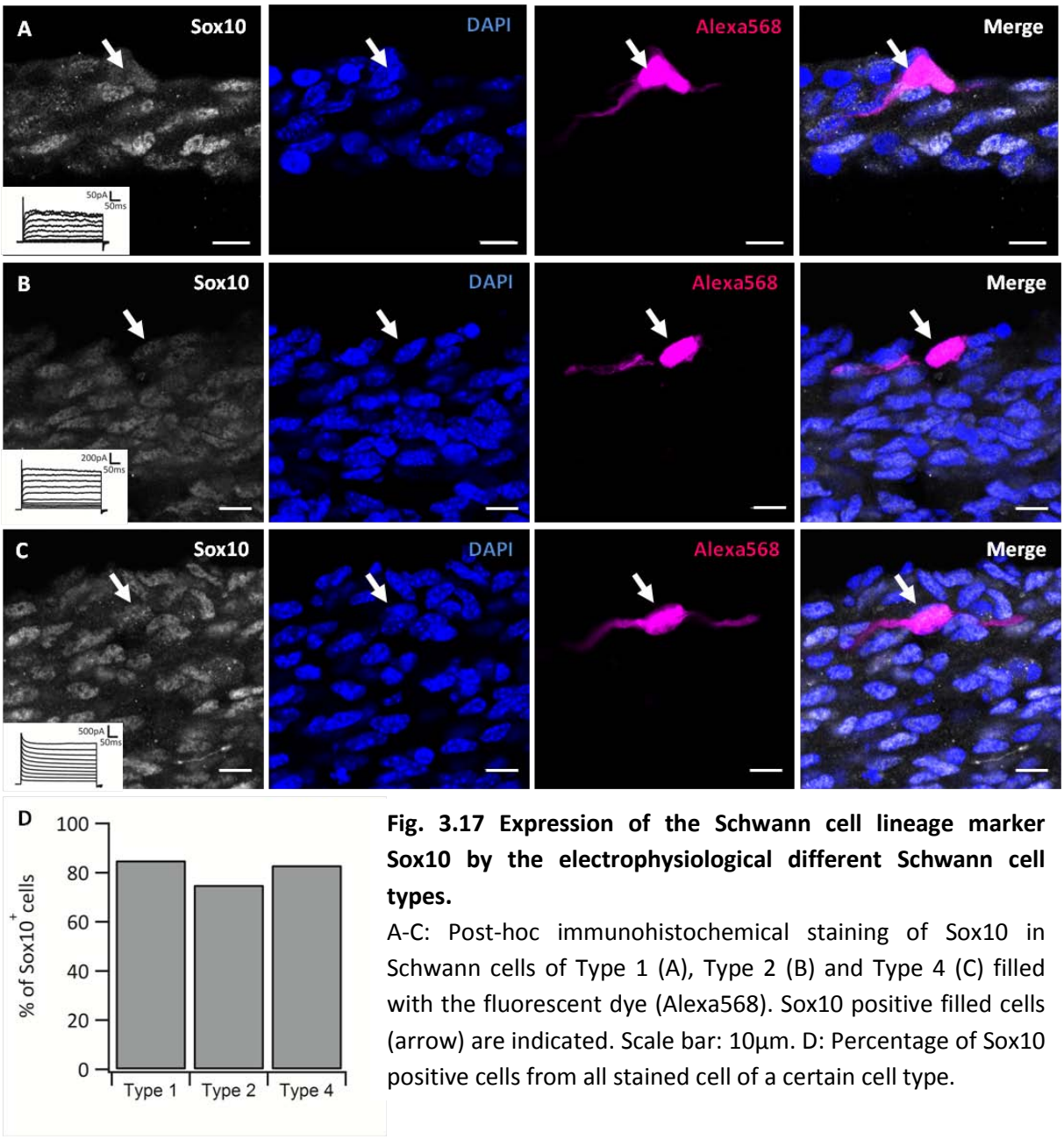

Fig. 3.17 Expression of the Schwann cell lineage marker Sox10 by the electrophysiological different Schwann cell types.

A-C: Post-hoc immunohistochemical staining of Sox10 in Schwann cells of Type 1 (A), Type 2 (B) and Type 4 (C) filled with the fluorescent dye (Alexa568). Sox10 positive filled cells (arrow) are indicated. Scale bar: 10µm. D: Percentage of Sox10 positive cells from all stained cell of a certain cell type.

Type 4 cells are only present in the older age group (P0-02) investigated in this study. Staining of these cells for Sox10 demonstrated that five out of six cells are positive for Sox10 (Fig. 3.17).

In summary the specific marker for the Schwann cell lineage, the transcription factor Sox10, was present in all four electrophysiological different cell types. The majority of the tested cells (83%) labeled positive for Sox10. The remaining cells didn't show the expression of Sox10. Thus, our results suggest that the majority of cells with electrophysiological properties described in chapter3.2. belong to the Schwann cell lineage.

3.5.2. GLIAL FIBRILLARY ACIDIC PROTEIN (GFAP)

To further classify the four electrophysiological different Schwann cell type we use the marker glial fibrillary acidic protein (GFAP). GFAP is a protein which appears relatively late in the embryonic development in the processes of the cells (Jessen, Morgan et al. 1990). It is down regulated in Schwann cell as soon as they start to build myelin, while GFAP is selectively expressed in non-myelinating Schwann cells during their whole live time (Jessen, Morgan et al. 1990). We have used this marker to distinguish between relatively undeveloped Schwann cell types in the lineage (GFAP negative) and more advanced immature and non-myelinating cells (GFAP positive).

The immunohistochemical staining for GFAP was in three Type 1 cells performed. All three cells were negative for this specific marker of the Schwann cell lineage. The stainings were carried out in slices from animals older than E18 to ensure that GFAP is already expressed. All three investigated Type 2 Schwann cells express GFAP. The slices with the filled cells from this cell type were collected from animals between P0 and P02. The GFAP signal is clearly located in the processes of this Schwann cell type (Fig. 3.18). In some cases the filamentous structure of GFAP was altered because of the preparation processes and the fragile composition of this protein. Nevertheless a clear overlay between the more fragmented GFAP signal and the process of the filled cell could be observed. The brightest and nicest staining from all was observed in a Type 3 Schwann cell. Even if we could only stain one cell of this type, the result was the clearest. There was a clear and almost total overlay between the GFAP signal and the filled process of the Type 3 cell (Fig. 3.18). The result for the Schwann cells of Type 4 is more complex. Four out of five cells express GFAP in their processes. Figure 3.18 shows one cell of Type 4 with GFAP positive processes and one cell with GFAP negative processes. This is in agreement with an older study from Jessen et al. 1990 that shows that Schwann cells start to down regulate GFAP as soon as they start to myelinate (Jessen, Morgan et al. 1990).

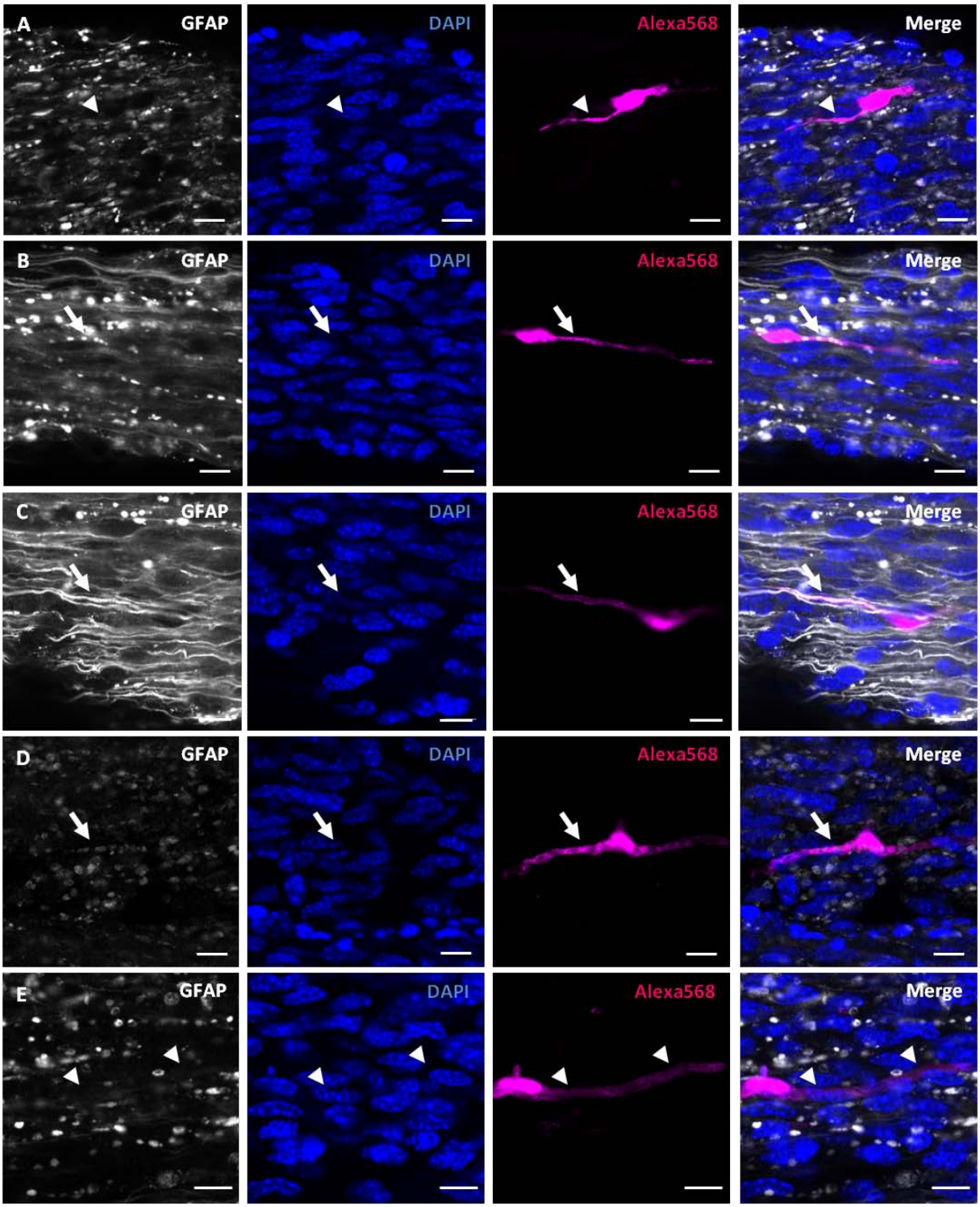

Fig. 3.18 Expression of the Schwann cell marker GFAP by the electrophysiological different Schwann cell types.

A-E: Post-hoc immunohistochemical staining for GFAP of fluorescent dye filled Schwann cells of Type 1 (A), Type 2 (B), Type 3 (C) and Type 4 (D,E). Arrow points toward cells/processes that express GFAP (B,C,D) and arrowhead points toward cells/processes that don't express GFAP (A, E). Scale bar: 10µm.

In summary, Schwann cells of Type 1 are the only cells that do not express GFAP and therefore seems to be the earliest Schwann cell type that was patched in our preparation. Schwann cells of Type 2 und 3 are clearly positive for GFAP, whereas Schwann cells of Type 4 show a more complex picture. The majority of Type 4 cells are GFAP positive, but we also find GFAP negative cells. This result indicates already that Type 4 cells might be in a transition state and start to down regulate GFAP already.

3.5.3. MYELIN BASIC PROTEIN (MBP)

The myelin basic protein (MBP) is one of the major components of the myelin sheath (Greenfield, Weise et al. 1982, Agrawal and Agrawal 1991, Gow, Friedrich et al. 1992). There are only two types of cells in the nervous system that express this protein: myelinating oligodendrocytes in the CNS and myelinating Schwann cells in the PNS (Gow, Friedrich et al. 1992). We aimed to use MBP labeling of dye-filled cells in order to distinguish more mature cells from other types of the Schwann cell lineage.

At the first step we wanted to monitor the myelination in the sciatic nerve slice. The process of myelination in the PNS of mice starts directly after birth at P0 and increases rapidly during the first two postnatal weeks (Stewart, Morgan et al. 1993, Jessen and Mirsky 2005). Therefore we expect no or only a few MBP positive cells in the sciatic nerve slice of the first age group from E16-18. With increasing age we expect an increase of MBP positive cells in the sciatic nerve slice in mice from P0 to P2.

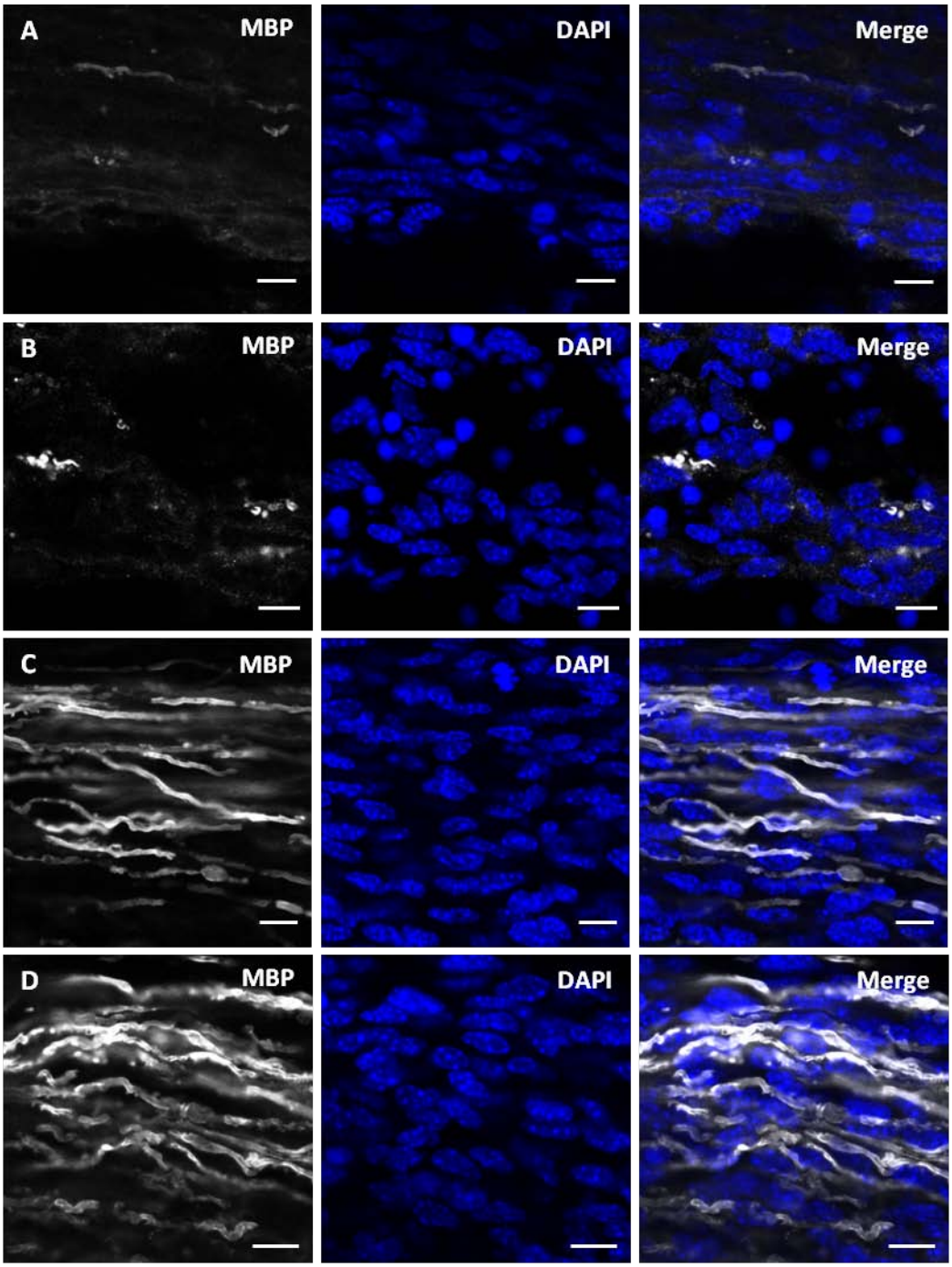

Fig. 3.19 Expression of the myelinating Schwann cell marker MBP in different ages.
A-D: Immunohistochemical staining for MBP in E18 (A), P0 (B), P01 (C) and P02 (D) slices. A clear increase in the MBP signal starting from P0 is visible. Scale bar: 10µm.

We found that in E18 and P0 slices there is almost no detectable MBP signal; only a very few short structures are stained. These structures might represent the first cells that start to differentiate into myelinating Schwann cells and therefore start to express MBP. Starting from P01 there is a large increase in the MBP signal, which is even higher in slices from P02 animals (Fig. 3.19). Already at this relatively early developmental stage large elongated MBP

positive Schwann cell sheath are visible, which run in most of the cases parallel to each other. Hence we conclude that starting from P0 with increasing age the MBP signal in the sciatic nerve increases. As some of our electrophysiological different Schwann cells types (Type 3 and 4) are only present in cells after birth, we hypothesize that a group of these cells might be more mature and represent the group of myelinating Schwann cells. To proof this hypothesis, fluorescent dye filled cells were stained for MBP. As MBP is expressed only in the processes of myelinating Schwann cells, we expected a staining only in the processes of this special cell type in the Schwann cell lineage.

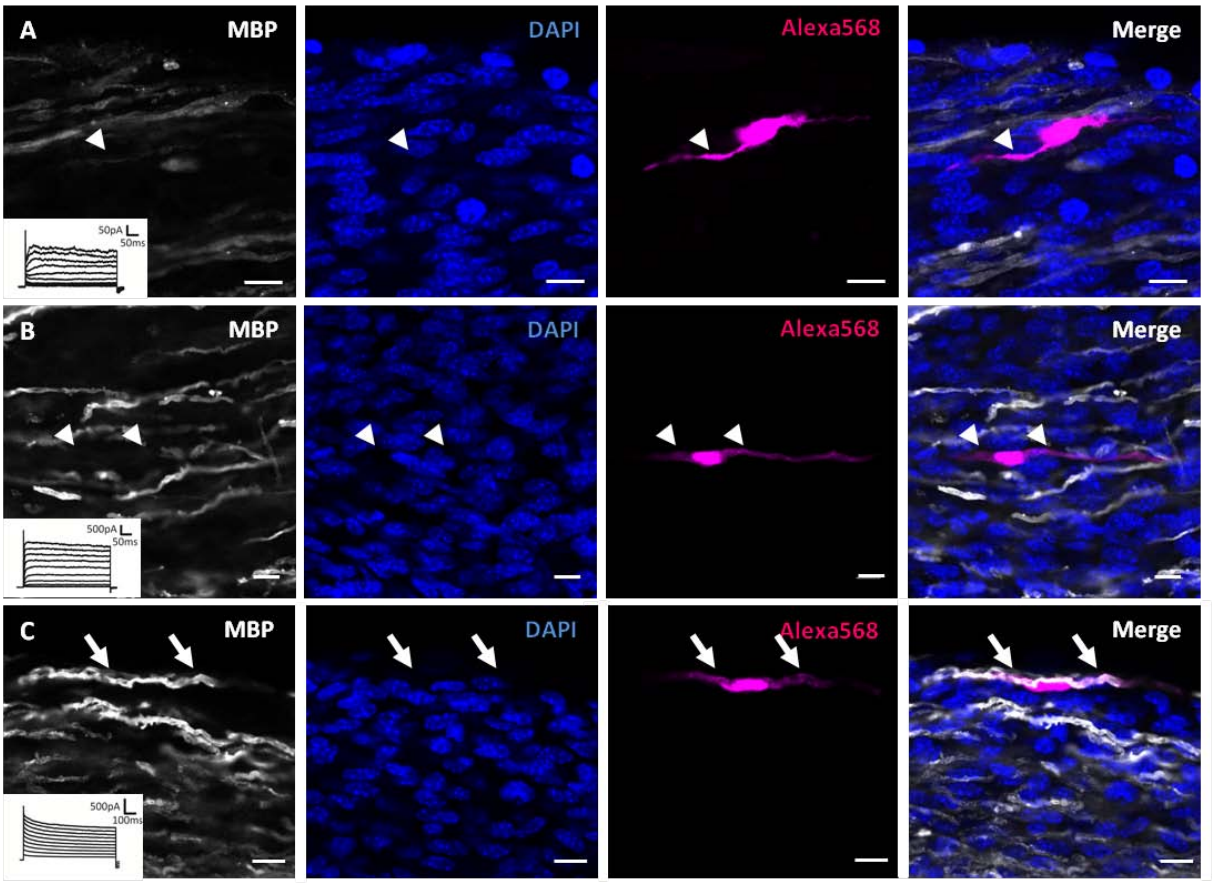

Fig. 3.20 Expression of myelin basic protein (MBP) in the electrophysiological different Schwann cell types.

A-C: Post-hoc immunohistochemical staining of MBP in Type 1 (A), Type 2 (B) and Type 4 (C) Schwann cells. MBP positive processes are marked with an arrow (C) and MBP negative processes (A, B) are marked with an arrowhead. Scale bar: 10µm.

We found that all tested Schwann cells of Type 1 (n=4) and Type 2 (n=7) are negative for the myelin basic protein (MBP). The majority of stainings were performed in slices between P0 and P02. There was no overlay between the MBP signal and the filled processes of the cell. Because of the rare appearance of Type 3 Schwann cells, no staining for MBP was

performed. Therefore we cannot make any conclusion about this cell type and its expression of this special protein. All tested cells Schwann cells of Type 4 are positive for MBP (n=17). In these cells a clear overlay between the filled processes of the cell and the MBP signal was visible (Fig. 3.20).

In summary: Our MBP staining shows that with increasing age of the animal the MBP signal produced by the myelinating Schwann cells is enhanced. In consensus with the literature we are able to demonstrate that the myelination in the mouse sciatic nerve starts around P0 and increases fast in the first days of life. As only Schwann cells of Type 4 express MBP we can clearly state that this cell is the myelinating Schwann cell. This distinct property distinguishes Type 4 Schwann cells from other cell types investigated in this study.

3.5.4. IONIZED CALCIUM-BINDING ADAPTOR MOLECULE 1 (IBA1)

Beside Schwann cells we find a small population of macrophages in the sciatic nerve of mice (Finzsch, Schreiner et al. 2010). To exclude that the investigated cells in this study belong to the population of macrophages we used specific markers to label these cells. Two markers are commonly used to consider macrophages: (1) the ionized calcium-binding adapter molecule 1 (IBA1) and (2) Cluster of Differentiation 68 (CD68) are known as markers for macrophage (Mueller, Leonhard et al. 2003). A previous study shows that IBA1 and CD68 mark the same cell population (Mueller, Leonhard et al. 2003). Other studies demonstrate that CD68 is specific maker for active macrophages and microglia (Venneti, Lopresti et al. 2009). We first wanted to clarify this inconsistency in the literature and select the right marker for our application, we performed double-labeling of CD68 and IBA1 in mouse sciatic nerve slices.

The total number of IBA1+/CD68+ cells, as well as the number of IBA1+/CD68- and IBA1-/CD68+ cells was defined in the sciatic nerve slices. In four out of five slices only IBA1+/CD68+ cells (9 out of 233 DAPI positive cells), but no IBA1+/CD68- or IBA1-/CD68+ cells, were found, indicating that there is a complete overlay between these two different macrophage markers (Fig.3.21).

Only in one slice we could find in addition to IBA1+/CD68+ cells (6 cells) a population of cells that was IBA1-/CD68+ (3 cells). As the majority of our stainings show complete overlay between the two different markers and in addition the staining of IBA1 has less background

and appeared less granulated, we decided to use IBA1 as a marker for macrophages in our study. Remarkably we found that the proportion of $IBA1^+$ cell is with 3.18±1.3% (n=4 slices from four different animals; 9 out of 115 DAPI positive cells) in E16-18 animals and with 4.45±1% (n=3 slices from three different animals; 5 out of 118 DAPI positive cells) in P0-P02 very low in our preparation (Fig. 3.21). As the activation of macrophages and the increase of the number of macrophages in the nerve are often used as indicators for healthiness of the tissue (Griffin, George et al. 1993, Mueller, Wacker et al. 2001), the low number of these cells also emphasizes the good preparation and recording conditions that we achieved with our preparation (in addition to criteria described in chapter 3.1).

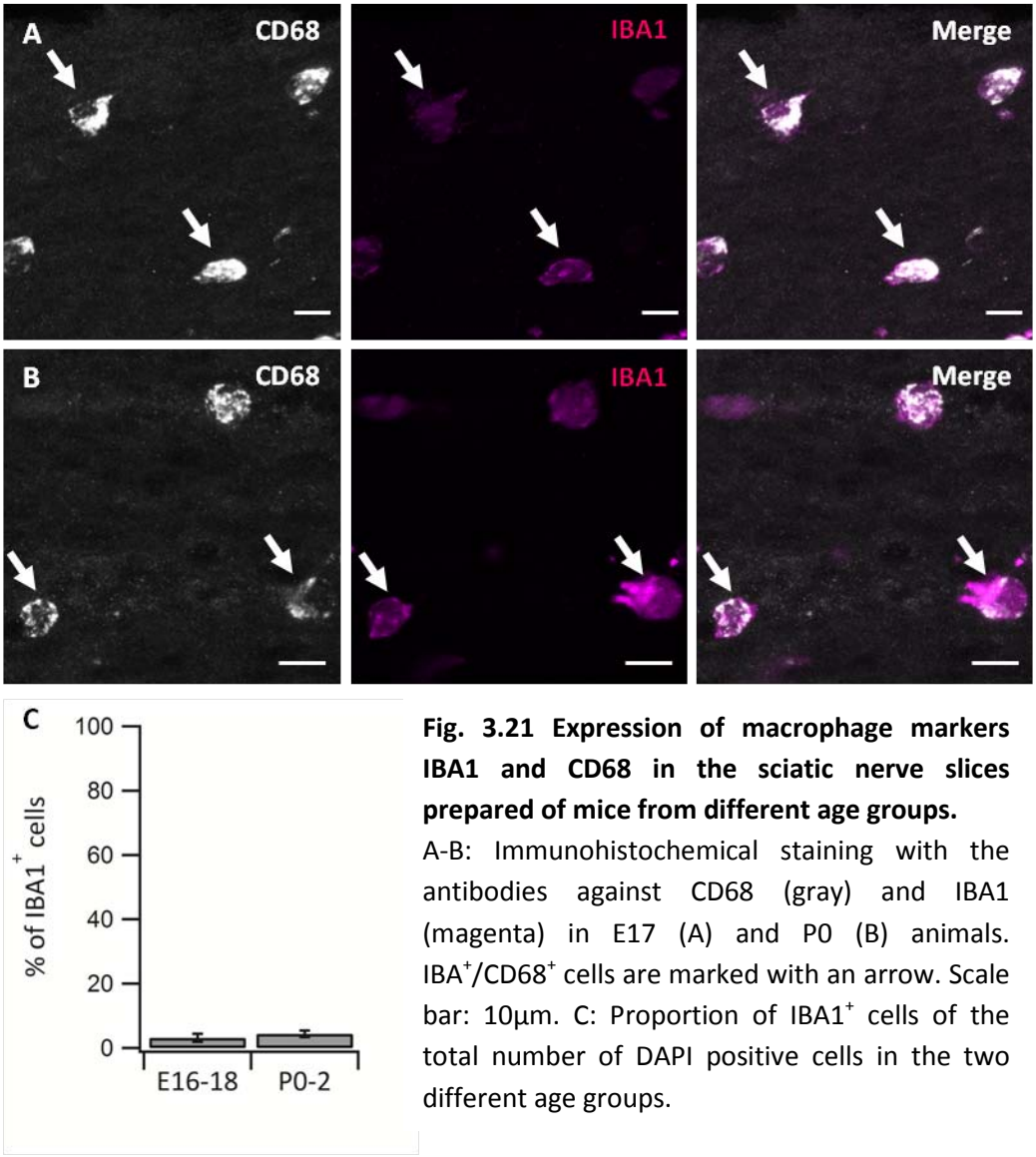

Fig. 3.21 Expression of macrophage markers IBA1 and CD68 in the sciatic nerve slices prepared of mice from different age groups.
A-B: Immunohistochemical staining with the antibodies against CD68 (gray) and IBA1 (magenta) in E17 (A) and P0 (B) animals. $IBA^+/CD68^+$ cells are marked with an arrow. Scale bar: 10µm. C: Proportion of $IBA1^+$ cells of the total number of DAPI positive cells in the two different age groups.

Next we want to verify that none of the four electrophysiologically different Schwann cell types, described in our study, belongs to the group of macrophages. The result of the post-hoc IBA1 staining showed no overlay between the IBA1 signal and the fluorescent signal of the filled cell in all four Schwann cell types (Type 1: n=9; Type 2: n=5; Type 3: n=2; Type 4: n=5).

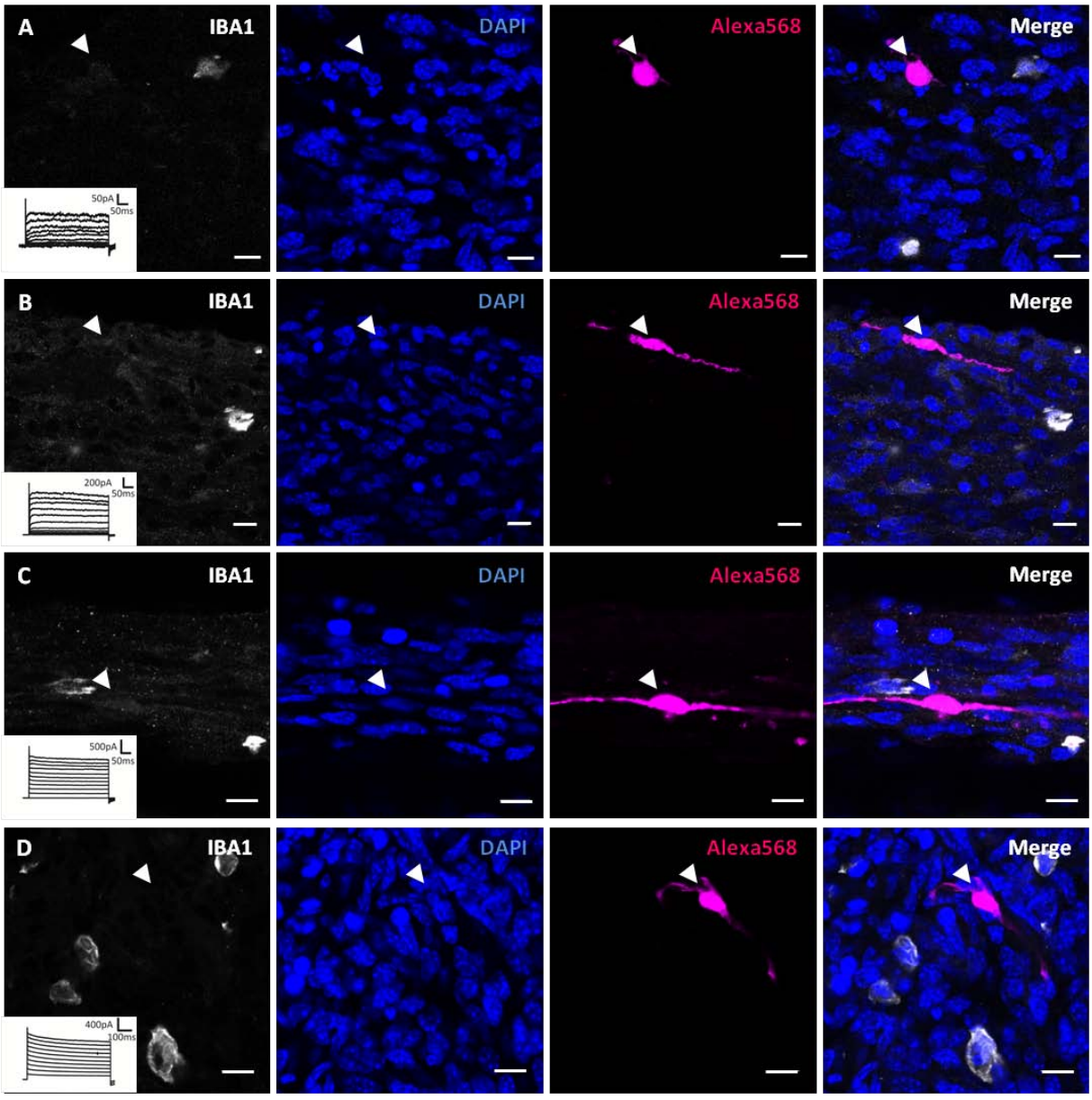

Fig. 3.22 Four electrophysiological different Schwann cell types do not express the macrophage marker IBA1.

A-D: Representative examples of immunohistochemical labelling of the recorded cells with an antibody against IBA1: Type 1 (n=9; A), Type 2 (n=5; B), Type 3 (n=2; C) and Type 4 (n=5; D) Schwann cells. The response to depolarizing voltage steps of the different recorded cells is shown as inset in the first panel. All cells are negative for the marker (indicated with an arrowhead). Scale bar: 10µm.

As all recorded cells stained negatively for IBA1, we sought for a possibility to perform a positive control experiment. We know from patch-clamp recordings in the CNS the current pattern of microglia (the CNS counterpart of the macrophages). The current pattern of these cells is characterized by a very small leak and steady state voltage-gated current, even smaller than that of Type 1 Schwann cells (Kettenmann and Ilschner 1993, Boucsein, Kettenmann et al. 2000). Microglia appears as small roundish cells in the CNS. We were looking for this type of cell in the sciatic nerve slice. We found small roundish cells, verified their current pattern in response to ten depolarizing voltage steps from -80mV to 20mV with 10mV increment and stained them post-hoc for IBA1. The result was that two small roundish cells showed the typical current pattern for microglia cells and were in addition positive for IBA1 (Fig. 3.23).

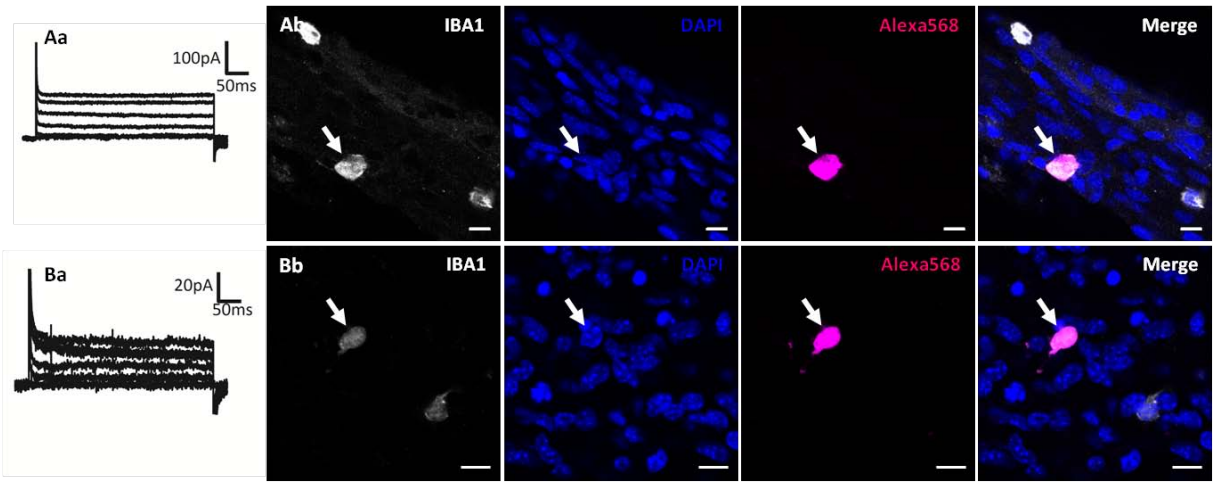

Fig. 3.23 Electrophysiological properties and immunohistochemical staining of IBA1 positive cells in the sciatic nerve.
Aa and Ba: Current pattern in response to ten depolarizing voltage steps starting from -80 to +20mV with 10mV increment (without leak subtraction) of two recorded cells. Ab and Bb: Post-hoc staining of the same cells for IBA1. Both cells appeared positive. The soma of the positive cells is indicated by an arrow. The IBA1 staining is presented in gray, the Alexa568-filling is presented in magenta and the DAPI staining is shown in blue. Scale bar: 10µm.

Based on our finding we conclude that the four electrophysiologically different Schwann cell types investigated in our study are not macrophages. Comparable to the brain, IBA1 positive cells show a specific current pattern (Kettenmann and Ilschner 1993, Boucsein, Kettenmann et al. 2000) which is distinct from current pattern of the investigated Schwann cell types.

Summary of chapter 5

The investigation of the molecular marker expression in the four electrophysiologically distinct Schwann cell types revealed clear differences between the cells. Type 1 Schwann cells are Sox10+, GFAP- and MBP-. This expression pattern indicates that the cell type is a cell of the Schwann cell lineage (Sox10+), which is relatively immature as it is GFAP- and MBP-. Schwann cells of Type 2 show the following marker profile: Sox10+, GFAP+ and MBP-. The Sox10+ signal reveals that the cell belongs to Schwann cell lineage, as it is GFAP+ it seems to be more developed then Type 1 cells. Schwann cells of Type 3 are Sox10+ and GFAP+. The cell belongs as well to the Schwann cell lineage (Sox10+). As we have not performed the MBP staining for Type 3 cells we cannot make any statement about the myelination status of these cells. The marker profile of Type 4 Schwann cell is the following: Sox10+, GFAP+/-, MBP+. This Schwann cell (Sox10+) is the only type that is expressing MBP and is only present in the age group from P0-2. Both facts indicate that Type 4 Schwann cell represent myelinating Schwann cells.

3.6. Expression of functional glutamate receptors in the four different Schwann cell types

So far we could demonstrate that the four electrophysiological different Schwann cell types differ in their morphological appearance and in the expression of different Schwann cell markers. In the next step we wanted to investigate the expression of functional glutamate receptors in the different Schwann cell types. To do so, we applied the neurotransmitter glutamate at the different Schwann cell types and recorded the response induced by the activation of receptors expressed at the cell surface. To deliver glutamate to the patched cell we used the fast pressure-application system (PDES-01 AM, NPI Electronic Instruments). Application of the drugs via the fast pressure application system has several advantages: precise localization of the pressure application pipette as well as exact timing of the neurotransmitter application.

Establishing of the pressure application in sciatic nerve slices

All experiments have been performed in the presence of the following drug cocktail: inhibitor for voltage-gated sodium channels (TTX, 1µM), $GABA_A$ receptors (Picrotoxin, 100µM), $GABA_B$ receptors (CGP, 5µM), NMDA receptors (CPP, 10µM), metabotropic glutamate receptors (LY341495, 50µM), nicotinic acetylcholine receptors (Mecamylamine,

50 or 100µM), α7-containing nicotinic acetylcholine receptors (MLA, 200nM), muscarinic acetylcholine receptors (atropine, 10µM) presented in the bath. The drug cocktail was used to isolate exclusively the current response mediated by AMPA/kainate receptors in Schwann cells. As previously described AMPA receptors desensitize over time (Sun, Olson et al. 2002). Therefore to inhibit desensitization of AMPA receptors and to enhance the response we included cyclothiazide (CTZ, 50µM) into the bath solution (Sun, Olson et al. 2002, Balannik, Menniti et al. 2005). Details about the used drugs are specified in the table 7. The amplitude as well as the kinetic of the current depends among other things mainly from the size of the pressure application pipette opening and the position and distance of the pressure pipette from the patched cell (Fig. 3.24). To standardize our recordings we used pipettes with the same opening size and positioned the pipette always in the same distance to the patched cell.

At the beginning of each experiment the cell was patched and electrophysiologically characterized as described in chapter 3.2. Subsequently the tip of the pressure-application pipette containing 1 mM glutamate, was positioned at a distance of 18-23µm from the middle of the soma and glutamate (1mM) was applied to the patched cell using the following drug application parameters: 30psi for 5ms.

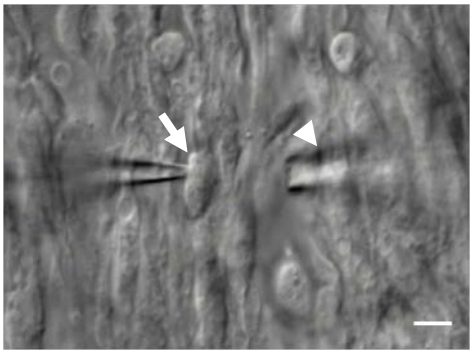

Fig. 3.24 Typical experimental arrangement for whole cell patch-clamp recording combined with pressure application of glutamate in the sciatic nerve slice.
The picture represents differential interference contrast (DIC) image of a patched Schwann cell (arrow) and the positioned pressure application pipette (arrowhead) in a 100µm thick sciatic nerve slice. The distance between the two pipettes was roughly 20µm. Scale bar: 10µm

Tab. 7 Overview of the channel and receptor blockers and antagonists

Toxin	Abbreviation	blocked channel or receptor
Tetrodotoxin	**TTX**	selective reversible inhibitor of voltage-gates sodium channels
Cyclothiazide	**CTZ**	positive allosteric modulator of AMPA receptors, that inhibits AMPA receptor desensitization
Picrotoxin		non-competitive antagonist for the $GABA_A$ receptor
Pyridoxalphosphate-6-azophenyl-2',4'-disulfonic acid tetrasodium salt	**PPADS**	non-selective P2 purinergic antagonist
(3-Aminopropyl) ethylphosphinic acid hydrochloride	**CGP**	competitive antagonist of the $GABA_B$ receptors
(2S)-2-Amino-2-[(1S,2S)-2-carboxycycloprop-1-yl]-3-(xanth-9-yl) propanoic acid	**LY341495**	highly potent antagonist of metabotropic glutamate receptors
	CPP	potent selective and competitive antagonist of NMDA receptors
Mecamylamine hydrochloride	**Mec**	non-competitive nicotinic acetylcholine receptor antagonist
Methyllycaconitine	**MLA**	potent antagonist for α7-containing nicotinic acetylcholine receptors
Atropine		competitive antagonist of the muscarinic acetylcholine receptors

The application of glutamate leads to the receptor activation at the Schwann cell. The generated response is shown in Fig. 3.25. The rise of the inward current starts shortly after the time-point of glutamate application (in all figures labeled with a black arrow). After the response reaches the peak a long lasting decay was followed. The jitter in the response onset most likely depends from the speed of the application system, the distance of the pressure-application pipette from the patched cell and the composition of the nerve tissue surrounding the pressure application pipette and the patched cell, and other factors. Therefore the onset of the response differs from cell to cell slightly, the average time

between the start of the pressure application and the response onset was 17,4±2ms (n=50). Furthermore the amplitude of the evoked current likely depends on the distance from the pressure-application pipette to the receptors and the structure of the tissue between the pressure-application pipette and the patched cell. To standardize the application parameters we positioned the tip of the pressure application pipette always in the same distance from the middle of the cell (18-23µm) and we used pipettes with almost the same opening (3-4.5µm), and we assumed that the slice tissue had always similar composition.

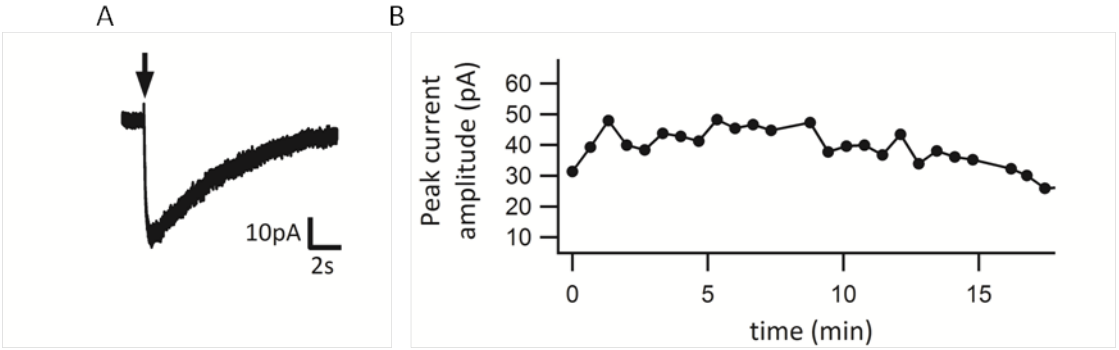

Fig. 3.25 Repetitively pressure application of glutamate.
A: Representative average of five current responses of a Schwann cell to 1mM glutamate applied via fast pressure application system. The arrow indicates the application time point. B: An example time-course of the peak current amplitude measured after pressure application of glutamate.

Fast pressure application of glutamate reliable elicited an inward current in different Schwann cell types (Fig. 3.26). Dependent from the Schwann cell type the percentage of cells that responded to glutamate differed.

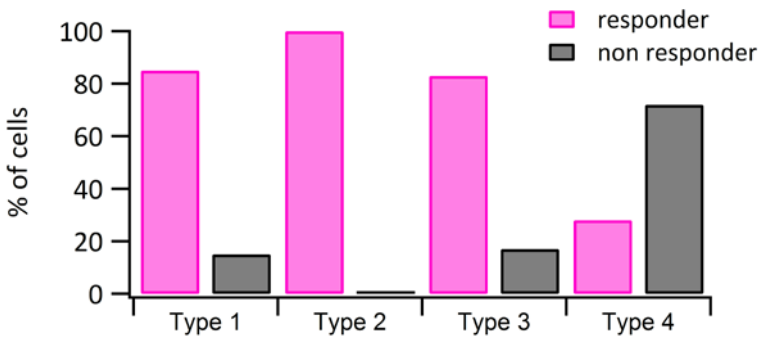

Fig. 3.26 Response of the different Schwann cell types to the pressure application of 1mM glutamate in sciatic nerve slices.
Bar graphs represent the percentage of responding (magenta) and non-responding (gray) cells.

The majority of Type 1 Schwann cells react to the pressure application of glutamate. 17 out of 20 Type 1 Schwann cells (85% of the cells) show an inward current as response to glutamate application, three cells failed to show a response. Responses are detectable in both age groups, their average peak current amplitude is with 62.2±14pA in E16-18 animals

(n=10) and 84.6±32pA in P0-2 animals (n=5) not statistically different (t-test, p>0.05) (Fig. 3.29). Schwann cells of Type 2 always showed a response to glutamate (n=21). The responses were present in both age groups with comparable average peak current amplitude of 39.7±8pA in E16-18 animals (n=10) and 41.5±9pA in P0-P02 animals (n=11) (Fig. 3.29). 83% (4 out of 5 cells) of the Type 3 Schwann cells show an inward current upon pressure application of glutamate. All cells of this Schwann cell type were recorded in animals between P0-2. The average peak current amplitude was 49.5±19pA (n=4). Schwann cells of Type 4 are inhomogeneous related to the current response after glutamate application. In contrast to the three other Schwann cell types only four out of 19 Type 4 cells (21% of the cells) respond to the glutamate application with a clear inward current. As Type 4 cells are only present in the second age group (P0-2), all cells were recorded in the single age group after birth. The elicited inward currents show an average peak current amplitude of 53.7±40pA (n=3). 11 out of 19 cells (53% of Type 4 cells) show no response to glutamate application. In 21% of Type 4 cells (4 out of 19) a small outward current of 8.5±2pA (n=4) could be observes. This outward current was only reported in Type 4 Schwann cell and was not further characterized (Fig. 3.29).

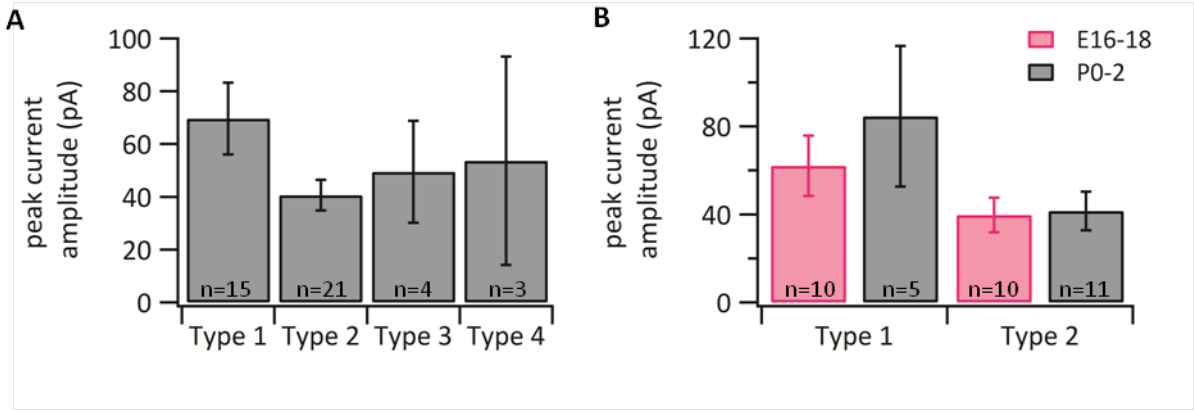

Fig. 3.27 Pressure application of glutamate elicits inward currents in the different Schwann cell types.

A: Average peak current amplitude of the responding cells. B: Comparison of the average peak current amplitude in Type 1 and Type 2 Schwann cells from animals of the two different age groups, E16-18 (magenta) and P0-P2 (black). In (A) and (B) data shown mean±SEM.

In summary, Schwann cells in the mouse sciatic nerve differ in their expression of functional glutamate receptors. Schwann cells of Type 2 appear to express always functional receptors at their surface. The majority of Type 1 (85%) and Type 3 (81%) cells convey a reliable inward current in response to the pressure application of glutamate. Furthermore Schwann cells of

Type 1 show slightly higher average peak current amplitude. Schwann cells of Type 4 are the cells with the highest percentage of cells that don't response to glutamate application; nevertheless 21% of these cells show a clear and stable response.

Although pressure-application of drugs has several advantages, one of its major drawbacks (when combined with whole-cell patch-clamp recordings) is that it may cause movement of the tissue and appearance of the 'current' response triggered by this mechanical artefact. Therefore, we wanted to test whether such type of artefacts occurs in our system and whether they affect glutamate-induced currents in Schwann cells.

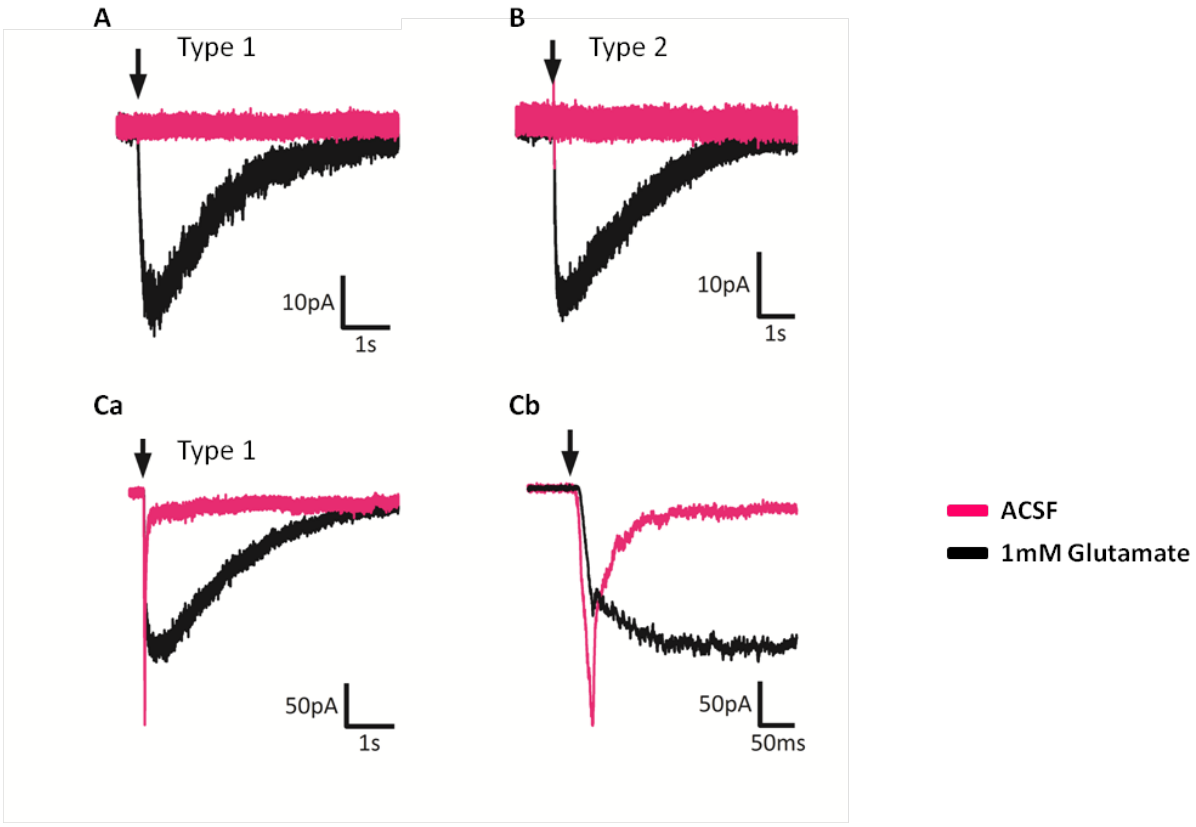

Fig. 3.28 Pressure application of ACSF and glutamate to different Schwann cell types.
A-B: Averaged current responses of Type 1 (A) and 2 (B) Schwann cells to ACSF (magenta) and glutamate (1mM, black) application. Arrow represents the time of the ACSF or glutamate pressure application. A-B: Cells revealed a clear response to glutamate (black) and no response to ACSF (magenta) application. All traces represent averages of 5 single traces. Ca: Only Schwann cell that shows response to glutamate and to ACSF. Cb: Enlargement of the traces in Da. Traces in A and B are averages of 5 single traces.

In these experiments we first patch-clamped a Schwann cell and characterized it electrophysiologically (as described in chapter 3.2.). Pressure application pipette contained ACSF, which was applied to the patched cells using the same application parameters

(pressure: 30psi, duration: 5ms) which we used for glutamate application (see above). In total we applied ACSF to eight cells, and in four of them ACSF application was followed by a glutamate application (Fig. 3.28). In the majority of Schwann cells no current caused by the mechanical or any other destruction of the tissue was observed. Only one out of these eight cells showed a clear outward deflection in response to the ACSF application (Fig. 3.28). However the kinetics was completely different from the kinetic of glutamate mediated currents. The deflections caused by ACSF were characterized by a fast rise (11.4±1ms) and decay (5.9±2ms) (Fig. 3.28). Therefore we conclude that this happens very rarely and that we are able to discriminate responses to glutamate, which are characterized by a slower kinetic, from the deflection to the applied ACSF by their kinetic differences.

3.6.1. AMPA RECEPTOR EXPRESSION BY DIFFERENT SCHWANN CELL TYPES

In the previous chapter we have identified a glutamate-mediated current in the different Schwann cell types. The drug cocktail that was used in the former experiments indicate that the current was mediated by AMPA/kainate receptors. As an additional proof that the current is not mediated by receptors not blocked by our used drug cocktail, we applied the non-competitive AMPA receptor antagonist GYKI53655. Different studies document that a low concentration of GYKI53655 (~20µM) almost exclusively inhibits AMPA receptor mediated responses and only a high concentration affects the kainate dependent response (Paternain, Morales et al. 1995, Wilding and Huettner 1995, Bleakman, Ballyk et al. 1996).

To control that our fast pressure-application system works reliable and the response is stable over several minutes, we applied during several control experiments glutamate over a longer period repetitively and monitored the recorded response (n=3, Fig. 3.25). The long-term experiments clearly show that the response to the pressure application is stable over several minutes (Fig. 3.25). In addition the recording time of 40s is long enough; during that time the current decays back to the baseline.

At the beginning of each experiment the cell was patched and electrophysiologically characterized as described in the chapter 3.2. Glutamate was applied via pressure-application system. After a stable response was evoked, the antagonist was applied via the bath solution. The glutamate response was monitored during the whole time in the different Schwann cell types (Fig. 3.29).

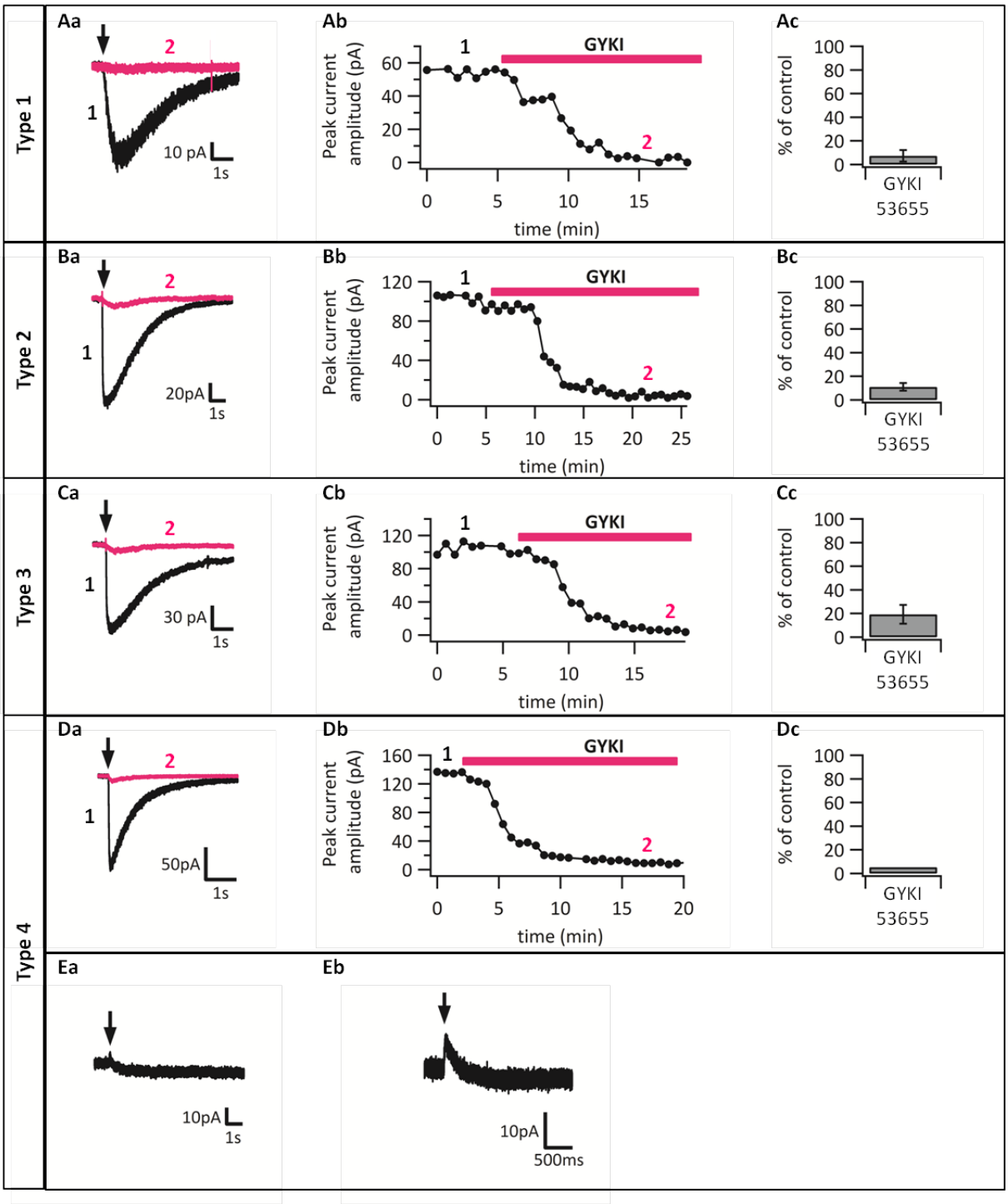

Fig. 3.29 Pressure application evoked glutamate responses at different Schwann cell types are almost completely abolished by the AMPA receptor antagonist GYKI53655.

Aa, Ba, Ca, Da: Averaged example traces under control conditions (black) and with GYKI53655 in the bath (magenta) of the four different Schwann cell types. Arrow indicates the point in time of the glutamate application. Ab, Bb, Cb, Db: Time course of the antagonist wash-in. The numbers indicate the time-point at which the traces in part a of the figure were collected. The magenta bar indicates the application time of GYKI53655. Ac, Bc, Cc, Dc: Bar graph showing the effectiveness of the GYKI53655 application in % of the control. Data present in mean±SEM. E: Example trace of Type 4 cells which show no response (Ea) or an outward (Eb) current after pressure application of glutamate.

Fig. 3.29 represents the responses of the different Schwann cell types to pressure-applied glutamate. All four different Schwann cell types are able to response to glutamate. The application of GYKI53655 via bath shows in the different Schwann cell types the typical wash-in kinetic (Fig. 3.29). The inhibitory effect of GYKI53655 was after approximately five to seven minutes observed (Fig. 3.29). After additional 10 to 15 minutes an almost complete block was visible in the different Schwann cell types. In Type 1 cells only 7.4±5% (n=3), in Type 2 cells 11±3% (n=6), Type 3 cells 19±8% (n=4), and Type 4 cells 5% (n=1) of the original current remained at the time-point when the effect of the antagonist has reached its steady-state. We therefore conclude that the majority of the glutamate evoked inward current in different Schwann cell types was mediated by AMPA receptors.

Investigation of the AMPA receptor subunit composition in Schwann cells

As mentioned in the introduction, the sensitivity to toxins can be used as a property to investigate the expression of GluA2-lacking AMPA receptors. Philanthotoxin, a polyamine toxin, is selectively blocking GluA2-lacking AMPA receptors and shows no effect at GluA2-containing receptors (Verdoorn, Burnashev et al. 1991, Jonas and Burnashev 1995). Therefore we use philanthotoxin to indicate the involvement of GluA2-containing AMPA receptors in our glutamate evoked inward current.

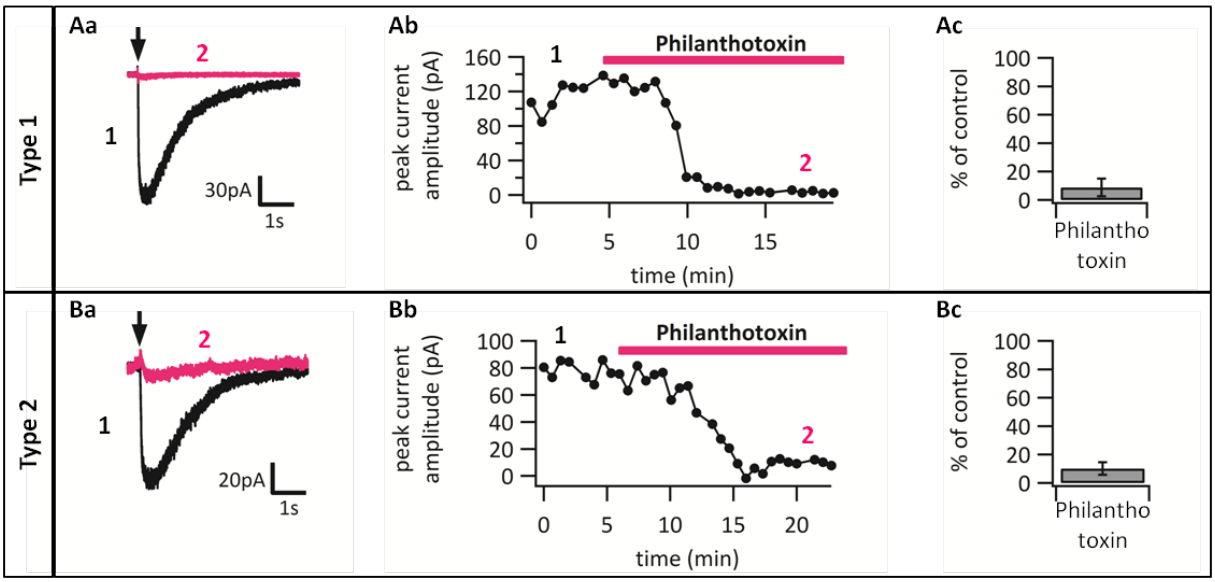

Fig. 3.30 Schwann Cells of Type 1 and Type 2 express GluA2-containing AMPA receptors.
Aa-Ba: Averaged example traces of 5 single traces before (black) and after philanthotoxin application (10µM, magenta). Arrow indicates the time-point of pressure application. Ab-Bb: Time course of philanthotoxin application. The numbers indicate the time-point at which the traces in part a of the figure were collected. The magenta bar indicates the duration of the antagonist application. Ac-Bc:

Summary bar graph shows the effect of the philanthotoxin application as % from the control condition without philanthotoxin. Data present in mean±SEM.

The application of philanthotoxin was performed in Schwann cells of Type 1 and Type 2. Philanthotoxin was applied via the bath and a clear wash-in kinetic after five to seven minutes was observed. The majority of the inward current elicited by the pressure application of glutamate was inhibited by philanthotoxin in Schwann cells of Type 1 and 2. In Schwann cell of Type 1 the glutamate-induced current was inhibited by 91.1±6% (n=2), while in Type 2 cells it was inhibited by 89.8±4% (n=4) after the application of philanthotoxin via bath. This experiment shows that the majority of the AMPA receptors expressed by the Schwann cells of Type 1 and Type 2 are sensitive to philanthotoxin. Therefore we can conclude that a high proportion of the AMPA receptors in these two types of Schwann cells are lacking edited GluA2-subunit. The application to Type 3 cells was not possible because of the rare appearance of this cell type. In addition as only a minority (21%) of Type 4 Schwann cell respond to glutamate with an inward current, philanthotoxin application was not performed in this cell type.

Summary of Chapter 6

The investigation of the presence of glutamate receptors with the help of the pressure-application system shows that the different Schwann cells types express functional glutamate receptors at their surface. The majority of Type 1 cells (85% of the recorded cells) express AMPA receptors lacking the GluA2-subunit. We could in all investigated Type 2 cells observe a response to the pressure application of glutamate. Furthermore the majority of these receptors are from the AMPA type lacking the GluA2-subunit. Also the majority of Type 3 cells (83% of the cells) express functional glutamate receptors of the AMPA type. In contrast, in the majority of Type 4 cells (58%) we could not observe a response to the application of glutamate. Nevertheless, in 4 out of 19 cells the pressure-application of glutamate leads to an inward current.

3.7. GLUTAMATE-MEDIATED INTERACTION BETWEEN SCHWANN CELLS AND AXONS IN THE SCIATIC NERVE OF MICE

So far we could demonstrate that Schwann cells in the mouse sciatic nerve express functional glutamate receptors in our slice preparation. In the next step of our study we wanted to investigate whether a direct connection via the neurotransmitter glutamate between Schwann cells and axons in the sciatic nerve is possible. It has been shown previously that axons in peripheral nerves are able to release neurotransmitters, in particular glutamate and acetylcholine, along the axons (Zakharenko, Chang et al. 1999, Wieraszko and Ahmed 2009). The released neurotransmitter may subsequently bind to the corresponding receptors expressed by Schwann cells. To test this hypothesis, we performed patch-clamp experiments of Schwann cells in sciatic nerve slice and stimulated the nerve axons electrically. We assumed that if the neurotransmitter glutamate is released along the axons, electrical stimulation of axons may trigger this release. The released neurotransmitter binds at the receptors expressed by Schwann cells und leads to the observed inward current.

We used electrical stimulation of the axons in the sciatic nerve to trigger the release of neurotransmitter along the axons. In addition we patch-clamped the cells and recorded the current in response to the electrical stimulation. Different stimulation paradigms (single pulse, 2-pulses and a train of pulses), stimulation pipettes (monopolar and bipolar stimulation with silver-chloride and tungsten electrodes) and stimulation positions were used during our study. Figure 3.31 summarizes the major stimulation models used in our study.

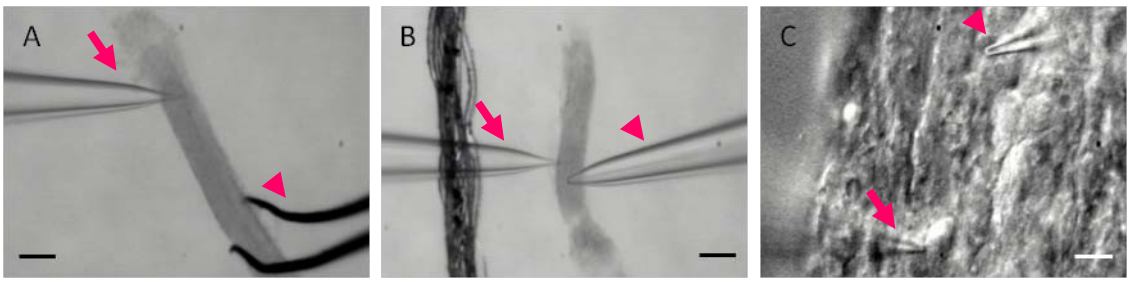

Fig. 3.31 Different experimental arrangements used for stimulation of axons combined with patch-clamp recordings of Schwann cells in the sciatic nerve slices.
A: Bipolar electrode (Tungsten) is used for stimulation of axons. B: Monopolar electrode is used for stimulation of axons. Monopolar electrode consists of a silver-chloride wire placed into the glass pipette which is filled with ACSF. C: Higher magnification of stimulation with monopolar electrode. The electrode opening is much smaller than in B. In all panels arrowhead points to stimulation electrode, and arrow points to the patch-pipette. Scale bar: 60µm (A,B), 10µm (C).

The experiments were performed with the antagonist for NMDA receptors (CPT, 1µM) and a blocker of the desensitization of AMPA receptors (CTZ, 50µm) in the bath. We started our experimental series using monopolar stimulation with a glass pipette, positioned closely to the cell (around 20-40µm, Fig. 3.31) or more far away (around 100-200µm, Fig. 3.31) from the patched cell. This model was based on stimulation experiments performed in different regions of the central nervous system to investigate the interaction between neurons and glial cells, especially oligodendrocyte precursor cells (Bergles, Roberts et al. 2000, Kukley, Capetillo-Zarate et al. 2007).

In total 21 Type 2 Schwann cells were patched. In 52% of the Type 2 cells a current was generated in response to electrical stimulation. In 14% of the cells only a single response could be obtained by monopolar electrical stimulation. We were not able to elicit a repetitive response to monopolar stimulation. In these cells a further characterization was not possible. Different reasons that might explain that observation will be discussed in the discussion part. In 48% (10 out of 21) of these cells no currents could by elicited by electrical stimulation of the axons. In most of the experiments different stimulation positions and different stimulation intensities were tried. Nevertheless a current could by not detected. There could be different explanations for this phenomenon that will be discussed in the discussion part.

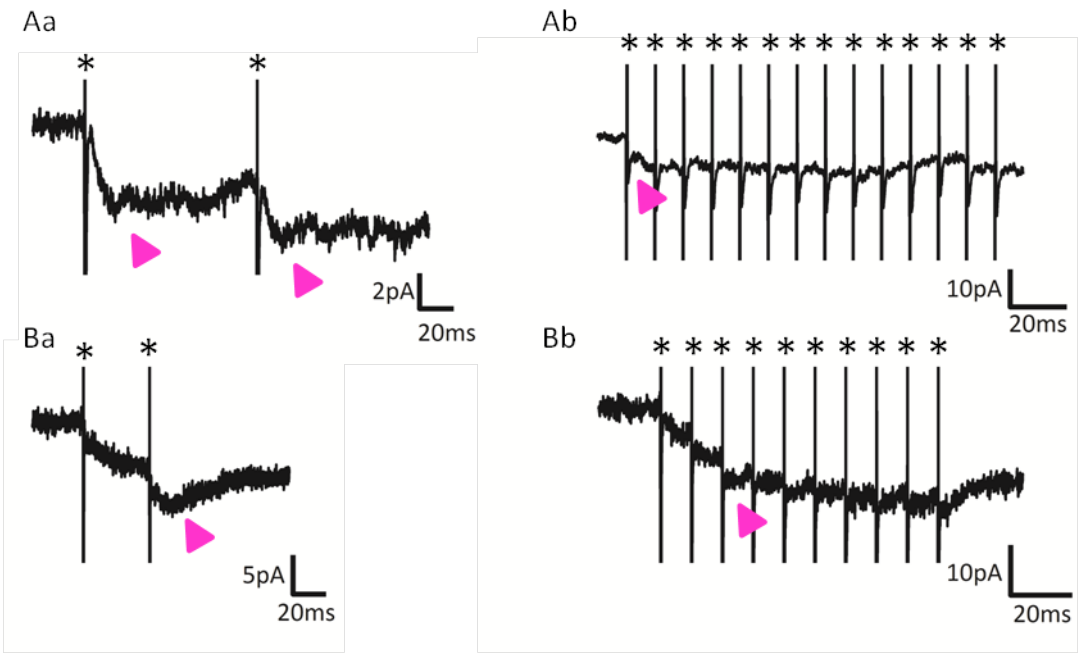

Fig. 3.32 Currents elicited by electrical stimulation of axons in the sciatic nerve slice.
Aa: Typical fast response of Type 2 cells after paired-pulse stimulation. Ab: The same cell shows a response to a train of stimuli 14@100Hz. Ba: Typical slow response to paired-pulse stimulation of a Type 2 cell. Bb: Response of the same cell to a train of stimuli (10@100Hz). The star indicates the stimulus artefact and the arrowhead indicates the response.

Fig. 3.32 shows two typical responses of Type 2 Schwann cells to electrical stimulation. The amplitude of the currents in Schwann cells which responded to electrical stimulation of axons varies between 5 and 12pA (average: 8.8±0.8pA, n=11). The kinetic of the current divided the Type 2 cells in two categories. The first category is characterized by a relatively fast rise time, which varies from 3 to 13ms (average: 7.4±2ms, n=5) and the second category is marked by a slower rise time between 32 and 52ms (average: 42.3±6ms, n=3). Fig. 3.33 indicates the difference in the onset kinetic between the two categories of Type 2 cells.

To further investigate the stimulated current recorded in Type 2 cells, we patched a Schwann cell in the sciatic nerve slice and stimulated the surrounding axons. After a stable response was established TTX, an inhibitor of voltage-gated sodium channels, was applied via the bath. These experiments were conducted to explore the dependence of the stimulated currents from the activation of voltage-gated sodium channels. These recordings could only be obtained in three stable Type 2 cells. Figure 3.33 shows the effect of TTX on the currents in Schwann cells elicited by electrical stimulation of axons.

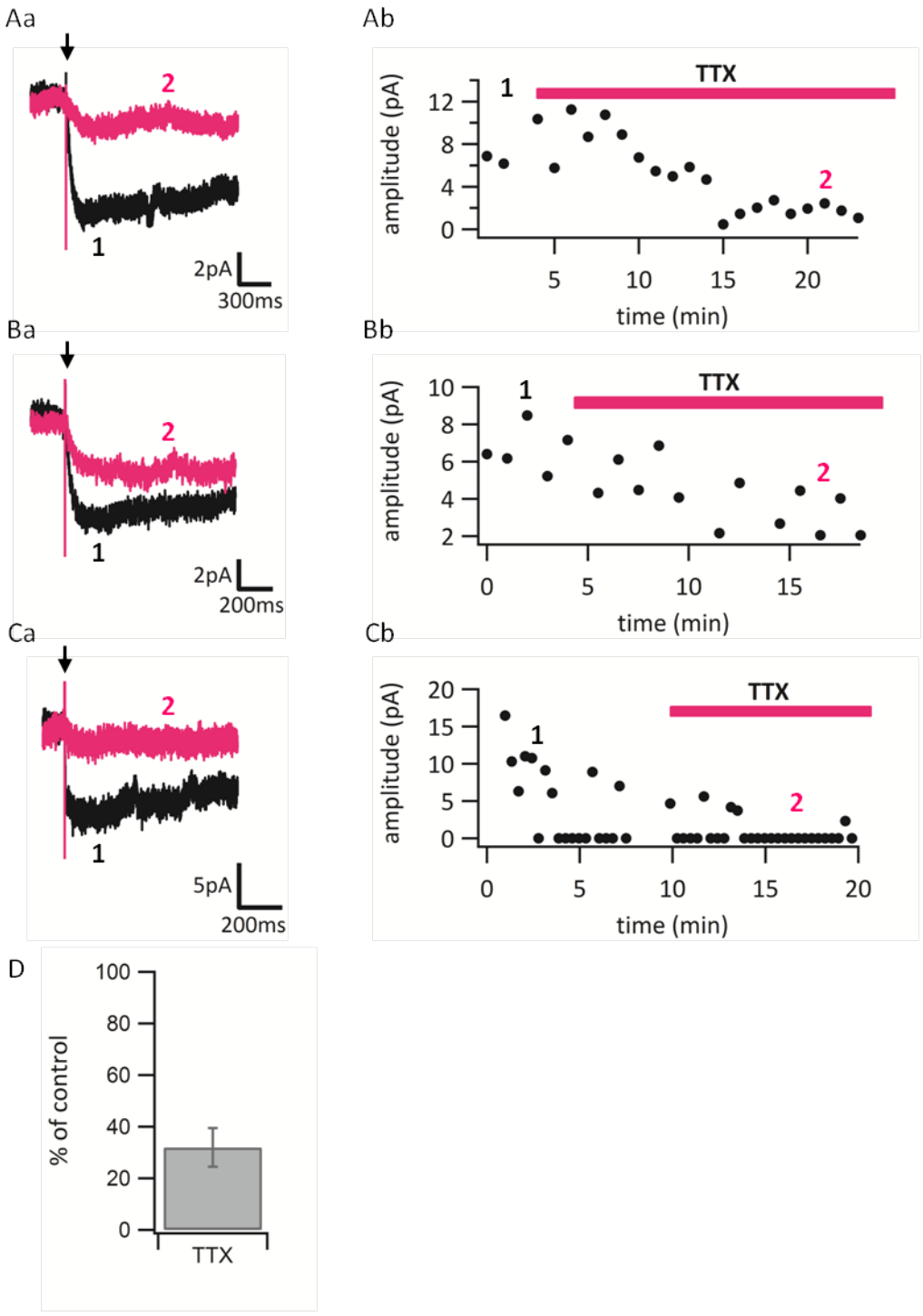

Fig. 3.33 Partial block of the stimulated current by the voltage-gated sodium channel blocker TTX in Type 2 Schwann cells.

Aa, Ba, Ca: Example traces before (black) and during (magenta) TTX application of three different Type 2 cells. Ab, Bb, Cb: Time course of the peak amplitude before and during TTX application. D: Summary bar graph of the averaged current left over during the TTX application. Data presented in mean±SEM.

In all three investigated cells TTX only partially inhibits the current evoked by electrical stimulation of axons. In two cells the majority of the current was inhibited by TTX by (72-79%), while in the third cell the current was inhibited by TTX only by 54% (Fig. 3.33). One possible explanation of this partial block might be the existence of TTX-insensitive voltage-gated sodium channels in peripheral nerve axons (Buchanan, Harper et al. 1996). Further details will be discussed in the discussion part.

An additional described feature of TTX-insensitive currents is the relatively slow activation time, which is more than two times slower than that described for TTX-sensitive currents (Kostyuk, Veselovsky et al. 1981, Elliott and Elliott 1993). This might explain the slower currents as a result of the participation of slow TTX-resistance sodium channels. Nevertheless additional experiments still need to be done, to proof whether the current is of synaptic origin or founded by neurotransmitter spillover or by the activation of metabotropic glutamate receptors. Further details will be debated in the discussion part.

Summary of Chapter 7

Our experiments show that approximately 50% of the recorded Type 2 cells respond to the electrical stimulation of axons with a small inward current. We observed two categories of currents in Type 2 cells. The first category was dominated by a faster kinetic, while the second category was characterized by a much slower kinetic. Furthermore, we demonstrated that the current in Schwann cells, evoked by electrical stimulation of axons, are partially inhibited by TTX (68.1±7.5%), an inhibitor of voltage-gated sodium channels. These findings indicate that the recorded currents are mediated by TTX-dependent action potential. The unblocked currents might be elicited by TTX-insensitive voltage-gated sodium channels expressed by axons in the peripheral nerve (Kostyuk, Veselovsky et al. 1981, Caffrey, Eng et al. 1992, Akopian, Sivilotti et al. 1996), see discussion part.

4. DISCUSSION

The establishment of the preparation of mouse sciatic nerve slices for electrophysiological recordings enables us the first time to investigate the electrophysiological properties of Schwann cells in slices. In addition the first time a combination of electrophysiological and morphological characterization was performed. Furthermore the whole study was realized in early developmental stages in the Schwann cell lineage starting from E16 to P02. All this achievements enables us to have a closer look at Schwann cells in a critical period of the development in the peripheral nervous system.

4.1. CLASSIFICATION OF THE ELECTROPHYSIOLOGICAL DIFFERENT SCHWANN CELL TYPES INTO THE EXISTING SCHWANN CELL LINEAGE

Our first electrophysiological investigations showed that we can, dependent from the age differentiate up to four different Schwann cell types. We performed our experiments in two different age groups. The youngest investigated age group was E16-E18. At this age group we expected in accordance with the literature Schwann cell precursor cells and immature Schwann cells in the sciatic nerve (Jessen, Brennan et al. 1994, Jessen and Mirsky 1999, Jessen and Mirsky 2005). Our recordings in the early age group show the presents of two different Schwann cell types (Type 1 and Type 2).

Schwann cells of Type 1 were characterized by a small voltage-independent leak and a small voltage-dependent total steady state outward current (Tab. 4). This cell type has by far the highest membrane resistance (3.37±0.5 GΩ). Further investigation exhibit the absence of voltage-gated sodium channels in this cell type. The application of 4-AP and the use of different pre-pulse protocols reveal the absence of an I_A-like current (Fig. 3.8.). It is established that 4-AP is blocking dependent from the concentration I_D-like currents (low concentration, 50µm) and in addition I_A-like potassium currents (high concentration of 4-AP, 5mM)(Storm 1990, Beck, Ficker et al. 1992, Albert and Nerbonne 1995, Locke and Nerbonne 1997). The experiments performed to investigate the presence of voltage-gated potassium channels were carried out with a high concentration of 4-AP (5mM), assuming that we block I_D- and I_A-like currents. These experiments show that the group of Type 1 Schwann cells is inhomogeneous in this feature. Half of the cells express only the slow activating and slow inactivating I_K-like current, while the other half expresses the faster I_D-like current and the

slow activating and inactivating I_K-like current (Fig. 3.9.). Schwann cells of Type 1 are characterized by the expression of a small amount of slower I_D- and/or I_K-like potassium channels. Baker et al. published 1992 a study performed in rabbit neonatal sciatic nerve. They investigated cultured Schwann cells with the help of whole cell patch clamp recordings. They found a Schwann cells type, called Type II, that is characterized by slow activating potassium channels (activation gating time constant around 15ms) (Baker, Howe et al. 1993). This activation gating time constant of around 15ms is comparable with the $Tau_{activation}$ (as well around 15-16ms) of the slow activating potassium channel present in each Type 1 Schwann cell investigated in our study. The morphological investigation exhibit the particular shape of the cell type. It is characterized by a small roundish soma, from that several primary processes originate. This cell type is the shortest of all Schwann cell types investigated in our study with the finest processes. In contrast to all other Schwann cell types more than two primary processes can arise from the nucleus (Fig. 3.11.). Another special feature of this Schwann cell Type 1 is the branching of the processes, no other Schwann cell type branches that much. The marker profile of this cell type is as well unique. First of all the majority of cells are positive for Sox10, the major marker of the Schwann cell lineage that is mainly located in the nucleus (Finzsch, Schreiner et al. 2010). The few cells that are negative for Sox10 might result from the patching process. During that process the cytoplasm of the cell gets replaced by the internal solution of the patch pipette. Rehberg et al. described the transfer of Sox10 out of the nucleus in the cytoplasm (Rehberg, Lischka et al. 2002). If the majority of Sox10 is transferred to the cytoplasm, it might be washed out during the patching process and the cell appeared to be $Sox10^-$. Schwann cells of Type 1 are negative for GFAP and MBP. The negative results for MBP, a typical marker for myelinating Schwann cells, and the appearance of the cell before birth indicate an early position in the Schwann cell lineage development (Jessen and Mirsky 2005). As the cell type is negative for GFAP, it suggested that it presents a very early Schwann cell type, like a Schwann cell precursor, which is known to be GFAP negative (Jessen, Morgan et al. 1990, Jessen and Mirsky 2005). The electrophysiological and morphological characterization, as well as the marker profile and its presence before birth suggest that Schwann cells of Type 1 present an early Schwann cell progenitor (Fig. 4.1).

Schwann cells of Type 2 are present in the age group before birth and after birth. They are characterized by a small voltage-independent leak current (12.26±2.3pA) and the largest

steady state outward current (664.14±56pA) of all Schwann cell types (Tab. 4). The majority of cells (71%) express TTX-sensitive voltage-gated sodium channels, which show similar activation properties (~ 0.15ms) and reach the maximum between -10 and -20mV like sodium channels expressed in the CNS by neurons and NG2 cells (Steinhauser, Kressin et al. 1994, Gilly, Gillette et al. 1997, Catterall 2000). It is the only Schwann cell types in our preparation that express voltage-gated sodium channels. A study performed in cultured rabbit Schwann cells of the sciatic nerve and the vagus nerve showed the presence of sodium channels with a much slower activation kinetic (time-to-peak between 0.96 and 1.15ms) (Howe and Ritchie 1990). The differences between our results and the study of Howe and Ritchie may result from the fact that the experiments where performed in different species (our studies was performed in mice and the other study was performed in rabbits) and in a different age rage (our study: E16 to P02; Howe study: adult animals). In addition, the Schwann cells in the Howe study were cultured several days before the electrophysiological investigation, therefore a change in the channel distribution and properties may occur.

A large proportion of the total outward currents are elicited by voltage-gated potassium channels. The further investigation of this channels indicate that Type 2 Schwann cells express an I_A-like current that is blocked by 4-AP and could be investigated with the help of two different pre-pulse protocols (Fig. 3.8). The $Tau_{activation}$ of the I_A-like potassium current (2.4±0.3ms) was comparable with potassium channels expressed by one cultured rabbit Schwann cells type. Bake et al. characterized in cultured rabbit neonatal sciatic nerve Schwann cells with the help of whole cell patch clamp recordings a cell type, called Type I, in 1993. The cell type is marked by a fast gating time constant, which was below 3ms (Baker, Howe et al. 1993). The investigation of the slower voltage-dependent potassium channels exhibits the presence of two different components in all Schwann cells of Type 2. They express an I_D-like current with a faster rise than I_K-like currents and a slower rise as an I_A-like current. The I_D current expressed by Type 2 cells seems to have the same kinetic properties like that of the Type 1 Schwann cells, both show a $Tau_{activation}$ of 4.7±1ms (Type 1) and 4.9±0.2ms (Type 2). This might indicate that both Schwann cells express the same I_D-like channels. Also comparisons with I_D-like currents expressed by different neurons in the CNS designate similar kinetic properties. Isolated superior colliculus-projecting (SCP) visual cortical neurons express as well I_D-like channels with an activation kinetic of approximately

4ms (Albert and Nerbonne 1995). In addition, I_D-like channels could be observed in callosal-projecting visual cortical neurons. They also exhibit similar $Tau_{activation}$ of 3ms (Locke and Nerbonne 1997). The second slow activating and slow inactivating voltage-dependent potassium channel expressed by Type 2 cells shows an even slower $Tau_{activation}$ with 37.2±4ms than I_K-like currents expressed by Type 1 Schwann cells. Nevertheless the activation kinetic is still in the rage of I_K-like currents investigated in neurons (Storm 1990). The difference in the activation kinetic indicates that Schwann cells of Type 1 and 2 might differ in the expression of distinct subtypes of I_K channels. Further investigation of the sustained voltage-gated potassium channels with the help of 4-AP and TEA indicate that the majority (87%) of voltage-dependent channels expressed by Schwann cell of Type 2 are sensitive for 4-AP. Although 4-AP is not completely specific for I_D channels, a higher sensitive of I_D channels for 4-AP was reported (Beck, Ficker et al. 1992, Albert and Nerbonne 1995, Locke and Nerbonne 1997). In addition, the results from our pre-pulse protocol experiments indicate that 2/3 of the sustained current is mediated by the I_D-like current with the faster $Tau_{activation}$. To summarize, 2/3 of the sustained current is mediated by the 4-AP sensitive I_D-like current, the pre-pulse protocol experiments confirm this. The percentage of the current blocked by TEA is with 44% much lower, also the results from the pre-pulse protocols indicate that 1/3 of the slow activating sustained current is mediated by the I_K-like current with a slow $Tau_{activation}$. A study performed 1998 in cultured trout lateral line nerves shows the presence of a cell that exhibit fast activating potassium channels comparable with our results, which are partially blocked by 4-AP and TEA (Rabe, Ritz et al. 1998). Rabe and his colleagues investigated one Schwann cell type, which possess voltage-gated potassium channels partially sensitive to 4-AP (around 70% of the current was blocked) and with a minor sensitivity to TEA (Rabe, Ritz et al. 1998). We conclude that Schwann cells of Type 2 express a subset of voltage-dependent potassium channels; I_A, I_D and I_K like channels could be determined during our experiments.

The morphology of Type 2 Schwann cells is characterized by a bipolar appearance. In the vast majority two primary processes originate from the elongated soma. The processes are not branched and the cell is longer than Type 1 cells. The cells of Type 2 are positive for the marker Sox10 and GFAP and they are negative for MBP. The appearance of the cells before and after birth indicates that it is one of the Schwann cell progenitors. As the cells are positive for GFAP, they might not belong to the early Schwann cell precursors (Jessen,

Morgan et al. 1990, Jessen and Mirsky 2005). In addition, the probability of patching this Schwann cell type was in both age groups relatively high. This effect might reflect the relatively high availability of this Schwann cell type in the tissue during our recorded age groups. In accordance to the literature immature Schwann cells are the major Schwann cell type present in the mouse nerve shortly before and after birth (Jessen, Brennan et al. 1994, Jessen and Mirsky 2005). Furthermore the absence of MBP, a major marker for the myelination together with the appearance of the cells before birth indicates that Schwann cells of Type 2 don't represent myelinating Schwann cells. The morphological distinction between Schwann cells of Type 1 and Type 2 might indicate the development from the progenitor (Type 1) to the more advanced stage with a closer contact to a few axons by their two elongated non branched primary processes (Type 2). In summary the discussed results might indicate that Schwann cells of Type 2 represent the group of immature Schwann cells.

Schwann cells of Type 3 are only present in the age group after birth, which indicates already that they represent a more mature Schwann cell type in the lineage (Jessen and Mirsky 2005). In addition this type was only rarely patched during the whole study, which may indicate that the cell is only infrequently present in the investigated age group. Otherwise, this effect may occur because of a subjective pre-selection of the patched cells. Type 3 Schwann cells are characterized by a large voltage-independent leak current (93.3±15pA) and the smallest voltage-dependent steady state outward current (86.9±23pA). The membrane resistance is with 0.08±0.01GΩ smaller than in Type 1 and Type 2 cells. Sharp electrode recording of cells of the medial stellar nerves of three species of squid (*Loligo forbesi*, *Loligo vulgaris*, *Loligo bleekeri*) show the presence of a cell type that shares the profil of voltage-dependent outward currents with the Type 3 Schwann cell investigated in our study (Inoue, Tsutsui et al. 2002). The morphology of the cell is characterized by a bipolar shape: two primary processes originate from the two poles of the elongated soma. This cell type exhibits the longest processes, which are never branched. The processes are thicker than that of Type 1 but thinner than that of Type 4. The few stainings performed in this type show that it belongs to the Schwann cell lineage ($Sox10^{+}$) and that it is positive for GFAP. As the cell is only superficial investigated we can only speculate about its position in the Schwann cell lineage. As it is present only after birth and it is positive for GFAP, we can exclude that it represents an early Schwann cell precursor or an immature Schwann cell (Jessen, Morgan et al. 1990, Jessen and Mirsky 2005). Former studies show that at the day of

birth the cells start to differentiate into myelinating Schwann cells; around the second postnatal week the maturation of non-myelinating Schwann cells follows (Jessen and Mirsky 1998, Jessen and Mirsky 1999). The number of non-myelinating Schwann cell is at the date of birth and early postnatal very low (Jessen and Mirsky 2005), which is in accordance with the low number of this cell type found in the nerve during our recordings . Another cell type that is only present after birth and where the cell number decreases by aging is the pro-myelinating Schwann cell (Friede and Samorajski 1968). We therefore assume that Schwann cell of Type 3 re-presents the group of pro-myelinating or non-myelinating Schwann cells (Fig. 4.1).

Schwann cells of Type 4 are as well as Type 3 cells only present after birth and therefore representing a more mature stage of the Schwann cell lineage. This cell type is characterized by the highest voltage-independent leak current (141.5±12pA) and a relatively small voltage-dependent steady state outward current (283.7±32pA) in comparison with the other Schwann cell types. Likewise Type 3 cell they reveal a low membrane resistance (0.06±0.01GΩ). Both cell types that are present only after birth express in comparison with the cells that are already present before birth a high amount of leak channels and a low amount of voltage-gated channels. In addition the cells after birth are characterized by a strong decrease in the membrane resistance. We therefore conclude that the maturation of Schwann cells is characterized by a strong change in the electrophysiological properties. Schwann cells of Type 4 appear in a bipolar shape. Two primary processes arise from the soma. These cells possess the thickest processes from all investigated cell types (2.92±0.2µm). The processes are long and never branched. Brown et al. performed in the most medial third order giant axons from adult *Loligo forbesi* and Loligo vulgaris a morphological study that showed an elongated Schwann cell with an elongated soma and two long processes that surround single axons (Brown, Bone et al. 1991). This described cell type seems to share characteristic properties with the Type 4 Schwann cell of this study. The appearance after birth and the fact that the probability to patch a cell of this type increased by age, as well as the thickness of the processes already indicate that Type 4 cells may represent the myelinating Schwann cells. The marker profile of this cell Type is supporting our assumption. Schwann cells of Type 4 are always positive for the myelination marker MBP, a major marker of myelinating Schwann cells. However some of the Type 4 cells are positive for GFAP, which is a marker of immature and non-myelinating Schwann cells (Jessen

and Mirsky 2005). This affect can be explained by the gradually down-regulation of proteins during the development and the start of myelination. The latest investigates age in our study was P2, in this age the transition of pro-myelinating Schwann cells to myelinating Schwann cells, and therefore the process of the protein down-regulation, might not be fully finished in all cells (Jessen, Morgan et al. 1990, Jessen and Mirsky 2005). Our results suggest that Schwann cell of Type 4 represent the myelinating Schwann cell (Fig. 4.1).

During all our recording and cell fillings we never saw a cell-to-cell coupling (neither with Lucifer yellow nor with Alexa568). Therefore we conclude that Schwann cell coupling in Schwann cells of the mouse sciatic nerve in the age between E16 and P2 was not present. In contrast to our results, cell coupling was reported for Schwann cells surrounding the giant axon of the squid (Brown, Bone et al. 1991). Another study performed in freshly dissociated and cultures Schwann cells shows that the coupling of Schwann cells disappear in mature myelinating Schwann cells and was as well preserved in non-myelinating Schwann cells (Konishi 1990). It might be that the used dyes (Lucifer Yellow (457Da) or Allexa568 (~600Da)) are too large to fit through the pores of the expressed gap junction, although different studies using these dyes could demonstrate cell coupling in different cell types (Butt and Ransom 1989, Konishi 1990, Kukley, Kiladze et al. 2008) and other studies report the permeability of molecules with a size up to 1000Da (Anzini, Neuberg et al. 1997, Simon and Goodenough 1998, Evans and Martin 2002). Some earlier studies were performed with a smaller dye (376Da) (Balice-Gordon, Bone et al. 1998). In addition the charge of the dye may also play a role for the permeability of the gap junctions (Cao, Eckert et al. 1998).

Our study provided the first time a combination of electrophysiological and morphological characterization of mammalian Schwann cells in situ. In addition the marker expression of the different cells was investigated. We could discriminate four different Schwann cell types and characterized them in detail. We tried to integrate our work in the already existing knowledge about the Schwann cell lineage development (Fig. 4.1).

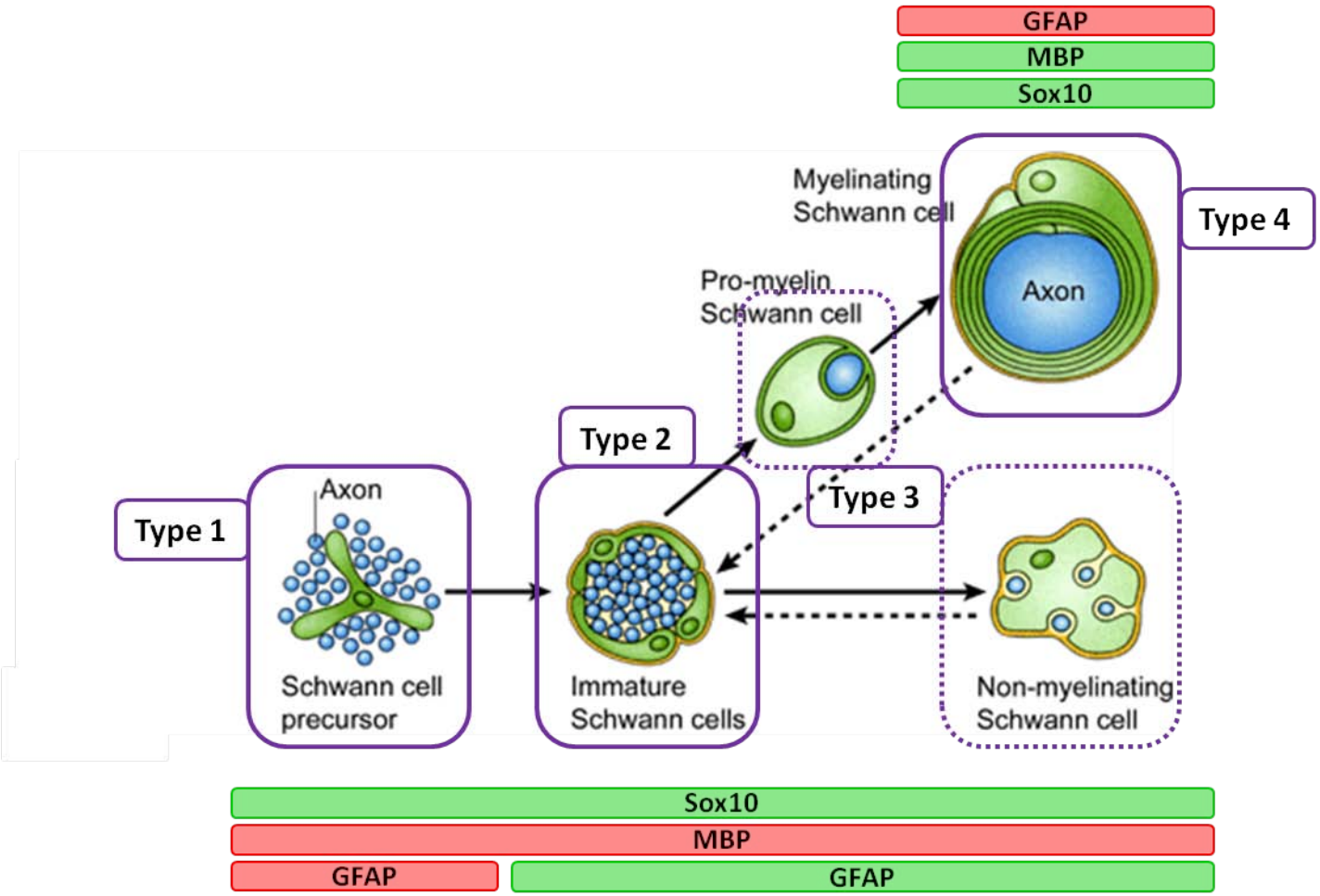

Fig. 4.1 Summary overview of the electrophysiological different Schwann cell types.
The overview summarizes the classification of the electrophysiological different Schwann cell types (purple boxes) into the already established Schwann cell lineage. The bar below and above the drawing indicate the expression (green) or the absence (red) of different important Schwann cell marker. Reproduced and modified from (Jessen and Mirsky 2005).

4.2. EXPRESSION OF FUNCTIONAL NEUROTRANSMITTER RECEPTORS AT THE DIFFERENT SCHWANN CELL TYPES

We investigated the expression of functional glutamate receptors of Schwann cells in the mouse sciatic nerve with the help of the fast pressure application system. The exploration showed that the Schwann cell types differ in their expression of functional glutamate receptors. All investigated Schwann cells of Type 2 and 21% of Type 4 cells respond with an inward current to the application of glutamate. The majority of Type 1 cells (85%) and Type 3 (83%) express as well functional glutamate receptors. Type 1 and 2 Schwann cells show in both age groups a response to the application of glutamate. The amplitude was comparable between the different types and age groups (Fig. 3.27). The inward current recorded in Type 1 and Type 2 cells could be reliable inhibited with the AMPA/kainate antagonist GYKI35655. Dependent from the Schwann cell type the efficacy of the antagonist was between 80% (Type 2) and 95% (Type 1). We therefore conclude that the majority of receptors responsible for the glutamate evoked response are from the AMPA/kainate type. Former experiments performed in squid Schwann cells showed as well a change of the membrane potential in response to the application of glutamate. Different studies showed a glutamate dependent depolarization which was followed by a long lasting hyperpolarizsation which was dependent from glutamate and acetylcholine (Lieberman, Abbott et al. 1989, Evans, Reale et al. 1991, Evans, Reale et al. 1991, Lieberman 1991, Lieberman and Sanzenbacher 1992). A clear relationship between the de- and hyperpolarization could not be drawn after the performed experiments. Nevertheless they clearly show the presence of functional glutamate receptors at Schwann cells. Lieberman et al. concluded during their study in 1992 that the depolarizing current was generated by TTX-sensitive glutamate gated Na^+ channel (Lieberman and Sanzenbacher 1992). Our experiments indicate that the majority of the current elicit by the pressure application of glutamate is generated by AMPA/kainate receptors. So far, the above mentioned experiments performed from different research groups in Schwann cells of the squid gaint axon are the only investigations of functional glutamate receptors of Schwann cell. Further studies in vertebrate show with the help of immunohistochemistry the presence of glutamate receptors at Schwann cell processes in the human skin and of AMPA receptors in Schwann cells of the peripheral vestibular system of guinea pig and rat (Dememes, Lleixa et al. 1995, Kinkelin, Brocker et al. 2000). Schwann cells of Type 1 and 2, which seem to be the more immature types, express functional glutamate receptors in both investigated age groups (Fig. 3.27). Furthermore, a down regulation of the receptors in more developed

myelinating Schwann cells (Type 4) might happen, as the percentage of receptor expressing cells drops in Type 4 Schwann cells. Another possible explanation for the decrease in the number of responding Type 4 cells could be a change of the localization of the receptors, as it is already shown for voltage-dependent channels (Mi, Deerinck et al. 1995). A special concentration of glutamate receptors at the end of the processes close to the node of Ranvier might happen in myelinating Schwann cells. As Type 4 Schwann cells are quite long and the cell expresses a lot of voltage-independent leak channels, we might not be able to record the response of the receptors at the end of the Schwann cell processes because of the space clamp problem.

Furthermore we investigated the subunit composition of the AMPA/kainate receptors present in Type 1 and 2 Schwann cells. Our experiments show that the majority of the receptors are sensitive to philanthotoxin, a specific inhibitor for GluA2-lacking AMPA/kainate receptors. We therefore conclude that the AMPA/kainate receptors expressed by Schwann cells are in the majority Ca^{2+} permeable. As the current is not completely blocked, a minor proportion of the current might be mediated by receptors containing the GluA2-subunit. Former studies underline our results and show the presence of GluA2, GluA3 and GluA4 in Schwann cells with the help immunohistochemical staining (Dememes, Lleixa et al. 1995).

As we executed our experiments with the help of the pressure application system (valve switch time <1 ms) a statement about the activation kinetics of the receptors cannot be drawn. The time that the system needs to release the glutamate as well as the time that is needed to reach the receptor is by far longer than the actual opening time of the receptors. The activation kinetics of AMPA receptors in oligodendrocyte precursor cells was in several studies characterized by a rise time of 200-350µs (Bergles, Roberts et al. 2000, Kukley, Capetillo-Zarate et al. 2007). In neurons the activation kinetic of AMPA receptors was described by a rise time of 150-250µs (Geiger, Lubke et al. 1997, Liu and Cull-Candy 2002). In addition CTZ was added in all experiments, which is as well changing the amplitude and the kinetic properties of the receptor (Bergles, Roberts et al. 2000, Fucile, Miledi et al. 2006, Hald, Ahring et al. 2009). One study performed in oligodendrocyte precursor cells described an increase in the amplitude of the current mediated by AMPA receptors and an approximately 3 fold increase in the decay time in response to the application of CTZ (Bergles, Roberts et al. 2000). Furthermore different studies performed in neurons showed

at least a 2.5 fold increase in the amplitude of the AMPA mediated current and in addition a 2 fold increase in the rise time and at least a 4 fold increase in the decay time (Liu and Cull-Candy 2002, Hald, Ahring et al. 2009).

We can conclude that Schwann cells are able to express functional glutamate receptors of the AMPA/kainate type and that with the process of maturation the number of receptors get down regulated or the distribution of the receptors at the cell surface changes. In addition we could show that the majority of receptors in Type 1 and 2 Schwann cells are sensitive to philanthotoxin and therefore lacking the GluA2-subunit, which means they are permeable for Ca^{2+} ions.

4.3. DO SCHWANN CELLS AND AXONS INTERACT WITH EACH OTHER?

With the pressure application experiments the presence of functional AMPA/kainate receptors at different Schwann cell types could be demonstrated. It is known that AMPA/kainate receptors are one of the receptors present in the synaptic cleft and involved in synaptic activation in response of pre-synaptic glutamate release. The last part of our investigation deals with the possible interaction between Schwann cells and axons. If the receptors are positioned close to the release site of the axon, a synaptic like interaction could be possible. A former immunohistochemical study shows the presence of the neurotransmitter receptors, in this case ACh receptors, which are mainly located at the cell surface facing the neighboring axon (Rawlins and Villegas 1978). This fact indicates the possibility that the expressed receptors are located closely to the neighboring release site of the axon. In addition a sniffer patch study performed at Xenopus neurons and loading experiments with non-metabolizable analog of glutamate in the mouse sciatic nerve indicate the release of neurotransmitter along the axons (Zakharenko, Chang et al. 1999, Wieraszko and Ahmed 2009). To investigate a synaptic like interaction between the axons and the Schwann cell, axons were electrical stimulated and the Schwann cell response was recorded. Our investigation shows the presence of evoked currents in a small proportion of Type 2 Schwann cells (Fig. 3.32). A possible explanation for the relatively low success rate could be explained by the small number of axons that may contact one single Schwann cell. Former studies show that especially myelinating Schwann cells have only contact to one single axon. In addition during the process of radial sorting and the maturation of the sciatic nerve the number of axons, which are in contact with one single Schwann cell, decreases (Webster 1971, Webster, Martin et al. 1973, Jessen and Mirsky 2005). Furthermore our morphological

results show that Schwann cells of Type 2, 3 and 4 possess only two major processes which are not or only rarely branched (Fig. 3.15). Most probably these two processes are in contact with the same or at most two different axons. If these few axons are destroyed during the process of cutting or during the positions of the electrodes, we are not able to detect any response evoked by electrical stimulation. If the low success rate is caused by the destruction of the axons, an enhancement in the slice preparation is needed.

The analyses of the kinetics of the evoked currents indicate the presence of two different groups of responses. The first group is characterized by a faster activation kinetic (7.4±2ms). Nevertheless, in comparison with evoked synaptic-like currents in OPC the response recorded in our cells is much slower (655±44µs (Kukley, Capetillo-Zarate et al. 2007), 406±24µs (Lin, Huck et al. 2005)). This might be caused by the added CTZ, which is known to slow down kinetic properties of the AMPA receptor. A 3fold increase of the rise time in the presence of CTZ could be reported in evoked OPC responses in the hippocampus (Bergles, Roberts et al. 2000). Furthermore the rise time of evoked currents in neurons differ between synapses, e.g. hippocampal pyramidal neurons reveal a rise time between 1 and 3 ms (Williams and Johnston 1991). These facts indicate that the evoked fast response in Schwann cells of Type 2 may represent the presence of a synaptic-like interaction between the Schwann cell and the axon. To support the dependency of the recorded evoked responses from action potential dependent stimulation of the axons, TTX was added to the bath solution. The partially block of the evoked currents indicate that at least a proportion of the evoked current was dependent from the activation of TTX-sensitive voltage-gated sodium channels at the axon (Fig. 3.33). The current that was insensitive to TTX could represent the expression of TTX-insensitive sodium channels at axons in the sciatic nerve. The expression of TTX-insensitive sodium channels is very well described for sensory neurons in the PNS (Kostyuk, Veselovsky et al. 1981, Caffrey, Eng et al. 1992, Akopian, Sivilotti et al. 1996). All this arguments underline the possibility that the current evoked by electrical stimulation of the peripheral nerve axons is at least partial induced by a synaptic-like structure, where the release site at the axons and the receptors at the Schwann cell are in close proximity.

The kinetics of the second group of responses evoked by electrical stimulation of the axons is with 42.3±6ms much slower. This very slow rise time speaks against the presence of a synaptic-like structure between axons and Schwann cells. The slow evoked response could

be described by the spillover of neurotransmitter at the release site and the activation of glutamate receptors that are not directly positioned at the release site. This distance between the release site and the receptor position may cause the increase in the rise time. The effect of spillover is described as another way of communication for different regions in the CNS (Matsui and Jahr 2003, Szapiro and Barbour 2007). Further explanation for the long rise time could be the activation of metabotropic glutamate receptors. As these receptors act via a second messenger pathway, the activation time is much slower than that recorded in ionotropic receptors (Huang, Sinha et al. 2004). The activation of metabotropic glutamate receptors may lead to an opening of potassium channels via the second messenger pathway which results in the recorded current. Nevertheless further experiments are needed to clearly demonstrate the origin of the fast and slow evoked currents in Schwann cells after electrical stimulation.

REFERENCES

Agrawal, H. C. and D. Agrawal (1991). "Proteolipid protein and DM-20 are synthesized by Schwann cells, present in myelin membrane, but they are not fatty acylated." Neurochem Res **16**(8): 855-858.

Aguayo, A. J., G. M. Bray, L. C. Terry and E. Sweezey (1976). "Three dimensional analysis of unmyelinated fibers in normal and pathologic autonomic nerves." J Neuropathol Exp Neurol **35**(2): 136-151.

Akopian, A. N., L. Sivilotti and J. N. Wood (1996). "A tetrodotoxin-resistant voltage-gated sodium channel expressed by sensory neurons." Nature **379**(6562): 257-262.

Albert, J. L. and J. M. Nerbonne (1995). "Calcium-independent depolarization-activated potassium currents in superior colliculus-projecting rat visual cortical neurons." J Neurophysiol **73**(6): 2163-2178.

Alonso, G. (2000). "Prolonged corticosterone treatment of adult rats inhibits the proliferation of oligodendrocyte progenitors present throughout white and gray matter regions of the brain." Glia **31**(3): 219-231.

Amedee, T., E. Ellie, B. Dupouy and J. D. Vincent (1991). "Voltage-dependent calcium and potassium channels in Schwann cells cultured from dorsal root ganglia of the mouse." J Physiol **441**: 35-56.

Anzini, P., D. H. Neuberg, M. Schachner, E. Nelles, K. Willecke, J. Zielasek, K. V. Toyka, U. Suter and R. Martini (1997). "Structural abnormalities and deficient maintenance of peripheral nerve myelin in mice lacking the gap junction protein connexin 32." J Neurosci **17**(12): 4545-4551.

Arroyo, E. J., J. R. Bermingham, Jr., M. G. Rosenfeld and S. S. Scherer (1998). "Promyelinating Schwann cells express Tst-1/SCIP/Oct-6." J Neurosci **18**(19): 7891-7902.

Baker, M., J. R. Howe and J. M. Ritchie (1993). "Two types of 4-aminopyridine-sensitive potassium current in rabbit Schwann cells." J Physiol **464**: 321-342.

Baker, M. D. and J. M. Ritchie (1996). "Characteristics of type I and type II K+ channels in rabbit cultured Schwann cells." J Physiol **490 (Pt 1)**: 79-95.

Balannik, V., F. S. Menniti, A. V. Paternain, J. Lerma and Y. Stern-Bach (2005). "Molecular mechanism of AMPA receptor noncompetitive antagonism." Neuron **48**(2): 279-288.

Balice-Gordon, R. J., L. J. Bone and S. S. Scherer (1998). "Functional gap junctions in the schwann cell myelin sheath." J Cell Biol **142**(4): 1095-1104.

Baumann, N. and D. Pham-Dinh (2001). "Biology of oligodendrocyte and myelin in the mammalian central nervous system." Physiol Rev **81**(2): 871-927.

Beck, H., E. Ficker and U. Heinemann (1992). "Properties of two voltage-activated potassium currents in acutely isolated juvenile rat dentate gyrus granule cells." J Neurophysiol **68**(6): 2086-2099.

Benninger, Y., T. Thurnherr, J. A. Pereira, S. Krause, X. Wu, A. Chrostek-Grashoff, D. Herzog, K. A. Nave, R. J. Franklin, D. Meijer, C. Brakebusch, U. Suter and J. B. Relvas (2007). "Essential and distinct roles for cdc42 and rac1 in the regulation of Schwann cell biology during peripheral nervous system development." J Cell Biol **177**(6): 1051-1061.

Berger, T., J. Schnitzer, P. M. Orkand and H. Kettenmann (1992). "Sodium and Calcium Currents in Glial Cells of the Mouse Corpus Callosum Slice." Eur J Neurosci **4**(12): 1271-1284.

Bergles, D. E., J. D. Roberts, P. Somogyi and C. E. Jahr (2000). "Glutamatergic synapses on oligodendrocyte precursor cells in the hippocampus." Nature **405**(6783): 187-191.

Bevan, S., S. Y. Chiu, P. T. Gray and J. M. Ritchie (1985). "The presence of voltage-gated sodium, potassium and chloride channels in rat cultured astrocytes." Proc R Soc Lond B Biol Sci **225**(1240): 299-313.

Bleakman, D., B. A. Ballyk, D. D. Schoepp, A. J. Palmer, C. P. Bath, E. F. Sharpe, M. L. Woolley, H. R. Bufton, R. K. Kamboj, I. Tarnawa and D. Lodge (1996). "Activity of 2,3-benzodiazepines at native rat and recombinant human glutamate receptors in vitro: stereospecificity and selectivity profiles." Neuropharmacology **35**(12): 1689-1702.

Boesmans, W., C. Cirillo, V. Van den Abbeel, C. Van den Haute, I. Depoortere, J. Tack and P. Vanden Berghe (2013). "Neurotransmitters involved in fast excitatory neurotransmission directly activate enteric glial cells." Neurogastroenterol Motil **25**(2): e151-160.

Bosse, F. (2012). "Extrinsic cellular and molecular mediators of peripheral axonal regeneration." Cell Tissue Res **349**(1): 5-14.

Boucsein, C., H. Kettenmann and C. Nolte (2000). "Electrophysiological properties of microglial cells in normal and pathologic rat brain slices." Eur J Neurosci **12**(6): 2049-2058.

Boyd, J. G., V. Skihar, M. Kawaja and R. Doucette (2003). "Olfactory ensheathing cells: historical perspective and therapeutic potential." Anat Rec B New Anat **271**(1): 49-60.

Bremer, M., F. Frob, T. Kichko, P. Reeh, E. R. Tamm, U. Suter and M. Wegner (2011). "Sox10 is required for Schwann-cell homeostasis and myelin maintenance in the adult peripheral nerve." Glia **59**(7): 1022-1032.

Brinkmann, B. G., A. Agarwal, M. W. Sereda, A. N. Garratt, T. Muller, H. Wende, R. M. Stassart, S. Nawaz, C. Humml, V. Velanac, K. Radyushkin, S. Goebbels, T. M. Fischer, R. J. Franklin, C. Lai, H. Ehrenreich, C. Birchmeier, M. H. Schwab and K. A. Nave (2008). "Neuregulin-1/ErbB signaling serves distinct functions in myelination of the peripheral and central nervous system." Neuron **59**(4): 581-595.

Britsch, S., D. E. Goerich, D. Riethmacher, R. I. Peirano, M. Rossner, K. A. Nave, C. Birchmeier and M. Wegner (2001). "The transcription factor Sox10 is a key regulator of peripheral glial development." Genes Dev **15**(1): 66-78.

Brown, E. R., Q. Bone, K. P. Ryan and N. J. Abbott (1991). "Morphology and electrical properties of Schwann cells around the giant axon of the squids Loligo forbesi and Loligo vulgaris." Proc Biol Sci **243**(1308): 255-262.

Buchanan, S., A. A. Harper and J. R. Elliott (1996). "Differential effects of tetrodotoxin (TTX) and high external K+ on A and C fibre compound action potential peaks in frog sciatic nerve." Neurosci Lett **219**(2): 131-134.

Bush, T. G., T. C. Savidge, T. C. Freeman, H. J. Cox, E. A. Campbell, L. Mucke, M. H. Johnson and M. V. Sofroniew (1998). "Fulminant jejuno-ileitis following ablation of enteric glia in adult transgenic mice." Cell **93**(2): 189-201.

Butt, A. M. and B. R. Ransom (1989). "Visualization of oligodendrocytes and astrocytes in the intact rat optic nerve by intracellular injection of lucifer yellow and horseradish peroxidase." Glia **2**(6): 470-475.

Caffrey, J. M., D. L. Eng, J. A. Black, S. G. Waxman and J. D. Kocsis (1992). "Three types of sodium channels in adult rat dorsal root ganglion neurons." Brain Res **592**(1-2): 283-297.

Cahalan, M. D., K. G. Chandy, T. E. DeCoursey and S. Gupta (1985). "A voltage-gated potassium channel in human T lymphocytes." J Physiol **358**: 197-237.

Cao, F., R. Eckert, C. Elfgang, J. M. Nitsche, S. A. Snyder, H. u. DF, K. Willecke and B. J. Nicholson (1998). "A quantitative analysis of connexin-specific permeability differences of gap junctions expressed in HeLa transfectants and Xenopus oocytes." J Cell Sci **111 (Pt 1)**: 31-43.

Carroll, W. M., A. R. Jennings and L. J. Ironside (1998). "Identification of the adult resting progenitor cell by autoradiographic tracking of oligodendrocyte precursors in experimental CNS demyelination." Brain **121 (Pt 2)**: 293-302.
Catterall, W. A. (2000). "From ionic currents to molecular mechanisms: the structure and function of voltage-gated sodium channels." Neuron **26**(1): 13-25.
Causey, G. and H. Hoffman (1956). "The relation between the Schwann cell and the axon in peripheral nerves." J Anat **90**(1): 1-4.
Chanson, M., K. J. Chandross, M. B. Rook, J. A. Kessler and D. C. Spray (1993). "Gating characteristics of a steeply voltage-dependent gap junction channel in rat Schwann cells." J Gen Physiol **102**(5): 925-946.
Cherkas, P. S., T. Y. Huang, T. Pannicke, M. Tal, A. Reichenbach and M. Hanani (2004). "The effects of axotomy on neurons and satellite glial cells in mouse trigeminal ganglion." Pain **110**(1-2): 290-298.
Chiu, S. Y., P. Schrager and J. M. Ritchie (1984). "Neuronal-type Na+ and K+ channels in rabbit cultured Schwann cells." Nature **311**(5982): 156-157.
Clarke, L. E. and B. A. Barres (2013). "Emerging roles of astrocytes in neural circuit development." Nat Rev Neurosci **14**(5): 311-321.
Coetzee, W. A., Y. Amarillo, J. Chiu, A. Chow, D. Lau, T. McCormack, H. Moreno, M. S. Nadal, A. Ozaita, D. Pountney, M. Saganich, E. Vega-Saenz de Miera and B. Rudy (1999). "Molecular diversity of K+ channels." Ann N Y Acad Sci **868**: 233-285.
Dawson, M. R., A. Polito, J. M. Levine and R. Reynolds (2003). "NG2-expressing glial progenitor cells: an abundant and widespread population of cycling cells in the adult rat CNS." Mol Cell Neurosci **24**(2): 476-488.
Decker, L., C. Desmarquet-Trin-Dinh, E. Taillebourg, J. Ghislain, J. M. Vallat and P. Charnay (2006). "Peripheral myelin maintenance is a dynamic process requiring constant Krox20 expression." J Neurosci **26**(38): 9771-9779.
del Rio-Hortega, P. (1993). "Art and artifice in the science of histology. 1933." Histopathology **22**(6): 515-525.
Del Rio-Hortega P. (1920). “La microglia y su transformation en células en bastoncito y cuerpos gránulo-adiposos.” Trab del Lab de invest biol **18**, 37
Dememes, D., A. Lleixa and C. J. Dechesne (1995). "Cellular and subcellular localization of AMPA-selective glutamate receptors in the mammalian peripheral vestibular system." Brain Res **671**(1): 83-94.
Dingledine, R., K. Borges, D. Bowie and S. F. Traynelis (1999). "The glutamate receptor ion channels." Pharmacol Rev **51**(1): 7-61.
Dong, Z., A. Brennan, N. Liu, Y. Yarden, G. Lefkowitz, R. Mirsky and K. R. Jessen (1995). "Neu differentiation factor is a neuron-glia signal and regulates survival, proliferation, and maturation of rat Schwann cell precursors." Neuron **15**(3): 585-596.
Elliott, A. A. and J. R. Elliott (1993). "Characterization of TTX-sensitive and TTX-resistant sodium currents in small cells from adult rat dorsal root ganglia." J Physiol **463**: 39-56.
Evans, P. D., V. Reale, R. M. Merzon and J. Villegas (1991). "Mechanisms of axon-Schwann cell signaling in the squid nerve fiber." Ann N Y Acad Sci **633**: 434-447.
Evans, P. D., V. Reale, R. M. Merzon and J. Villegas (1991). "N-methyl-D-aspartate (NMDA) and non-NMDA type glutamate receptors are present on squid giant axon Schwann cells." J Exp Biol **157**: 593-600.
Evans, W. H. and P. E. Martin (2002). "Gap junctions: structure and function (Review)." Mol Membr Biol **19**(2): 121-136.

Fatt, P. and B. Katz (1950). "Some observations on biological noise." Nature **166**(4223): 597-598.
Fatt, P. and B. Katz (1952). "Spontaneous subthreshold activity at motor nerve endings." J Physiol **117**(1): 109-128.
Feltri, M. L., D. Graus Porta, S. C. Previtali, A. Nodari, B. Migliavacca, A. Cassetti, A. Littlewood-Evans, L. F. Reichardt, A. Messing, A. Quattrini, U. Mueller and L. Wrabetz (2002). "Conditional disruption of beta 1 integrin in Schwann cells impedes interactions with axons." J Cell Biol **156**(1): 199-209.
Finzsch, M., S. Schreiner, T. Kichko, P. Reeh, E. R. Tamm, M. R. Bosl, D. Meijer and M. Wegner (2010). "Sox10 is required for Schwann cell identity and progression beyond the immature Schwann cell stage." Journal of Cell Biology **189**(4): 701-712.
Fricker, F. R., N. Lago, S. Balarajah, C. Tsantoulas, S. Tanna, N. Zhu, S. K. Fageiry, M. Jenkins, A. N. Garratt, C. Birchmeier and D. L. Bennett (2011). "Axonally derived neuregulin-1 is required for remyelination and regeneration after nerve injury in adulthood." J Neurosci **31**(9): 3225-3233.
Friede, R. L. and T. Samorajski (1968). "Myelin formation in the sciatic nerve of the rat. A quantitative electron microscopic, histochemical and radioautographic study." J Neuropathol Exp Neurol **27**(4): 546-570.
Fucile, S., R. Miledi and F. Eusebi (2006). "Effects of cyclothiazide on GluR1/AMPA receptors." Proc Natl Acad Sci U S A **103**(8): 2943-2947.
Fujita, S. and T. Kitamura (1975). "Origin of brain macrophages and the nature of the so-called microglia." Acta Neuropathol Suppl **Suppl 6**: 291-296.
Garratt, A. N., S. Britsch and C. Birchmeier (2000). "Neuregulin, a factor with many functions in the life of a schwann cell." Bioessays **22**(11): 987-996.
Garratt, A. N., O. Voiculescu, P. Topilko, P. Charnay and C. Birchmeier (2000). "A dual role of erbB2 in myelination and in expansion of the schwann cell precursor pool." J Cell Biol **148**(5): 1035-1046.
Geiger, J. R., J. Lubke, A. Roth, M. Frotscher and P. Jonas (1997). "Submillisecond AMPA receptor-mediated signaling at a principal neuron-interneuron synapse." Neuron **18**(6): 1009-1023.
Gensert, J. M. and J. E. Goldman (1997). "Endogenous progenitors remyelinate demyelinated axons in the adult CNS." Neuron **19**(1): 197-203.
Geren, B. B. and F. O. Schmitt (1954). "The Structure of the Schwann Cell and Its Relation to the Axon in Certain Invertebrate Nerve Fibers." Proc Natl Acad Sci U S A **40**(9): 863-870.
Gilly, W. F., R. Gillette and M. McFarlane (1997). "Fast and slow activation kinetics of voltage-gated sodium channels in molluscan neurons." J Neurophysiol **77**(5): 2373-2384.
Gow, A., V. L. Friedrich, Jr. and R. A. Lazzarini (1992). "Myelin basic protein gene contains separate enhancers for oligodendrocyte and Schwann cell expression." J Cell Biol **119**(3): 605-616.
Greenfield, S., M. J. Weise, G. Gantt, E. L. Hogan and S. W. Brostoff (1982). "Basic-Proteins of Rodent Peripheral-Nerve Myelin - Immunochemical Identification of the 21.5k, 18.5k, 17k, 14k, and P2 Proteins." Journal of Neurochemistry **39**(5): 1278-1282.
Griffin, J. W., R. George and T. Ho (1993). "Macrophage systems in peripheral nerves. A review." J Neuropathol Exp Neurol **52**(6): 553-560.
Grove, M., N. H. Komiyama, K. A. Nave, S. G. Grant, D. L. Sherman and P. J. Brophy (2007). "FAK is required for axonal sorting by Schwann cells." J Cell Biol **176**(3): 277-282.

Hald, H., P. K. Ahring, D. B. Timmermann, T. Liljefors, M. Gajhede and J. S. Kastrup (2009). "Distinct structural features of cyclothiazide are responsible for effects on peak current amplitude and desensitization kinetics at iGluR2." J Mol Biol **391**(5): 906-917.
Hess, A. and A. I. Lansing (1953). "The fine structure of peripheral nerve fibers." Anat Rec **117**(2): 175-199.
Higginson, J. R. and S. C. Barnett (2011). "The culture of olfactory ensheathing cells (OECs)--a distinct glial cell type." Exp Neurol **229**(1): 2-9.
Howe, J. R. and J. M. Ritchie (1988). "Two types of potassium current in rabbit cultured Schwann cells." Proc R Soc Lond B Biol Sci **235**(1278): 19-27.
Howe, J. R. and J. M. Ritchie (1990). "Sodium currents in Schwann cells from myelinated and non-myelinated nerves of neonatal and adult rabbits." J Physiol **425**: 169-210.
Huang, L. Y., Y. Gu and Y. Chen (2013). "Communication between neuronal somata and satellite glial cells in sensory ganglia." Glia **61**(10): 1571-1581.
Huang, Y. H., S. R. Sinha, K. Tanaka, J. D. Rothstein and D. E. Bergles (2004). "Astrocyte glutamate transporters regulate metabotropic glutamate receptor-mediated excitation of hippocampal interneurons." J Neurosci **24**(19): 4551-4559.
Inoue, I., I. Tsutsui, N. J. Abbott and E. R. Brown (2002). "Ionic currents in isolated and in situ squid Schwann cells." J Physiol **541**(Pt 3): 769-778.
Isaac, J. T., M. C. Ashby and C. J. McBain (2007). "The role of the GluR2 subunit in AMPA receptor function and synaptic plasticity." Neuron **54**(6): 859-871.
Jaegle, M., W. Mandemakers, L. Broos, R. Zwart, A. Karis, P. Visser, F. Grosveld and D. Meijer (1996). "The POU factor Oct-6 and Schwann cell differentiation." Science **273**(5274): 507-510.
Jagalur, N. B., M. Ghazvini, W. Mandemakers, S. Driegen, A. Maas, E. A. Jones, M. Jaegle, F. Grosveld, J. Svaren and D. Meijer (2011). "Functional dissection of the Oct6 Schwann cell enhancer reveals an essential role for dimeric Sox10 binding." J Neurosci **31**(23): 8585-8594.
Jenq, C. B., K. Chung and R. E. Coggeshall (1986). "Postnatal loss of axons in normal rat sciatic nerve." J Comp Neurol **244**(4): 445-450.
Jessen, K. R., A. Brennan, L. Morgan, R. Mirsky, A. Kent, Y. Hashimoto and J. Gavrilovic (1994). "The Schwann cell precursor and its fate: a study of cell death and differentiation during gliogenesis in rat embryonic nerves." Neuron **12**(3): 509-527.
Jessen, K. R. and R. Mirsky (1998). "Origin and early development of Schwann cells." Microsc Res Tech **41**(5): 393-402.
Jessen, K. R. and R. Mirsky (1999). "Schwann cells and their precursors emerge as major regulators of nerve development." Trends Neurosci **22**(9): 402-410.
Jessen, K. R. and R. Mirsky (2005). "The origin and development of glial cells in peripheral nerves." Nat Rev Neurosci **6**(9): 671-682.
Jessen, K. R., L. Morgan, H. J. Stewart and R. Mirsky (1990). "Three markers of adult non-myelin-forming Schwann cells, 217c(Ran-1), A5E3 and GFAP: development and regulation by neuron-Schwann cell interactions." Development **109**(1): 91-103.
Jonas, P. and N. Burnashev (1995). "Molecular mechanisms controlling calcium entry through AMPA-type glutamate receptor channels." Neuron **15**(5): 987-990.
Karadottir, R., N. B. Hamilton, Y. Bakiri and D. Attwell (2008). "Spiking and nonspiking classes of oligodendrocyte precursor glia in CNS white matter." Nat Neurosci **11**(4): 450-456.
Katz, B. (1971). "Quantal mechanism of neural transmitter release." Science **173**(3992): 123-126.
Katz, B. (2003). "Neural transmitter release: from quantal secretion to exocytosis and beyond." J Neurocytol **32**(5-8): 437-446.

Kettenmann, H. and S. Ilschner (1993). "Physiological properties of microglia." Clin Neuropathol **12**(5): 306-307.
Kimelberg, H. K. (2007). "Supportive or information-processing functions of the mature protoplasmic astrocyte in the mammalian CNS? A critical appraisal." Neuron Glia Biol **3**(3): 181-189.
Kinkelin, I., E. B. Brocker, M. Koltzenburg and S. M. Carlton (2000). "Localization of ionotropic glutamate receptors in peripheral axons of human skin." Neurosci Lett **283**(2): 149-152.
Komiyama, A. and K. Suzuki (1992). "Age-related differences in proliferative responses of Schwann cells during Wallerian degeneration." Brain Res **573**(2): 267-275.
Konishi, T. (1989). "Voltage-dependent potassium channels in mouse Schwann cells." J Physiol **411**: 115-130.
Konishi, T. (1990). "Dye coupling between mouse Schwann cells." Brain Res **508**(1): 85-92.
Kostyuk, P. G., N. S. Veselovsky and A. Y. Tsyndrenko (1981). "Ionic currents in the somatic membrane of rat dorsal root ganglion neurons-I. Sodium currents." Neuroscience **6**(12): 2423-2430.
Kuhlbrodt, K., B. Herbarth, E. Sock, I. Hermans-Borgmeyer and M. Wegner (1998). "Sox10, a novel transcriptional modulator in glial cells." J Neurosci **18**(1): 237-250.
Kukley, M., E. Capetillo-Zarate and D. Dietrich (2007). "Vesicular glutamate release from axons in white matter." Nat Neurosci **10**(3): 311-320.
Kukley, M., M. Kiladze, R. Tognatta, M. Hans, D. Swandulla, J. Schramm and D. Dietrich (2008). "Glial cells are born with synapses." FASEB J **22**(8): 2957-2969.
Levine, J. M. and R. Reynolds (1999). "Activation and proliferation of endogenous oligodendrocyte precursor cells during ethidium bromide-induced demyelination." Exp Neurol **160**(2): 333-347.
Li, Y., G. I. Tennekoon, M. Birnbaum, M. A. Marchionni and J. L. Rutkowski (2001). "Neuregulin signaling through a PI3K/Akt/Bad pathway in Schwann cell survival." Mol Cell Neurosci **17**(4): 761-767.
Lieberman, E. M. (1991). "Role of glutamate in axon-Schwann cell signaling in the squid." Ann N Y Acad Sci **633**: 448-457.
Lieberman, E. M., N. J. Abbott and S. Hassan (1989). "Evidence that glutamate mediates axon-to-Schwann cell signaling in the squid." Glia **2**(2): 94-102.
Lieberman, E. M. and E. Sanzenbacher (1992). "Mechanisms of glutamate activation of axon-to-Schwann cell signaling in the squid." Neuroscience **47**(4): 931-939.
Lin, S. C., J. H. Huck, J. D. Roberts, W. B. Macklin, P. Somogyi and D. E. Bergles (2005). "Climbing fiber innervation of NG2-expressing glia in the mammalian cerebellum." Neuron **46**(5): 773-785.
Liu, F. Y., Y. N. Sun, F. T. Wang, Q. Li, L. Su, Z. F. Zhao, X. L. Meng, H. Zhao, X. Wu, Q. Sun, G. G. Xing and Y. Wan (2012). "Activation of satellite glial cells in lumbar dorsal root ganglia contributes to neuropathic pain after spinal nerve ligation." Brain Res **1427**: 65-77.
Liu, G. J. and M. R. Bennett (2003). "ATP secretion from nerve trunks and Schwann cells mediated by glutamate." Neuroreport **14**(16): 2079-2083.
Liu, S. J. and S. G. Cull-Candy (2002). "Activity-dependent change in AMPA receptor properties in cerebellar stellate cells." J Neurosci **22**(10): 3881-3889.
Locke, R. E. and J. M. Nerbonne (1997). "Three kinetically distinct Ca2+-independent depolarization-activated K+ currents in callosal-projecting rat visual cortical neurons." Journal of Neurophysiology **78**(5): 2309-2320.
Matsui, K. and C. E. Jahr (2003). "Ectopic release of synaptic vesicles." Neuron **40**(6): 1173-1183.

Maudlej, N. and M. Hanani (1992). "Modulation of dye coupling among glial cells in the myenteric and submucosal plexuses of the guinea pig." Brain Res **578**(1-2): 94-98.
Mayer, M. L. and N. Armstrong (2004). "Structure and function of glutamate receptor ion channels." Annu Rev Physiol **66**: 161-181.
Meier, C., R. Dermietzel, K. G. Davidson, T. Yasumura and J. E. Rash (2004). "Connexin32-containing gap junctions in Schwann cells at the internodal zone of partial myelin compaction and in Schmidt-Lanterman incisures." J Neurosci **24**(13): 3186-3198.
Mi, H., T. J. Deerinck, M. H. Ellisman and T. L. Schwarz (1995). "Differential distribution of closely related potassium channels in rat Schwann cells." J Neurosci **15**(5 Pt 2): 3761-3774.
Michailov, G. V., M. W. Sereda, B. G. Brinkmann, T. M. Fischer, B. Haug, C. Birchmeier, L. Role, C. Lai, M. H. Schwab and K. A. Nave (2004). "Axonal neuregulin-1 regulates myelin sheath thickness." Science **304**(5671): 700-703.
Miron, V. E., T. Kuhlmann and J. P. Antel (2011). "Cells of the oligodendroglial lineage, myelination, and remyelination." Biochim Biophys Acta **1812**(2): 184-193.
Mirsky, R., C. Dubois, L. Morgan and K. R. Jessen (1990). "04 and A007-sulfatide antibodies bind to embryonic Schwann cells prior to the appearance of galactocerebroside; regulation of the antigen by axon-Schwann cell signals and cyclic AMP." Development **109**(1): 105-116.
Mori, T., T. Wakabayashi, Y. Takamori, K. Kitaya and H. Yamada (2009). "Phenotype analysis and quantification of proliferating cells in the cortical gray matter of the adult rat." Acta Histochem Cytochem **42**(1): 1-8.
Mueller, M., C. Leonhard, K. Wacker, E. B. Ringelstein, M. Okabe, W. F. Hickey and R. Kiefer (2003). "Macrophage response to peripheral nerve injury: the quantitative contribution of resident and hematogenous macrophages." Lab Invest **83**(2): 175-185.
Mueller, M., K. Wacker, E. B. Ringelstein, W. F. Hickey, Y. Imai and R. Kiefer (2001). "Rapid response of identified resident endoneurial macrophages to nerve injury." Am J Pathol **159**(6): 2187-2197.
Nageotte J. (1910). “Phenomenes de secretion dans le protoplasma des cellules nevrogliques de la substance gris.” C R Soc Biol (Paris) **68**, 1068-1069
Nagy, J. I. and J. E. Rash (2000). "Connexins and gap junctions of astrocytes and oligodendrocytes in the CNS." Brain Res Brain Res Rev **32**(1): 29-44.
Nave, K. A. (2010). "Myelination and the trophic support of long axons." Nat Rev Neurosci **11**(4): 275-283.
Nodari, A., D. Zambroni, A. Quattrini, F. A. Court, A. D'Urso, A. Recchia, V. L. Tybulewicz, L. Wrabetz and M. L. Feltri (2007). "Beta1 integrin activates Rac1 in Schwann cells to generate radial lamellae during axonal sorting and myelination." J Cell Biol **177**(6): 1063-1075.
Oh, Y., J. A. Black and S. G. Waxman (1994). "Rat brain Na+ channel mRNAs in non-excitable Schwann cells." FEBS Lett **350**(2-3): 342-346.
Paolicelli, R. C., G. Bolasco, F. Pagani, L. Maggi, M. Scianni, P. Panzanelli, M. Giustetto, T. A. Ferreira, E. Guiducci, L. Dumas, D. Ragozzino and C. T. Gross (2011). "Synaptic pruning by microglia is necessary for normal brain development." Science **333**(6048): 1456-1458.
Parkhurst, C. N., G. Yang, I. Ninan, J. N. Savas, J. R. Yates, 3rd, J. J. Lafaille, B. L. Hempstead, D. R. Littman and W. B. Gan (2013). "Microglia promote learning-dependent synapse formation through brain-derived neurotrophic factor." Cell **155**(7): 1596-1609.
Paternain, A. V., M. Morales and J. Lerma (1995). "Selective antagonism of AMPA receptors unmasks kainate receptor-mediated responses in hippocampal neurons." Neuron **14**(1): 185-189.
Patlak, J. (1991). "Molecular kinetics of voltage-dependent Na+ channels." Physiol Rev **71**(4): 1047-1080.

Prinz, M. and J. Priller (2014). "Microglia and brain macrophages in the molecular age: from origin to neuropsychiatric disease." Nat Rev Neurosci **15**(5): 300-312.
Prodanov, D. and H. K. Feirabend (2007). "Morphometric analysis of the fiber populations of the rat sciatic nerve, its spinal roots, and its major branches." J Comp Neurol **503**(1): 85-100.
Rabe, H., H. J. Ritz and G. Jeserich (1998). "Voltage-gated potassium channels of Schwann cells from trout lateral line nerve: a combined electrophysiological and molecular characterization." Glia **23**(4): 329-338.
Rawlins, F. A. and J. Villegas (1978). "Autoradiographic localization of acetylcholine receptors in the Schwann cell membrane of the squid nerve fiber." J Cell Biol **77**(2): 371-376.
Rehberg, S., P. Lischka, G. Glaser, T. Stamminger, M. Wegner and O. Rosorius (2002). "Sox10 is an active nucleocytoplasmic shuttle protein, and shuttling is crucial for Sox10-mediated transactivation." Mol Cell Biol **22**(16): 5826-5834.
Robitaille, R. (1995). "Purinergic receptors and their activation by endogenous purines at perisynaptic glial cells of the frog neuromuscular junction." J Neurosci **15**(11): 7121-7131.
Rochon, D., I. Rousse and R. Robitaille (2001). "Synapse-glia interactions at the mammalian neuromuscular junction." J Neurosci **21**(11): 3819-3829.
Saijo, K. and C. K. Glass (2011). "Microglial cell origin and phenotypes in health and disease." Nat Rev Immunol **11**(11): 775-787.
Santos-Benito, F. F. and A. Ramon-Cueto (2003). "Olfactory ensheathing glia transplantation: a therapy to promote repair in the mammalian central nervous system." Anat Rec B New Anat **271**(1): 77-85.
Scherer, S. S., D. Y. Wang, R. Kuhn, G. Lemke, L. Wrabetz and J. Kamholz (1994). "Axons regulate Schwann cell expression of the POU transcription factor SCIP." J Neurosci **14**(4): 1930-1942.
Schmalbruch, H. (1986). "Fiber composition of the rat sciatic nerve." Anat Rec **215**(1): 71-81.
Shrager, P., S. Y. Chiu and J. M. Ritchie (1985). "Voltage-dependent sodium and potassium channels in mammalian cultured Schwann cells." Proc Natl Acad Sci U S A **82**(3): 948-952.
Simon, A. M. and D. A. Goodenough (1998). "Diverse functions of vertebrate gap junctions." Trends Cell Biol **8**(12): 477-483.
Sobko, A., A. Peretz, O. Shirihai, S. Etkin, V. Cherepanova, D. Dagan and B. Attali (1998). "Heteromultimeric delayed-rectifier K+ channels in schwann cells: developmental expression and role in cell proliferation." J Neurosci **18**(24): 10398-10408.
Somjen, G. G. (1988). "Nervenkitt: notes on the history of the concept of neuroglia." Glia **1**(1): 2-9.
Son, Y. J., J. T. Trachtenberg and W. J. Thompson (1996). "Schwann cells induce and guide sprouting and reinnervation of neuromuscular junctions." Trends Neurosci **19**(7): 280-285.
Sontheimer, H. (1994). "Voltage-dependent ion channels in glial cells." Glia **11**(2): 156-172.
Stassart, R. M., R. Fledrich, V. Velanac, B. G. Brinkmann, M. H. Schwab, D. Meijer, M. W. Sereda and K. A. Nave (2013). "A role for Schwann cell-derived neuregulin-1 in remyelination." Nat Neurosci **16**(1): 48-54.
Steinhauser, C., K. Kressin, E. Kuprijanova, M. Weber and G. Seifert (1994). "Properties of voltage-activated Na+ and K+ currents in mouse hippocampal glial cells in situ and after acute isolation from tissue slices." Pflugers Arch **428**(5-6): 610-620.
Stewart, H. J., L. Morgan, K. R. Jessen and R. Mirsky (1993). "Changes in DNA synthesis rate in the Schwann cell lineage in vivo are correlated with the precursor--Schwann cell transition and myelination." Eur J Neurosci **5**(9): 1136-1144.
Storm, J. F. (1990). "Potassium currents in hippocampal pyramidal cells." Prog Brain Res **83**: 161-187.

Sun, Y., R. Olson, M. Horning, N. Armstrong, M. Mayer and E. Gouaux (2002). "Mechanism of glutamate receptor desensitization." Nature **417**(6886): 245-253.
Szapiro, G. and B. Barbour (2007). "Multiple climbing fibers signal to molecular layer interneurons exclusively via glutamate spillover." Nat Neurosci **10**(6): 735-742.
Taveggia, C., G. Zanazzi, A. Petrylak, H. Yano, J. Rosenbluth, S. Einheber, X. Xu, R. M. Esper, J. A. Loeb, P. Shrager, M. V. Chao, D. L. Falls, L. Role and J. L. Salzer (2005). "Neuregulin-1 type III determines the ensheathment fate of axons." Neuron **47**(5): 681-694.
Topilko, P., S. Schneider-Maunoury, G. Levi, A. Baron-Van Evercooren, A. B. Chennoufi, T. Seitanidou, C. Babinet and P. Charnay (1994). "Krox-20 controls myelination in the peripheral nervous system." Nature **371**(6500): 796-799.
Traynelis, S. F., L. P. Wollmuth, C. J. McBain, F. S. Menniti, K. M. Vance, K. K. Ogden, K. B. Hansen, H. Yuan, S. J. Myers and R. Dingledine (2010). "Glutamate receptor ion channels: structure, regulation, and function." Pharmacol Rev **62**(3): 405-496.
Venneti, S., B. J. Lopresti, G. Wang, R. L. Hamilton, C. A. Mathis, W. E. Klunk, U. M. Apte and C. A. Wiley (2009). "PK11195 labels activated microglia in Alzheimer's disease and in vivo in a mouse model using PET." Neurobiol Aging **30**(8): 1217-1226.
Verdoorn, T. A., N. Burnashev, H. Monyer, P. H. Seeburg and B. Sakmann (1991). "Structural determinants of ion flow through recombinant glutamate receptor channels." Science **252**(5013): 1715-1718.
Villegas, J. (1972). "Axon-Schwann cell interaction in the squid nerve fibre." J Physiol **225**(2): 275-296.
Villegas, J. (1975). "Characterization of acetylcholine receptors in the Schwann cell membrane of the squid nerve fibre." J Physiol **249**(3): 679-689.
Villegas, J., P. D. Evans and V. Reale (1987). "Modulation of the membrane potential of the Schwann cell of the squid giant nerve fiber." J Physiol (Paris) **82**(4): 322-326.
Virchow R. (1858). “Cellularpathologie” Berlin
Wanner, I. B., N. K. Guerra, J. Mahoney, A. Kumar, P. M. Wood, R. Mirsky and K. R. Jessen (2006). "Role of N-cadherin in Schwann cell precursors of growing nerves." Glia **54**(5): 439-459.
Webster, H. D. (1971). "The geometry of peripheral myelin sheaths during their formation and growth in rat sciatic nerves." J Cell Biol **48**(2): 348-367.
Webster, H. D., R. Martin and M. F. O'Connell (1973). "The relationships between interphase Schwann cells and axons before myelination: a quantitative electron microscopic study." Dev Biol **32**(2): 401-416.
Wegner, M. (1999). "From head to toes: the multiple facets of Sox proteins." Nucleic Acids Res **27**(6): 1409-1420.
Weiner, J. A., N. Fukushima, J. J. Contos, S. S. Scherer and J. Chun (2001). "Regulation of Schwann cell morphology and adhesion by receptor-mediated lysophosphatidic acid signaling." J Neurosci **21**(18): 7069-7078.
Wieraszko, A. and Z. Ahmed (2009). "Axonal release of glutamate analog, d-2,3-3H-Aspartic acid and l-14C-proline from segments of sciatic nerve following electrical and magnetic stimulation." Neurosci Lett **458**(1): 19-22.
Wilding, T. J. and J. E. Huettner (1995). "Differential antagonism of alpha-amino-3-hydroxy-5-methyl-4- isoxazolepropionic acid-preferring and kainate-preferring receptors by 2,3-benzodiazepines." Mol Pharmacol **47**(3): 582-587.
Williams, S. H. and D. Johnston (1991). "Kinetic properties of two anatomically distinct excitatory synapses in hippocampal CA3 pyramidal neurons." J Neurophysiol **66**(3): 1010-1020.

Wilson, G. F. and S. Y. Chiu (1990). "Ion channels in axon and Schwann cell membranes at paranodes of mammalian myelinated fibers studied with patch clamp." J Neurosci **10**(10): 3263-3274.
Wilson, G. F. and S. Y. Chiu (1990). "Potassium channel regulation in Schwann cells during early developmental myelinogenesis." J Neurosci **10**(5): 1615-1625.
Woodhoo, A. and L. Sommer (2008). "Development of the Schwann cell lineage: from the neural crest to the myelinated nerve." Glia **56**(14): 1481-1490.
Yu, W. M., M. L. Feltri, L. Wrabetz, S. Strickland and Z. L. Chen (2005). "Schwann cell-specific ablation of laminin gamma1 causes apoptosis and prevents proliferation." J Neurosci **25**(18): 4463-4472.
Zakharenko, S., S. Chang, M. O'Donoghue and S. V. Popov (1999). "Neurotransmitter secretion along growing nerve processes: comparison with synaptic vesicle exocytosis." J Cell Biol **144**(3): 507-518.
Ziskin, J. L., A. Nishiyama, M. Rubio, M. Fukaya and D. E. Bergles (2007). "Vesicular release of glutamate from unmyelinated axons in white matter." Nat Neurosci **10**(3): 321-330.
Ziskind-Conhaim, L. (1988). "Physiological and morphological changes in developing peripheral nerves of rat embryos." Brain Res **470**(1): 15-28.
Zorick, T. S., D. E. Syroid, A. Brown, T. Gridley and G. Lemke (1999). "Krox-20 controls SCIP expression, cell cycle exit and susceptibility to apoptosis in developing myelinating Schwann cells." Development **126**(7): 1397-1406.

ACKNOWLEDGEMENT

First of all, I would like to thank my supervisor, Dr. Maria Kukley, for giving me the opportunity to perform my PhD thesis in her lab in the Centre for Integrative Neuroscience (CIN) and for her constant scientific support and advice during my project.

A special thanks to my co-supervisors, Prof. Dr. Olga Garaschuk and Prof. Dr. Bernd Antkowiak for their great scientific comments on my project and assistance.

To all members of the AG Kukley and the CIN doctoral students, especially Balint, Ting-Jiun, Bartosz, Ruxandra, Hartwig, Florian, Luise and Charlie for motivating me during the years of my study, for their interest to my work, critical and fruitful discussions, and for just being a great team – inside and outside the lab. In particular, I am grateful to Daniela for kindly providing me with expert technical assistance, friendship and moral support.

Finally, I want to thank my beloved family, especially my parents. Thank you for believing in me during any period of my doctoral thesis and for supporting me whenever I was doubtful. The last two people I want to thank are my husband Jens and my daughter Mia. I especially thank you two for your endless patience, support and love. I am deeply grateful to Mia and Jens because they have given up so much to make my dissertation a priority in our lives. They shared all the ups and downs with me. You made me manage this, so it only seems right that I dedicate my dissertation to them.